國 立 交 通 大 學

機 械 工 程 學 系

碩 士 論 文

放置可移動陶瓷粒子在一水平加熱銅板上對 FC-72 池沸騰熱傳增強研究

Enhancement of FC-72 Pool Boiling Heat Transfer by Movable Ceramic Particles on a Horizontal Plate

研 究 生：吳 錫 寰

指 導 老 師：林 清 發 教授

中 華 民 國 103 年 1 月

誌謝

兩年半的研究生活終於畫下句點。在交通大學我學到很多，也得到很多，許多不如意的事開心的事依然歷歷在目，也因為這樣讓我變得更加圓滿，我喜歡新竹，我喜歡交大，這裡的研究氣息、人文風氣我都很喜歡，在這裡我要跟交大說一聲：謝謝。

在研究所的這段期間，很感謝林清發教授的細心指導。他是位真正的學者，同時也是最好的老師，而且具備了高度的道德及人文素養。兩年多下來的陶冶，我從什麼都不懂的小子慢慢變成稍微有點物理概念的研究生，我從老師身上學到的遠比我想得多更多，至於今後我會永遠記得老師的指導、教誨。再來則是要感謝博士班汪書磊學長的指導，雖然我們之間曾經發生過摩擦或是意見不合，但我始終相信學長的出發點是為我好，希望之後你一切順利。再來是感謝我最敬重對我最好的學長葉庭鈞，不僅在我的生活、研究想法甚至是我的思考，我的一切你都毫無保留的與我分享給我意見，也徹底改變了我的價值觀，讓我變成一個隨順圓滿的人，我想我們之間已經不是用同學就可以形容，你更像是我的哥哥。在這裡也要親自跟你說聲謝謝，我想我們在追求目標的過程中，一定會再相遇。同時也感謝學妹與學弟：李貞儀、江奕勳你們的活力熱血為實驗室注入了一股新的氣息，也謝謝你們的幫忙讓我的實驗才可以順利完成，有你們真好。謝謝你們讓我度過碩士生涯最開心的一學期，希望能夠莫忘加入實驗室的初衷，在未來路上將自己的目標與理想發揚光大並加以實踐。家魁你永遠都是我的好夥伴 謝謝你聽我訴苦也謝謝你的關心。仕文老大也感謝你在我寫論文時給我很多意見，陪我聊天。同學薛正宏與我共同經歷了很多事情千言萬語大概也只有感謝與祝福。

在此也要感謝家人、王門的冠丞、顯文、建銘，謝謝你們在我實驗遇到困難時幫我忙，以及保杰、 國淳時常鼓勵我以及其他關心過我的人，沒有你們的支持與鼓勵我是無法走到今天的。他日我若有一點小小成就，那必然是你們曾經有過的莫大幫助所造就的。滴水之恩，必定湧泉以報。

最後，我要對未來可能會翻閱到此頁的人和我說句話：也許已經過了很久，或許現在已是十年、二十年甚至更久之後了，每個人都不應該向現實屈服而是要仍不斷地學習成長、朝目標前進。不論何者，我都要說，請創造更好的未來吧，為你我的家人朋友享受更好的未來，不論何時，不論幾歲，不論開心，不論難過，這都要放在心上。

吳錫寰

2014/1 於新竹交大

放置可移動陶瓷粒子在一水平加熱銅板上

對 FC-72 池沸騰熱傳增強研究

研 究 生：吳 錫 寰　　指 導 老 師：林 清 發 教授

國立交通大學機械工程學系

摘要

本論文針對放置可移動陶瓷粒子於加熱銅板上對 FC-72 池沸騰熱傳增強實驗研究。可移動顆粒放置於加熱銅板表面上並且由一個四方型的壓克力圍牆圍住，來防止可移動顆粒不會因為液體的流動，導致可移動顆粒被沖離了加熱銅板表面。在實驗中探討顆粒種類、顆粒直徑和顆粒的數量。在實驗參數範圍上，熱通量 q 從 0.1 到 6 W/cm^2，顆粒種類為氧化鋁和氮化矽，氧化鋁顆粒直徑有 1.0 和 1.6 mm，顆粒的數量從 100 到 1800(對於直徑為 1.0 mm 的顆粒)和 100 到 700(對於直徑為 1.6 mm 的顆粒)，而氮化矽顆粒直徑有 1.6 和 2.0 mm，顆粒的數量從 100 到 700(對於直徑為 1.6 mm 的顆粒)和 100 到 500(對於直徑為 2.0 mm 的顆粒)。

實驗數據以壁過熱度對應輸入的熱通量及熱傳係數表示，比較對於光滑加熱銅塊下熱傳增強的表現。放置可移動陶瓷氧化鋁粒子相較於光滑表面對於 FC-72 之池沸騰熱傳係數有 550%的增強效果。而對於放置可移動陶瓷氮化矽粒子相較於光滑表面，整體的沸騰熱傳係數有 560%的增強效果。甚至當加熱銅板上覆蓋滿顆粒(最多鋪滿兩層)對於整體的散熱效果有明顯的增強。但在高熱通量時，散熱效果有降低的趨勢，特別對於氧化鋁顆粒放置直徑 1.6 mm 的顆粒，散熱效果降低的趨勢很明顯，而對氮化矽而言散熱效果幾乎沒有降低。由數據呈現的圖形可得，熱傳增強的表現會因其不同的參數搭配而有不同的增強效果，理想且良好的熱傳增強表現在於適當的顆粒種類、顆粒直徑和顆粒數量的搭配。

由數據呈現的結果指出，放置可移動擾動粒子於加熱銅板上後對於整體的

散熱效果有增強的效果也有降低的效果。在高熱通量時，散熱效果有明顯降低的現象。

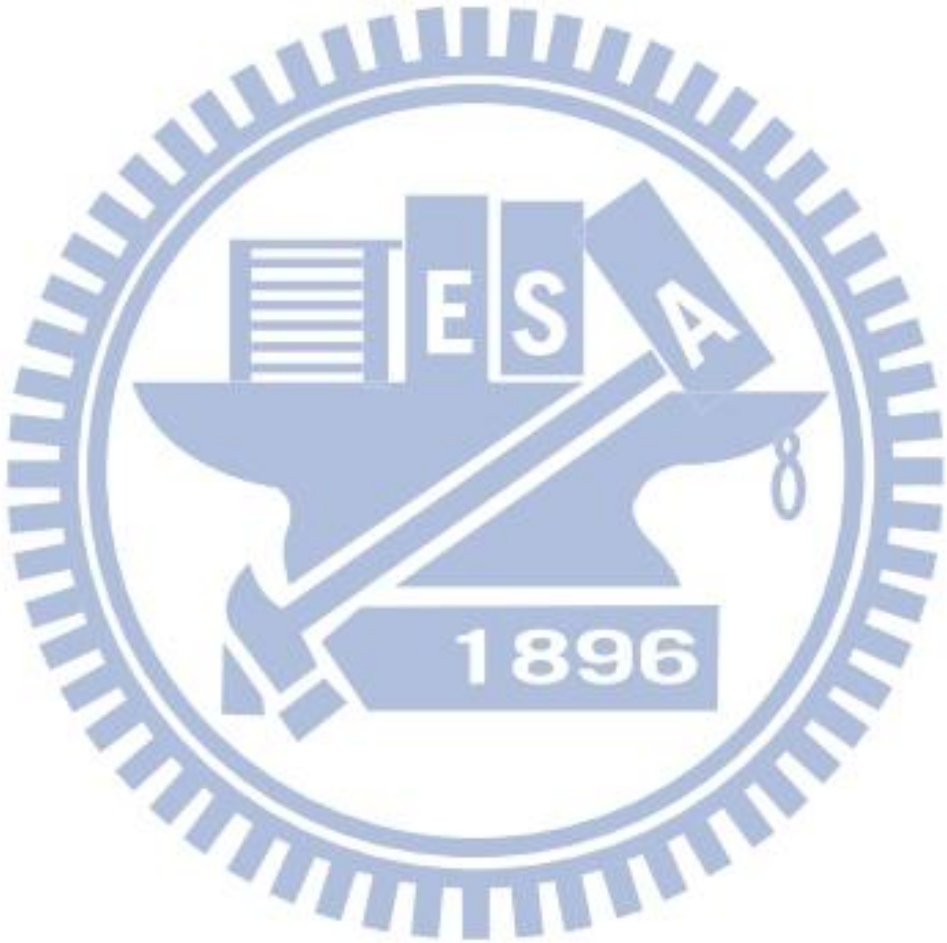

Enhancement of FC-72 Pool Boiling Heat Transfer by Movable Ceramic Particles on a Horizontal Plate

Student: His-Huan Wu **Advisor: Prof. Tsing-Fa Lin**

National Chiao Tung University

ABSTRACT

An experiment is carried out here to investigate how the saturated pool boiling heat transfer of liquid FC-72 over a horizontal heated copper plate of 3×3 cm^2 in surface area is affected by placing fine ceramic particles above the surface, intending to explore the possible pool boiling heat transfer enhancement by the boiling flow driven moving particles. Both zirconia and silicon nitride particles are tested. The particles are freely placed above the heated plate with a rectangular fence surrounding the plate so that the particles can be moved by the force induced by the boiling flow without being blown away. In the experiment, the imposed heat flux is varied from 0.1 to 6 W/cm^2 with the diameter of the particles fixed at 1.0 and 1.6 mm for the zirconia particles and at 1.6 and 2.0 mm for the silicon nitride particles. Besides, the total particle number placed on the plate ranges from 100 to 1800 for the small zirconia particles, from 100 to 700 for the particles at d_p=1.6 mm, and from 100 to 500 for the large silicon nitride particles at d_p=2.0 mm. The measured data are presented in terms of boiling curves and boiling heat transfer coefficients for the case with the presence and absence of the particles. The experimental parameters include the imposed heat flux level and the size, material and number of the particles.

The data obtained from the present study for the saturated pool boiling indicate that placing the movable ceramic particles on the heated plate can significantly

increase the pool boiling heat transfer coefficient of FC-72 at low and medium heat fluxes (wall superheats). For the zirconia particles the enhancement can be up to 550% over that for a bare surface for a certain combination of the experimental parameters. The best enhancement can be as high as 560% for the lighter silicon nitride particles. Even when more than one layer of particles is placed on the plate relatively significant boiling heat transfer enhancement can still be obtained. However, the boiling heat transfer enhancement varies nonmonotonically with the particle size, number and material and the heat flux applied, reflecting the complex mutual influences of the movable particles and bubble motion near the heated surface. An optimal boiling heat transfer enhancement could be procured by a suitable choice of the experimental parameters. Besides, the wall superheat for the incipient boiling can be substantially reduced by the moving ceramic particles. However, for cases at high heat flux (wall superheat) placing the large zirconia particles on the plate can noticeably reduce the boiling heat transfer. Moreover, the boiling heat transfer enhancement by the lighter ceramic particles is found to be somewhat better than that by the heavier metallic particles. Furthermore, the boiling heat transfer retardation at high heat flux by the ceramic particles in less severe.

The results from the visualization of the bubble and particle movement in the boiling flow over the copper plate reveals the complicate interactions between the particles and boiling flow, which is useful in identifying the mechanisms of enhancing and retarding the boiling heat transfer by the particles at different levels of the wall superheat. At high heat flux the retarding effect by the particles can be strong.

TABLE OF CONTENTS

LIST OF TABLES

LIST OF FIGURES

Experimental Apparatus

Data Reduction

Saturated Pool Boiling Heat Transfer

NOMENCLATURE

A	area, mm^2
c_p	specific heat, J/kg·K
d_p	diameters of particles, mm
N_p	numbers of particles
N_{pf}	maximum particle number forming a single particle layer
h	heat transfer coefficient, $W/m^2 \cdot K$
I	measured current from DC power supply, A
V	measured voltage from DC power supply, V
k	thermal conductivity, W/m·K
L	characteristic length, m
Nu_L	Nusselt number, $Nu_L = \frac{hL}{k_\ell}$
P	system pressure, kPa
Q	heat transfer rate, W
q_n	net wall heat flux, W/cm^2
Ra	Rayleigh number
T	temperature, ^oC
t	time, sec
W	plate width, cm

Greek Symbols

ν	kinematic viscosity, m^2/s
ρ_{zro_2}	zirconia density (ρ_{cu}=5948), kg/m^3
ρ_ℓ	liquid density, kg/m^3
ρ_p	particle density, kg/m^3
$\rho_{Si_3N_4}$	silicon nitride density (ρ_{ss}=3324), kg/m^3
μ	absolute viscosity, kg/m·s
β	coefficient of expansion, /K
σ	surface tension, N/m
δ	the distance between the thermalcouple tips and the upper surface of the copper plate, m
ΔT_w	wall superheat, K
ΔT_{ONB}	incipient boiling superheat, K

g gravity, m/s^2

α Thermal diffusion coefficient, m^2/s

i_{lv} Latent heat, kJ/kg

Subscripts

Cu copper

t total

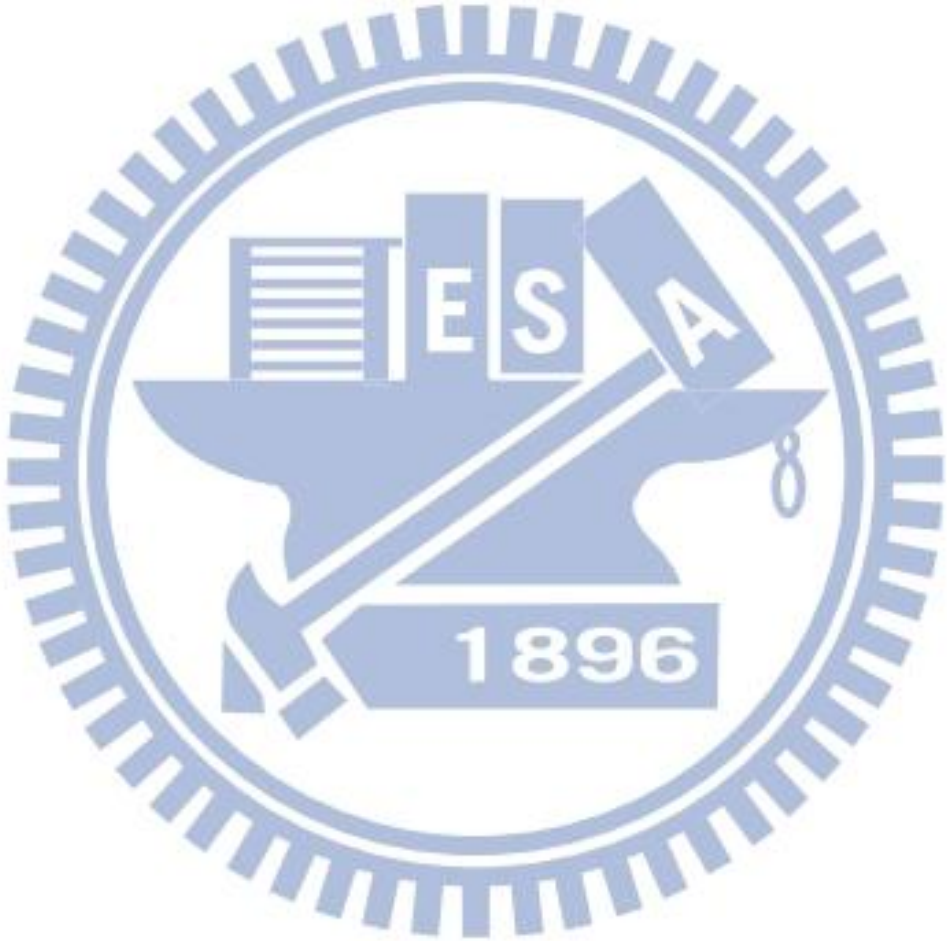

CHAPTER 1

INTRODUCTION

1.1 Motive of the Present Study

Recent significant technological advances in the electronics industry have led to a rapid miniaturization of integrated circuits. Consequently, the power dissipation density in various micro processors increases substantially during their normal operation. How to effectively remove the large amount of dissipating heat from the processors poses a great challenge to heat transfer research community. In order to transfer the large quantity of the dissipating heat from the chips with an ultra high microelectronic component density, highly efficient heat transfer methods are required to control their temperatures at allowable level. Although air cooling has been used commonly today over a long period of time, this method has reached its upper performance limit and is unable to solve the cooling problems encountered in the current electronics industry [1]. Therefore, cooling techniques have to be improved and heat transfer systems with better efficiency have to be used. Cooling based on liquid convection and liquid-vapor phase-change heat transfer have been considered. Among these, boiling heat transfer is regarded as one of the most effective methods in electronics cooling comparing with the methods based on single-phase heat transfer because of the exchange of latent heat is involved in the boiling processes. Methods to further improve the boiling heat transfer are therefore of great interest.

Over the past decades a number of passive boiling heat transfer enhancement methods have been proposed by modifying geometrical structure of the heated surface such as adding certain micro-structures, pin fins and grooves to the surfaces. Significant pool boiling heat transfer enhancement can be obtained. Besides, coating the surfaces with particles and covering the surfaces with screens have been known to be effective. These enhancement

methods are based on various forms of extended surface fixed firmly onto the surfaces or directly fabricated on the surfaces. Moreover, some active boiling heat transfer enhancement methods such as vibrating and rotating working fluids and/or heated surface by external forces were suggested. These methods are very effective. But they are not welcome because the need to use external force. In the present study, enhancement of FC-72 pool boiling heat transfer by placing a large number of movable small solid particles above a heating plate will be explored. The particles can be moved violently by the vigorous motion of the bubbly flow in the pool boiling on one end. On the other end, the violently moving particles can increase the bubble departing rate from the heated surface and the turbulence level of the boiling flow. These mutual interactions of the particles and bubbly flow can be beneficial in promoting the boiling heat transfer from the heated surface. However, the presence of a large number of the particles can impede the bubble departure from the heated surface and liquid inrush to the surface. This in turn will retard the boiling heat transfer. In the present investigation we intend to delineate the ranges of experimental parameters over which boiling heat transfer can be enhanced by the moving particles.

The working fluid FC-72 is a dielectric fluorocarbon liquid manufactured by the 3M Company and gains popularity in electronics cooling application. It not only has suitable phase-change temperature for thermal control of I.C. components but also owns the quality that does not foul the boiling surface. Importantly, FC-72 has less impact on our environment than alternative liquids like chlorofluorocarbons or organic liquids. Copper has properties of better thermal conductivity than most metals and is often considered to be suitable for heat dissipating elements. Thus the heat transfer enhancement characteristics of pool boiling of the dielectric liquid on a copper plate by placing movable solid particles above the heated surface immersed in FC-72 liquid are explored in the present study. In an earlier study [2] Wei in our laboratory obtained significant enhancement in pool boiling heat transfer of saturated FC-72 over a horizontal heated copper plate by placing copper and stainless steel (metallic) particles

on the plate when the, size and number of particles are suitably chosen for low and medium wall superheats. In this study we move further to investigate the possibility of enhancing saturated pool boiling heat transfer of FC-72 by the movable zirconia and silicon nitride (ceramic) particles. These ceramic particles are much lighter than the metallic particles tested by Wei [2]. Besides, the ceramic material has low thermal conductivity.

1.2 Literature Review

In what follows the literature relevant to the present study is briefly reviewed. Pool boiling heat transfer is a process of vigorous heat transfer resulting from latent heat exchange associated with liquid-to-vapor phase change in a quiescent liquid. Nukiyama [3] conducted a pioneering pool boiling experiment in 1934 and arranged the experimental heat transfer data as a form of the wall superheat versus the heat flux, which is known as the "boiling curve" today. After that, the pool boiling heat transfer research has received considerable attention.

The state of the art cooling technologies for handling heat dissipation in microelectronic equipments have been developed extensively over the past 30 years. Several products were released including Air-Cooled Modules, High Thermal Conduction Modules, and Liquid-Cooled Modules, as discussed by Bar-Cohen [4].

In an early attempt to improve pool boiling heat transfer by using a micro-configured surface, Miller et al. [5] found that vapor retention could be a function of the scale and geometry of the micro-configurations. They pointed out that the relation between the stability of the potential nucleation sites and the micro-configuration size and geometry required further investigation, so that the size and the site density of the cavities could be optimized for boiling heat transfer enhancement.

Slightly later a few studies have been carried out to examine the influences of the surface fabricated microstructures on the pool boiling heat transfer. These include boiling of FC-72 on micro-porous surfaces with particle coating tested by Chang and You [6] and by Vemuri and

Kim[7], adding micro-porous pin-fins and in the meantime coating particles to the surface investigated by Rainey and You [8,9], and fabricating micro-pin-fins and submicron-scale roughness on the surfaces by Honda et al. [10] and Wei et al. [11]. The study of Rainey and You [8, 9] concluded that the microporous coating can significantly enhance the boiling heat transfer performance over the pin-finned surfaces. In examining the pool boiling on the micro-pin-fin surfaces, Honda et al. [10] and Wei et al. [11] noted that the boiling curves were characterized by a very small increase in the wall superheat could cause a large increase in the heat flux. And increasing the fin height was found to provide better heat transfer in the nucleate boiling regime and result in a higher critical heat flux. Nucleation site interaction in pool boiling on an artificial surface was investigated by Zhang and Shoji [12] and by Yu et al. [13]. The hydrodynamic interaction can be also influenced by some factors, such as the liquid properties, subcooling, system pressure. The study of Yu et al. [13] concluded that the critical heat flux was dependent on the cavity density. The evaporation/boiling heat transfer regimes in the capillary wicking structures were identified and discussed by Li et al.[14] and Li and Peterson[15]. Anderson and Mudawar [16] reported that microstructures in the forms of fins, studs, grooves and vapor-trapping cavities on the boiling surface significantly shifted the boiling curve toward lower superheats while increasing the incipience excursion. Their results also suggest that the maximum boiling heat flux is a function of surface geometry and orientation but independent of the initial conditions, surface roughness, or the presence of large artificial cavities. Intending to augment boiling heat transfer, O'Connor and You [17] painted silver flakes on the boiling surface. Their experimental data show that the incipience boiling superheats are 70-85% lower and the nucleate boiling superheats are 70-80% lower than the bare surface. Besides, the critical heat flux is increased by 109%. O'Connor et al. [18] then compared two methods of generating surface microstructures, "spraying" and "painting", for pool boiling heat transfer enhancement. They noted that the incipient boiling superheat showed 33-55% reduction for the sprayed alumina and 63-85% reduction for the painted

diamond. The enhancement in the critical heat flux can be up to 47% for the sprayed alumina and 103% for the painted diamond microstructures. Chang and You [19] further studied the effects of coating different sizes of the diamond particles on the pool boiling heat transfer performances. They classified the coating thickness into two groups. For coatings thinner than 100 μm, increasing the coating thickness would generate a higher active nucleation density. But for coatings thicker than 100 μm, a further increase in the coating thickness does not always enhance the pool boiling heat transfer. They attributed this result to higher impedance for liquid-vapor exchange channels and higher thermal resistance for the thicker coating. Jung and Kwak [20] investigated the effects of submicron-scale roughness on the subcooled boiling heat transfer over a boiling surface anodized in DMF (dimethylforamide) and HF (hydrofluoric acid). Both surface treatments were found to increase the effective boiling area and served for increasing the nucleation sites and hence showed considerable enhancement in the boiling heat transfer. The critical heat flux also increases linearly. Honda and Wei [21] reviewed recent advances in enhancing boiling heat transfer from electronic components immersed in dielectric liquids through the use of surface microstructures and concluded that most of the surface microstructures were effective in decreasing the wall superheat at the boiling incipience. The nucleate boiling heat transfer also can be improved and the critical heat flux is raised. Rainey and You [22] and Rainey et al. [23] respectively studied the effects of the orientation and pressure on the pool boiling heat transfer from microporous surface. Their data show that nucleate boiling performance increases slightly for the surface inclined from 0^{o}(horizontal) to 45^{o} and then decreases for the inclination angle ranging from 90^{o} to 180^{o}. Moreover, for the plain and microporous surfaces increases in boiling performance and critical heat flux and decrease in the incipience wall superheat were noted as the pressure increased.

Chou et al. [24] arranged several grooved patterns on surfaces intending to enhance boiling heat transfer of distilled water. Their experimental data reveal that the radial grooved pattern has the best enhanced boiling heat transfer performance and the spiral or concentric

grooved pattern has poorer boiling heat transfer coefficient. The worst performance is noted for the grid or the spotted grooved pattern. All grooved patterns they investigated have better heat transfer performance than the plain surface and the denser groove is better than the sparser one for the same patterns.

Hasegawa et al. [25] covered a heat pipe with a woven screen to investigate the associated boiling characteristics and burnout phenomena. Their results disclose that the additional screen produces two opposite effects of inhibiting and enhancing the boiling heat transfer. Tsay et al. [26] explored pool boiling heat transfer enhancement by covering the boiling surface with a screen in distilled water. They found that the screen coverage could raise bubble generation frequency and enhance the boiling heat transfer. But the screen can also cover some nucleation sites and hence may retard the boiling heat transfer. They also noted that the boiling heat transfer became poorer at lowering the liquid level. They concluded that covering the heated surface with a screen could augment the pool boiling heat transfer if the mesh size was comparable with the bubble departure diameter. In boiling of methanol and HFE-7100, Liu et al. [27] pointed out that placing a fine mesh layer on the boiling surface enhanced nucleate boiling heat transfer at low wall superheat (ΔT_{sat}<10K) but an opposite trend resulted at a high superheat (ΔT_{sat}>10K). They also reported that the heat transfer in nucleate boiling always became worse with a coarse mesh on the boiling surface when compared with that on a smooth surface. Moreover, Franco et al. [28] used dielectric refrigerant R141b to investigate enhancement in the boiling heat transfer performance by covering the heated surface with wire meshes. The boiling heat transfer coefficient was noted to increase significantly, especially at relatively low heat fluxes. They also found that the wire mesh coverage on the heating surface resulted in slower transition to steady film boiling. In studying the effects of the wall superheat and the mesh layer covering on boiling heat transfer, Kurihara and Myers [29] tested several working fluids including water, acetone, n-hexane, carbon tetrachloride, and carbon disulfide. They found that active nucleation sites on the

heating plate increased due to the mesh covering and the boiling heat transfer coefficient was proportional to the one-third power of the bubble column numbers at high numbers.

Shi et al. [30] investigated pool boiling heat transfer in liquid saturated particle bed and fluidized bed of distilled water. The tests were conducted for glass beads, steel ball, find sand and Al_2O_3 particles. They showed that boiling heat transfer could be enhanced greatly by adding the solid particles into the liquid whether in the fixed or fluidized particle bed. The boiling heat transfer enhancement is closely related to the particle size (d_p=0.5, 1.0 and 2.0 mm), initial bed depth (H_p=3.0, 6.5, 9.5 and 13.4 mm) and heat flux applied. The best heat transfer enhancement is 120% for the particle diameter d_p=1.0 mm and bed height H_p=9.5 mm. A similar study was conducted by Matijevic et al. [31] using lead spheres to cover a heating surface. The spheres were packed as closely as possible into a single layer. They noted that boiling heat transfer from the heating surface to water could be enhanced substantially by the metallic spheres (d=3.0, 3.5, 3.6, 4.0 and 4.5 mm), and the smaller spheres resulted in a better enhancement of boiling heat transfer.

Heat transfer enhancement by employing nanofluids has become very popular recently. In nanofluids a very large number of nano particles (diameters smaller than 100 nm) are added into a working fluid which is considered to significantly increase thermal conductivity of the fluid. Wen and Ding [32] reported an enhancement of boiling heat transfer coefficient for about 40% with alumina water based nanofluids. On the other hand, by using the same nanoparticles in the same fluid, Bang and Chang [33] found that the boiling heat transfer coefficient deteriorated for about 20% when the nanoparticles are added.

Some active techniques to enhance boiling heat transfer were also proposed in the literature. Jeong and Kwon [34] found that the CHF augmentation in pool boiling of water due to ultrasonic vibration was closely related to its effects on the process of bubble generation and its departure. They noted that the rate of increase in CHF for downward facing surface ranged from 87~126% as the water subcooling varied from 5 to 40℃. Cipriani et al. [35] imposed

electric field on pool boiling of FC-72 over a heated platinum wire (d=0.1 and 0.2 mm)and found that the boiling heat transfer was strongly influenced by the presence of the electric field at a low wire superheat. An increase of the boiling heat transfer coefficient up to 400% was encountered with the maximum applied voltage. But it is almost unaffected by electrical force at high wire superheat. Through heated surface vibration, Navruzov et al. [36] demonstrated that boiling heat transfer of ethanol could be substantially enhanced at low imposed heat flux. The amplitude of the surface vibration is found to be a governing parameter for heat transfer enhancement at low-frequency vibrations. Besides, the vibration of the heat transfer surface significantly alters the heat transfer process both in subcooled boiling and in free convection. The single-phase heat transfer curves are 70-80% above the basic curve at increasing heat loads.

1.3 Objective of Present Study

The above literature review clearly reveals that considerable works have been carried out in the past to investigate the enhancement in the pool boiling heat transfer over a surface by passive methods through fabricating surface microstructures such as roughness and micro-pin-fins and by covering the surface with mesh screens and particle coating. All these microstructures are fixed firmly onto the boiling surface. Besides, some effective active heat transfer augmentation methods such as vibrating or rotating heating surface and/or fluid and applying electric field to vibrate a heating surface have been suggested. In an earlier experimental study, Wei [2] from our laboratory showed that placing small copper and stainless steel particles on a heated plate could result in a great increase in the FC-72 pool boiling heat transfer over the plate at low and medium wall superheats. But at high wall superheat the boiling heat transfer is impeded by the presence of the metallic particles on the plate to a certain degree. In this continuing study, we intend to explore the possibility of enhancing the pool boiling heat transfer of FC-72 over a wider range of the wall superheat by placing much lighter ceramic particles on the plate. Besides, we expect the retarding boiling

heat transfer at high wall superheat can be improved by placing the ceramic particles. We emphasize that the method proposed here is passive in nature. However, it behaves like an active heat transfer enhancement method.

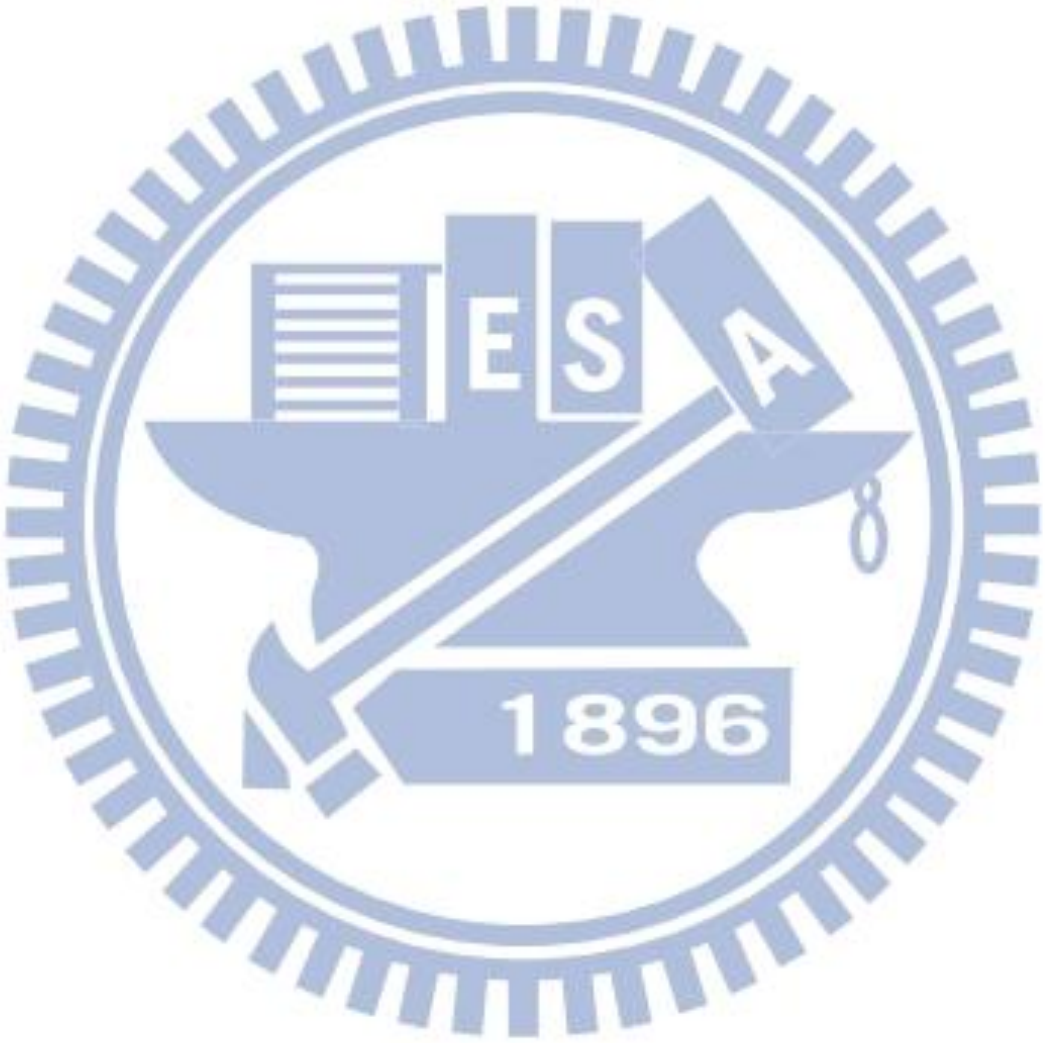

CHAPTER 2

EXPERIMENTAL APPARATUS AND PROCEDURES

A schematic arrangement of the experimental apparatus for the present investigation of the pool boiling heat transfer enhancement by movable ceramic particles driven by the boiling flow is similar to that employed in the previous study [2] and is shown in Fig. 2.1. The experimental system includes a main test chamber, a test heater assembly, and other auxiliary parts such as a D.C. power supply, a data acquisition unit and a high-speed photographic unit. The working fluid, FC-72, is a highly wetting dielectric fluorocarbon liquid produced by 3M Industrial Chemical Products Division, which has been considered as a good candidate fluid for liquid immersion cooling applications. It is chemically stable, dielectric, and has a relatively low boiling point (T_{sat}=56°C at atmospheric pressure). Some thermophysical properties of FC-72 are given in Table 2.1.

2.1 Main Test Chamber

The main test chamber is a hermetic stainless steel pressure vessel of 205 mm in height and 216 mm in diameter. An internal water condenser is installed inside the chamber and connects with a thermostat (LAUDA RK20) to maintain the bulk temperature of the working fluid in the chamber at the preset level. The maximum cooling power of the thermostat is 180W (at 20°C). We further use an external temperature controller (FENWAL MYSPEC Digital Temperature Controller) to control the bulk temperature of FC-72 liquid in the test chamber with an accuracy of ± 0.1°C. Besides, a cartridge heater is located near the bottom of the test chamber to provide additional heating during the degassing process. In order to prevent the heat

loss from the vessel to the ambient, a superlon layer of 10-mm thick is wrapped around the chamber. Moreover, a pressure transducer with an operating range of 0-200 kPa is located at the gate valve to measure the pressure of the work fluid. Meanwhile, the working fluid temperature is measured by two resistance temperature detectors (RTDs) located at the gate valve and at a selected location 5 cm above the bottom surface of the chamber with a calibrated accuracy of ± 0.1°C. An auxiliary tank of 10-liter liquid FC-72 is placed right above the test vessel and it is only used for subcooled pool boiling experiment to prevent regassing of the working fluid after degassing. A pressure transducer and a RTD are placed in the auxiliary tank to measure the internal gas pressure and liquid temperature. In addition, a test heater assembly is mounted to a stainless steel shelf to fix the PEEK (Polyether Ether Ketone) substrate. The working fluid is maintained at approximately 80 mm above the heated surface in the experiment.

2.2 Test Heater Assembly

A schematic of the test heater assembly is shown in Fig. 2.2. The assembly consists mainly of a film heater and it is adhered to the lower surface of a square copper plate by epoxy Omegabond 200. The plate is 10-mm thick with 30x30 mm^2 in surface area. The heater supplies the required power input to the copper plate. The copper plate is flush mounted onto a much larger PEEK block. Liquid FC-72 boils on the upper surface of the copper plate. More specifically, the copper plate is heated by D.C. current delivered from a D.C. power supply to the film heater. Besides, three calibrated copper-constantan thermocouples (T-type) with a calibrated accuracy of $\pm$ 0.2°C are installed at selected locations in the copper plate right below the boiling surface. They are used for the control and determination of the boiling surface

temperature. The detailed locations of the thermocouples installed in the copper plate are shown in Fig. 2.3. Note that the whole copper plate is inserted into a PEEK block which serves as a heat insulator ($k_T \approx 0.25 \mathrm{W/m \cdot K}$), intending to reduce the heat loss from the lateral and bottom surfaces of the plate to the ambient. Besides, the locations of thermocouples in the PEEK block are shown in Fig. 2.4.

2.3 Confinement of Particles and Experimental Parameters

Solid particles made from the same material and of uniform size are placed freely on the upper surface of the copper plate, as schematically shown in Fig. 2.5. In order to insure that the particles would not be blown away by the vigorous motion of the bubbles, we install an acryl fence of 2-cm high and 1-cm thick around the edges of the heating copper plate. In the present study tests will be conducted for zirconia and silicon nitride particles. The densities of zirconia and silicon nitride are measured before the experiment with $\rho_{ZrO_2} = 5948\, kg/m^3$ and $\rho_{Si_3N_4} = 3325\ kg/m^3$. These two sorts of ceramic particles are chosen here because the zirconia and silicon nitride have higher densities than liquid FC-72. But they are lighter than the copper and stainless steel particles tested by Wei [2]. Besides, the chosen particles should not be too small so that they float in the liquid above the plate and do not contact the heating surface. Moreover, they should not be too large and cannot be moved by the boiling flow. Here, the particle diameter is selected to be 1.0 and 1.6 mm for the zirconia particles, and 1.6 and 2.0 mm for silicon nitride particles. The chosen particle size and number for the cases tested here are summarized in Table 2.2. The measured data expressed in terms of boiling curves and boiling heat transfer coefficients will be compared with that of a bare heating surface.

2.4 DC Power Supply

The power generated in the film heater in the test heater assembly is provided by a programmable D.C. power supply (Gpc 3030D). It offers a maximum D.C. power of 180W for an output voltage of 60V and an output current of 3A. The power input to the copper block is transmitted through a GPIB interface to a personal computer. In order to measure the D.C. current, a precision ammeter (KYORITSU A.C./D.C. DIGITAL CLAMP METER) is arranged in series connection with the electric circuit. Besides, a YOKOGAWA data recorder is used to measure the voltage drop across the test heater assembly. All the voltage, current and power measurement devices are calibrated by a YOKOGAWA WT200 power meter according to the Center of Measurement Standards in Industrial Technology Research Institute of Taiwan.

2.5 Data Acquisition

A 20-channel YOKOGAWA data recorder (MX-100) combined with a personal computer is used to acquire and process the data from various transducers. All signals detected from the T-type thermocouples, RTDs, pressure transducer, ammeter, data recorders and power meter are all collected and converted by the internal calibration equations in the computer during the data acquisition.

2.6 Optical Measurement Technique

A high-speed camera along with a microscope is installed in front of the observation window to observe the boiling activity in the flow. The photographic apparatus consists mainly of a high speed digital video camera (IDT High-speed CMOS Camera), a micro-lens (Optem Zoom 16), and a three-dimensional positioning

mechanism. The high-speed motion analyzer can take photographs up to 143,307 frames/sec. In the present experiment the recording rate is 1000 frames/sec. After the experimental system reaches a statistical state, we start capturing the images of the particles and bubbles in the boiling flow. Besides, we store and display the images in the personal computer through an image-capturing software.

2.7 Experimental Procedures

The boiling surface is polished by fine sand paper (Number 3000, 2000 and 1000) and cleaned by ethyl alcohol before each experimental run. In each test, we place the chosen ceramic particles on the heated plate. Besides, we remove non-condensable gases existing in the empty test chamber by running a vacuum pump for about 15 minutes and then fill the FC-72 liquid into the chamber until the liquid level is higher than the heating plate for about 8 cm. Next, the FC-72 liquid in the test chamber is heated to the saturation state which is detected and maintained by a digital temperature controller. Moreover, the FC-72 liquid is boiled vigorously for 1 hour to further remove the dissolved non-condensable gases in it. After the working fluid pressure and temperature stabilize to one atmosphere and at the saturation state, we turn on the test heater. The imposed heat flux on the boiling surface is adjusted by controlling the electric current delivered to the heater from the D.C. power supply. Upon reaching the statistical state, we begin collecting the required heat transfer data and visualizing the boiling activity. Effects of the particle material, size and number density on the possible heat transfer enhancement are investigated in the experiment.

Table 2.1 Thermophysical properties of FC-72.

Properties at 25°C	**FC-72**
Appearance	Clear, colorless
Average Molecular Weight	338
Boiling Point (1atm)	56°C
Pour Point (1atm)	-90°C
Estimated Critical Temperature	449K
Estimated Critical Pressure	1.83×10^{6} Pa
Vapor Pressure	3.09×10^{4} Pa
Latent Heat of Vaporization h_{fg} (at normal boiling point)	88 J/g
Liquid Density ρ_{ℓ}	1680 kg/m^3
Absolute Viscosity μ	6.4×10^{-3} poises ; 6.4×10^{-4} kg/m·s
Kinematic Viscosity ν	3.8×10^{-3} stokes ; 3.8×10^{-7} m^2/ s
Liquid Specific Heat c_p	1100 J/kg·°C
Liquid Thermal Conductivity k	0.057 W/m·°C
Coefficient of Expansion β	0.00156 /°C
Surface Tension σ	10 dynes/cm ; 10^{-2} N/m

Table 2.2 Cases covered in present study

Particles	N_p	Particles	N_p
Zirconia (d_p=1.0 mm)	100	Silicon nitride (d_p=1.6 mm)	100
	300		200
	500		300
	700		400
	900		500
	1200		600
	1400		700
	1600		
	1800		
Zirconia (d_p=1.6 mm)	100	Silicon nitride (d_p=2.0 mm)	100
	200		200
	300		300
	400		400
	500		500
	600		
	700		

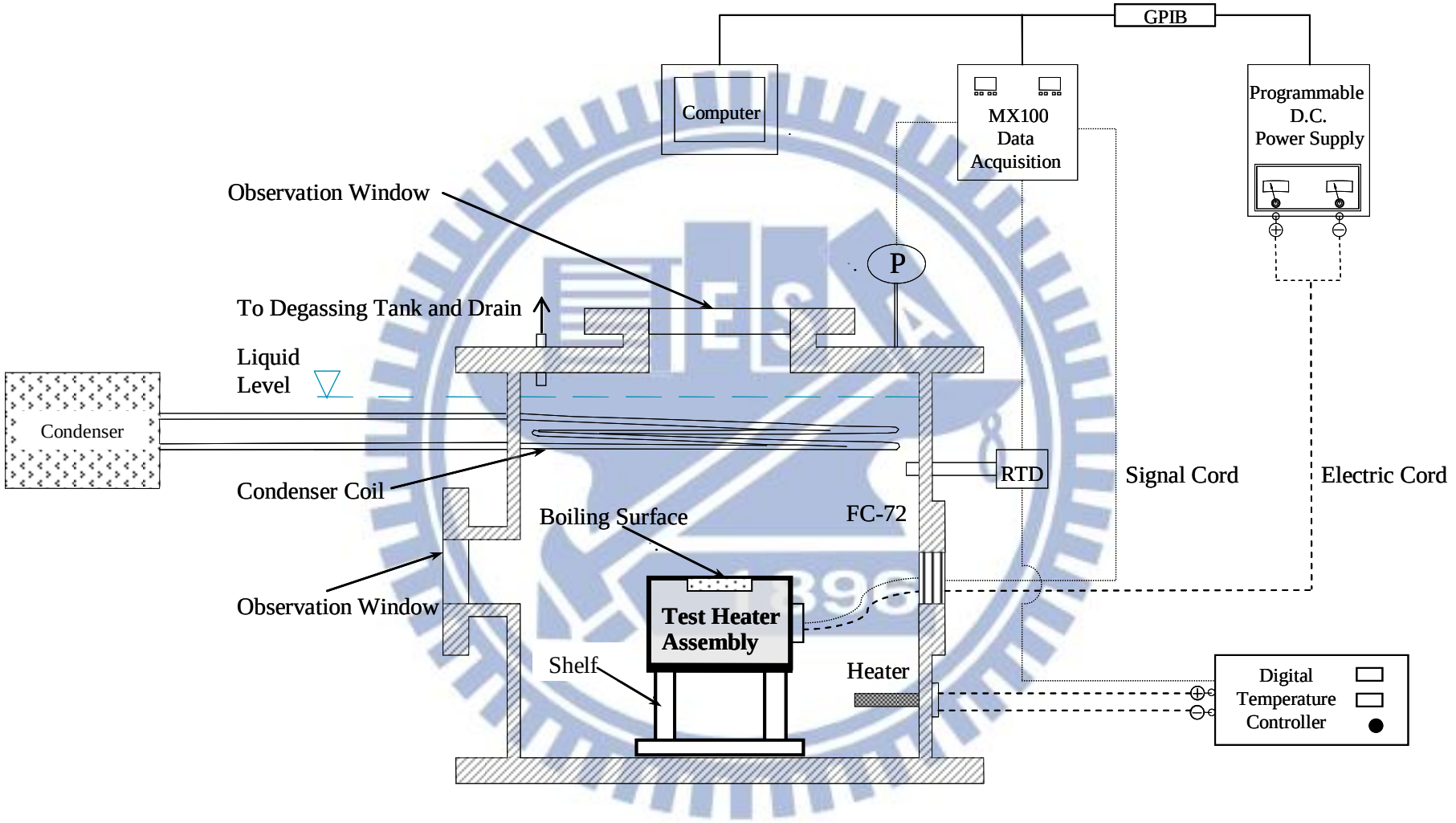

Fig. 2.1 Schematic diagram of the test apparatus.

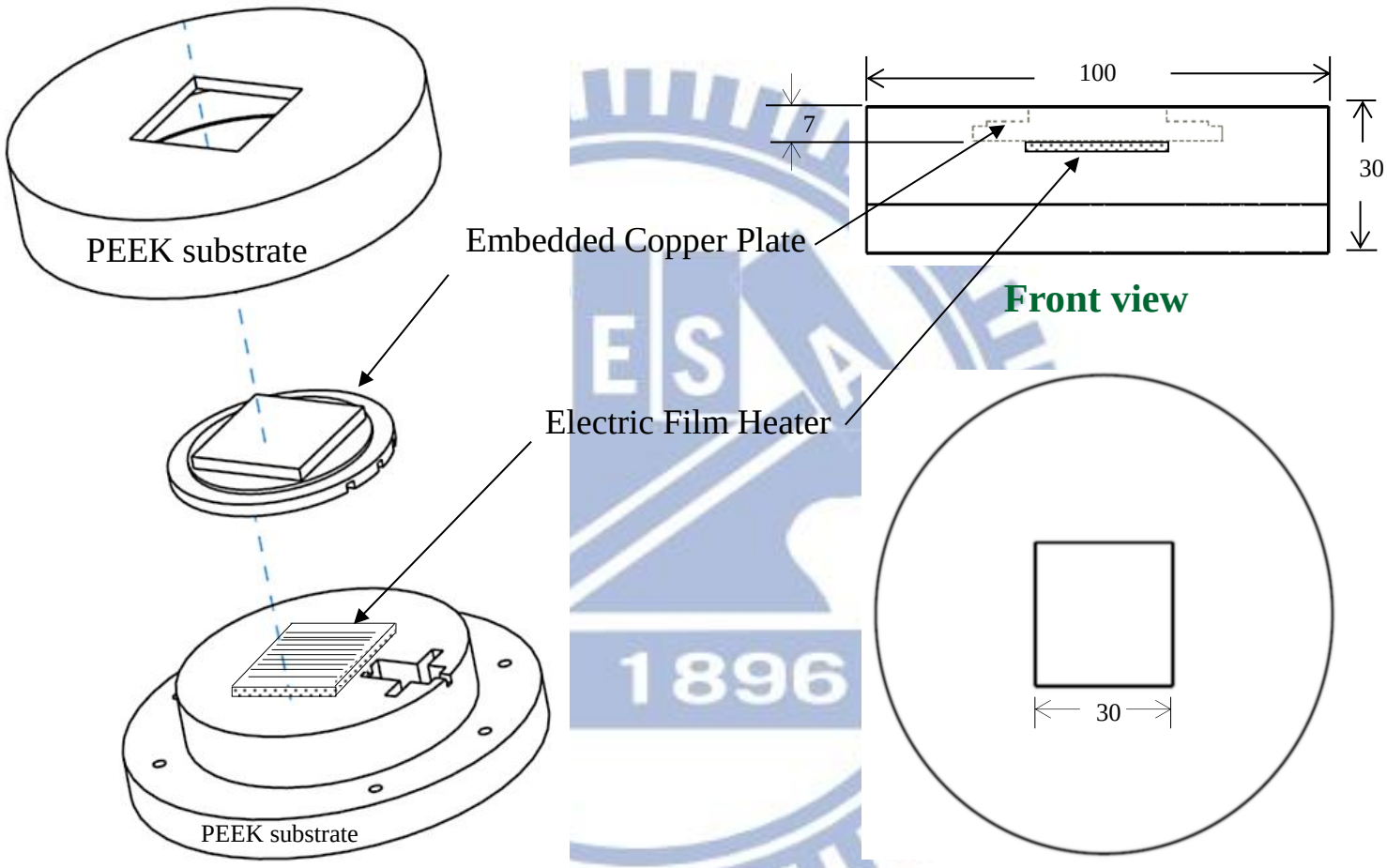

Fig. 2.2 Schematic diagram of the test heater assembly (not to scale).

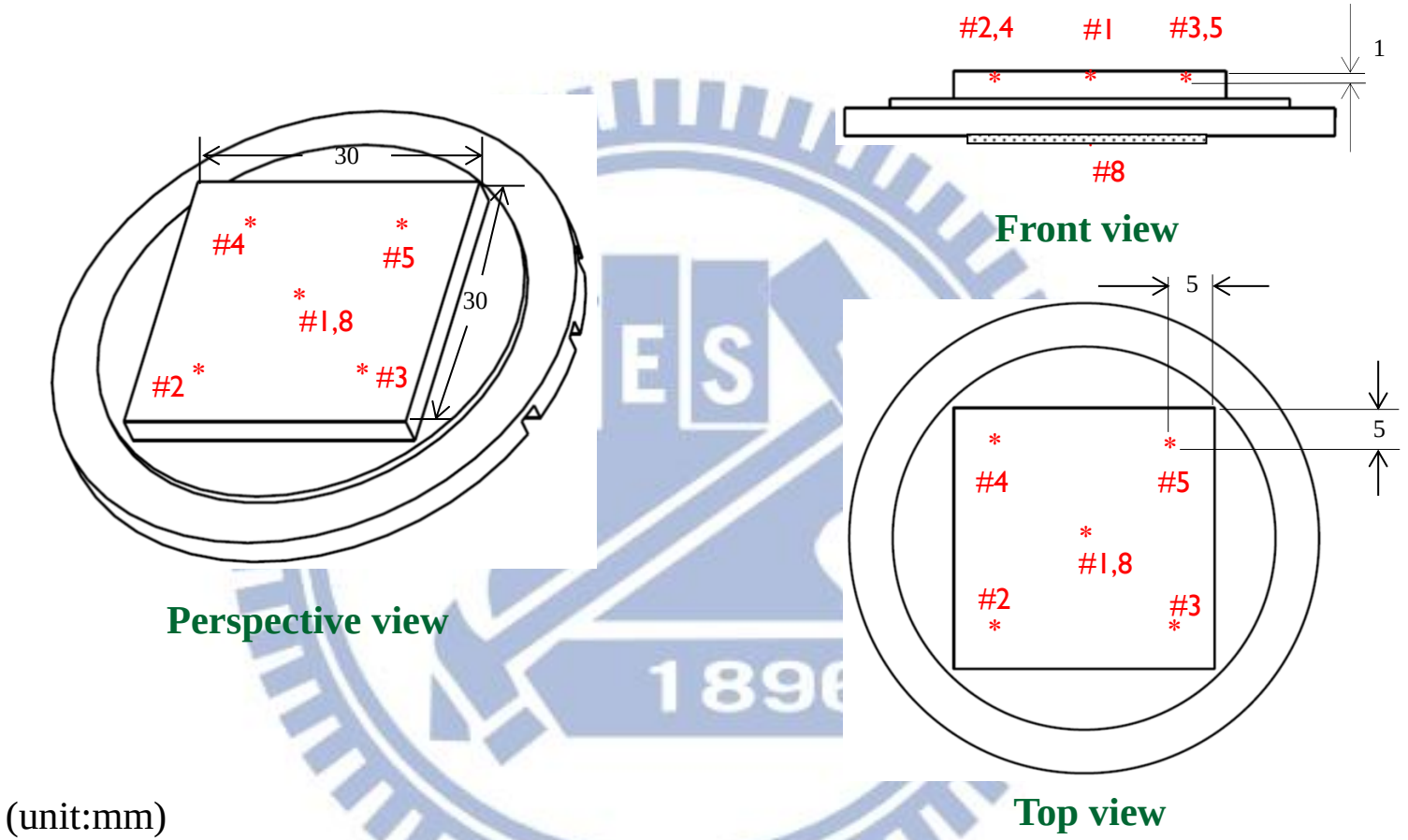

Fig. 2.3 Locations of three thermocouples in the copper plate and one thermocouple below the heater (not to scale).

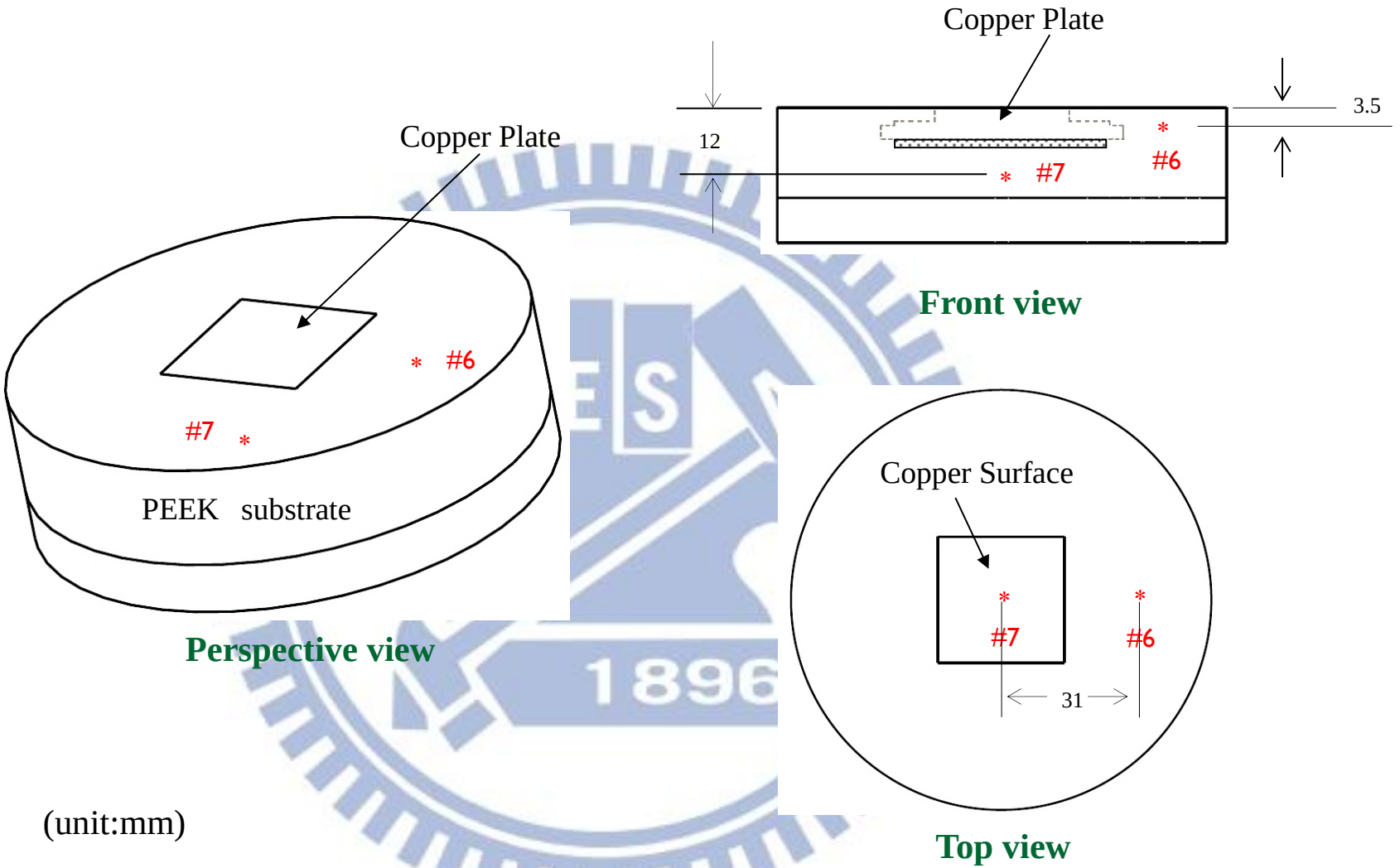

Fig. 2.4 Locations of two thermocouples in the PEEK block (not to scale).

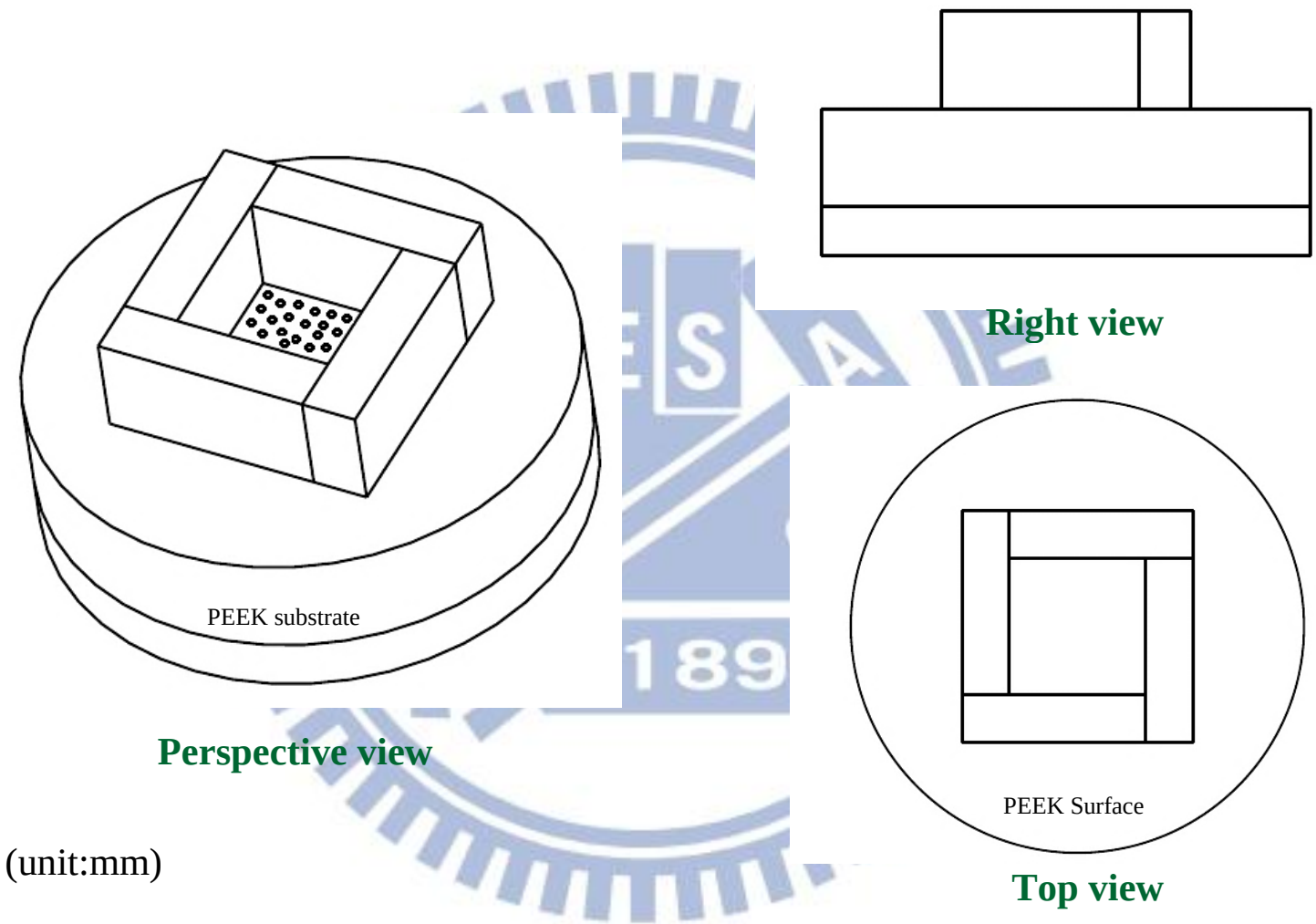

Fig. 2.5 Schematic diagram showing movable particles on heating surface with acryl rectangular enclosure (not to scale).

CHAPTER 3

DATA REDUCTION

3.1 Boiling Heat Transfer Coefficient

The space-average natural convection and boiling heat transfer coefficients over the upper surface of the heated square copper plate when the flow is at a statistical state are both defined as

$$h = {}^{q_n}/_{\Delta T_w} \tag{3.1}$$

where q_n is the net heat flux imposed on the upper surface and $\triangle T_w$ is the wall superheat defined as the difference between the average heated surface temperature and the saturated temperature of FC-72. The average heated surface temperature T_w is estimated from the measured average temperature from the thermocouples installed at different locations near the upper surface of the copper plate according to the steady-state one-dimensional conduction heat transfer. Specifically,

$$T_w = T_{Cu} - \left(q_n \times \frac{\delta}{k_{Cu}} \right) \tag{3.2}$$

where

T_{Cu} = the average measured temperature from the thermocouples (°C)

k_{Cu} = the thermal conductivity of copper (W/m·K)

δ = the vertical distance between the thermocouple tips and the upper surface of the copper plate (m)

The total power input Q_t to the copper plate can be obtained from the measured voltage drop across the film heater in the test heater assembly and the current passing through it,

$$Q_t = I \cdot V \tag{3.3}$$

where

Q_t = total power input to the upper surface of the copper plate (W)

I = electric current passing through the film heater (Amp.)

V = voltage drop across the film heater (Volts)

The substrate of the test section is made from PEEK, which have a much lower thermal conductivity ($k_T \approx 0.25 \mathrm{W/m \cdot K}$) than the copper ($k \approx 386 \mathrm{W/m \cdot K}$). In evaluating total heat loss from the heater assembly, we focus on heat transfer from the heater and copper plate surface to the PEEK. Figures 2.3 and 2.4 are the schematic diagrams of the thermocouples buried in the copper plate and PEEK block. The heat dissipation model used to estimate the heat loss is shown in Fig. 3.1, and the total heat loss can be estimated as follows:

$$\mathrm{Q_{loss}} = \mathrm{k_p} \cdot \frac{(\mathrm{T_8}-\mathrm{T_7})}{\mathrm{L_1}} \cdot \mathrm{A_1} + 4 \cdot \mathrm{k_p} \cdot \frac{(\mathrm{T_{Cu}}-\mathrm{T_6})}{\mathrm{L_2}} \cdot \mathrm{A_2} + \frac{2\pi \cdot \mathrm{k_p} \cdot \mathrm{L_3} \cdot (\mathrm{T_{Cu}}-\mathrm{T_6})}{\ln(\frac{\mathrm{r_6}}{\mathrm{r_{Cu,2}}})} + \frac{2\pi \cdot \mathrm{k_p} \cdot \mathrm{L_4} \cdot (\mathrm{T_{Cu}}-\mathrm{T_6})}{\ln(\frac{\mathrm{r_6}}{\mathrm{r_{Cu,3}}})} + \mathrm{k_p} \cdot \frac{(\mathrm{T_{Cu}}-\mathrm{T'_5})}{\mathrm{L_5}} \cdot \mathrm{A_5} + \mathrm{k_p} \cdot \frac{(\mathrm{T_{Cu}}-\mathrm{T'_6})}{\mathrm{L_6}} \cdot \mathrm{A_6} \tag{3.4}$$

where

T_6, T_7, T_8: the average measured temperatures at the measured locations inside the PEEK insulator, as schematically shown in Figs. 2.3 & 2.4

L_1, L_2, L_3, L_4, L_5, L_6: shortest distances between locations No.1~No.6 and the film heater or copper plate (m)

A_1, A_2, A_3, A_4, A_5, A_6: bottom and lateral surface areas of the copper plate

T'_5, T'_6: these two temperatures are calculated by using interpolation method based on T_6, as schematically shown in Fig. 3.2

Finally, the net imposed input heat flux to the upper surface of copper plate can be evaluated from the relation

$$q_n = \frac{Q_t - Q_{loss}}{A_{Cu}} \tag{3.5}$$

where A_{Cu} is the area of the upper surface of the copper plate.

3.2 Uncertainty Analysis

An uncertainty analysis is carried out here to estimate the uncertainty levels in the experiment. Kline and McClintock [37] proposed a formula for evaluating the uncertainty in the result F as a function of independent variables, $X_1, X_2, X_3 \cdots\cdots\cdots X_n$,

$$F=F\ (X_1, X_2, X_3 \cdots\cdots\cdots X_n) \tag{3.6}$$

The absolute uncertainty of F is expressed as

$$\delta F = \left\{ \left[\left(\frac{\partial F}{\partial X_1} \right) \delta X_1 \right]^2 + \left[\left(\frac{\partial F}{\partial X_2} \right) \delta X_2 \right]^2 + \left[\left(\frac{\partial F}{\partial X_3} \right) \delta X_3 \right]^2 + \cdots + \left[\left(\frac{\partial F}{\partial X_n} \right) \delta X_n \right]^2 \right\}^{\frac{1}{2}} \tag{3.7}$$

and the relative uncertainty of F is

$$\frac{\delta F}{F} = \left\{ \left[\left(\frac{\partial \ell nF}{\partial \ell nX_1} \right) \left(\frac{\delta X_1}{X_1} \right) \right]^2 + \left[\left(\frac{\partial \ell nF}{\partial \ell nX_2} \right) \left(\frac{\delta X_2}{X_2} \right) \right]^2 + \left[\left(\frac{\partial \ell nF}{\partial \ell nX_3} \right) \left(\frac{\delta X_3}{X_3} \right) \right]^2 + \cdots + \left[\left(\frac{\partial \ell nF}{\partial \ell nX_n} \right) \left(\frac{\delta X_n}{X_n} \right) \right]^2 \right\}^{\frac{1}{2}} \tag{3.8}$$

If $F = X_1^a X_2^b X_3^c \ldots\ldots$, then the relative uncertainty is

$$\frac{\delta F}{F} = \left\{ \left[a \left(\frac{\delta X_1}{X_1} \right) \right]^2 + \left[b \left(\frac{\delta X_2}{X_2} \right) \right]^2 + \left[c \left(\frac{\delta X_3}{X_3} \right) \right]^2 + \cdots\cdots \right\}^{\frac{1}{2}} \tag{3.9}$$

where $\frac{\partial F}{\partial X_i}$ and ∂X_i are, respectively, the sensitivity coefficient and uncertainty level associated with the variable X_i. The values of the uncertainty intervals ∂X_i are

obtained by a root-mean-square combination of the precision uncertainty of the instruments and the unsteadiness uncertainty, as recommended by Moffat [38]. The choice of the variable X_i to be included in the calculation of the total uncertainty level of the result F depends on the purpose of the analysis.

The uncertainties of the parameters in the present study are calculated as follows:

(1) Uncertainty of temperature difference, $\Delta T_w = T_w - T_{sat}$

$$\frac{\delta(T_w - T_{sat})}{(T_w - T_{sat})} = \left\{ \left[\left(\frac{\partial \ell n(T_w - T_{sat})}{\partial \ell n T_w} \right) \left(\frac{\delta T_w}{T_w} \right) \right]^2 + \left[\left(\frac{\partial \ell n(T_w - T_{sat})}{\partial \ell n T_{sat}} \right) \left(\frac{\delta T_{sat}}{T_{sat}} \right) \right]^2 \right\}^{\frac{1}{2}}$$

$$= \left\{ \left[\left(\frac{T_w}{T_w - T_{sat}} \right) \left(\frac{\delta T_w}{T_w} \right) \right]^2 + \left[\left(\frac{T_{sat}}{T_w - T_{sat}} \right) \left(\frac{\delta T_{sat}}{T_{sat}} \right) \right]^2 \right\}^{\frac{1}{2}}$$

$$= \left\{ \left[\frac{\delta T_w}{T_w - T_{sat}} \right]^2 + \left[\frac{\delta T_{sat}}{T_w - T_{sat}} \right]^2 \right\}^{\frac{1}{2}} \tag{3.10}$$

(2) Uncertainty of total power input, Q_t

$$Q_t = I \cdot V \tag{3.3}$$

and $$\frac{\delta Q_t}{Q_t} = \left[\left(\frac{\delta I}{I} \right)^2 + \left(\frac{\delta V}{V} \right)^2 \right]^{\frac{1}{2}} \tag{3.11}$$

(3) Uncertainty of net wall heat flux, q_n

$$q_n = \frac{Q_t - Q_{loss}}{A_{Cu}} \tag{3.5}$$

and

$$\frac{\delta q_n}{q_n}=\left\{\left[\left(\frac{\partial \ell n q_n}{\partial \ell n A_{Cu}}\right)\left(\frac{\delta A_{Cu}}{A_{Cu}}\right)\right]^2+\left[\left(\frac{\partial \ell n q_n}{\partial \ell n Q_t}\right)\left(\frac{\delta Q_t}{Q_t}\right)\right]^2+\left[\left(\frac{\partial \ell n q_n}{\partial \ell n Q_{loss}}\right)\left(\frac{\delta Q_{loss}}{Q_{loss}}\right)\right]^2\right\}^{\frac{1}{2}}$$

$$=\left\{\left[1\cdot\left(\frac{\delta A_{Cu}}{A_{Cu}}\right)\right]^2+\left[\left(\frac{Q_t}{Q_t-Q_{loss}}\right)\left(\frac{\delta Q_t}{Q_t}\right)\right]^2+\left[\left(\frac{Q_{loss}}{Q_t-Q_{loss}}\right)\left(\frac{\delta Q_{loss}}{Q_{loss}}\right)\right]^2\right\}^{\frac{1}{2}}$$

$$=\left\{\left[\frac{\delta A_{Cu}}{A_{Cu}}\right]^2+\left[\frac{\delta Q_t}{Q_t-Q_{loss}}\right]^2+\left[\frac{\delta Q_{loss}}{Q_t-Q_{loss}}\right]^2\right\}^{\frac{1}{2}} \tag{3.12}$$

Where

$$Q_{loss}=k_p\cdot\frac{(T_8-T_7)}{L_1}\cdot A_1+4\cdot k_p\cdot\frac{(T_{Cu}-T_6)}{L_2}\cdot A_2+\frac{2\pi\cdot k_p\cdot L_3\cdot(T_{Cu}-T_6)}{\ln(\frac{r_6}{r_{Cu,2}})}+\frac{2\pi\cdot k_p\cdot L_4\cdot(T_{Cu}-T_6)}{\ln(\frac{r_6}{r_{Cu,3}})}+k_p\cdot\frac{(T_{Cu}-T'_5)}{L_5}\cdot A_5+k_p\cdot\frac{(T_{Cu}-T'_6)}{L_6}\cdot A_6 \tag{3.4}$$

(4) Uncertainty of space-average heat transfer coefficient, *h*

$$h=q_n/\Delta T_{sat} \tag{3.1}$$

and

$$\frac{\delta h}{h}=\left\{\left[\left(\frac{\partial \ell n h}{\partial \ell n q_n}\right)\left(\frac{\delta q_n}{q_n}\right)\right]^2+\left[\left(\frac{\partial \ell n h}{\partial \ell n(T_w-T_{sat})}\right)\left(\frac{\delta(T_w-T_{sat})}{T_w-T_{sat}}\right)\right]^2\right\}^{\frac{1}{2}}$$

$$=\left\{\left[1\cdot\left(\frac{\delta q_n}{q_n}\right)\right]^2+\left[1\cdot\left(\frac{\delta T_w-T_{sat}}{T_w-T_{sat}}\right)\right]^2\right\}^{\frac{1}{2}}$$

$$=\left\{\left[\frac{\delta q_n}{q_n}\right]^2+\left[\frac{\delta T_w-T_{sat}}{T_w-T_{sat}}\right]^2\right\}^{\frac{1}{2}} \tag{3.13}$$

A summary of the results from the present uncertainty analysis is given in Table 3.1.

Table 3.1 Summary of the results from the uncertainty analysis.

Parameter	**Uncertainty**
Geometry	
Length & thickness (%)	± 0.167%
Area (%)	± 0.334%
Particle diameter (%)	± 10.0%
Particle density(%)	± 13.4%
Parameter measurement	
Temperature, T (°C)	± 0.05
Temperature difference, ΔT_w (°C)	± 0.36
System pressure, P (kPa)	± 0.5
Boiling heat transfer on the copper flat plate	
Total power input, Q_t (%)	± 5.9%
Imposed net heat flux, q_n (%)	± 8.3%
Heat transfer coefficient, h (%)	± 11.0%

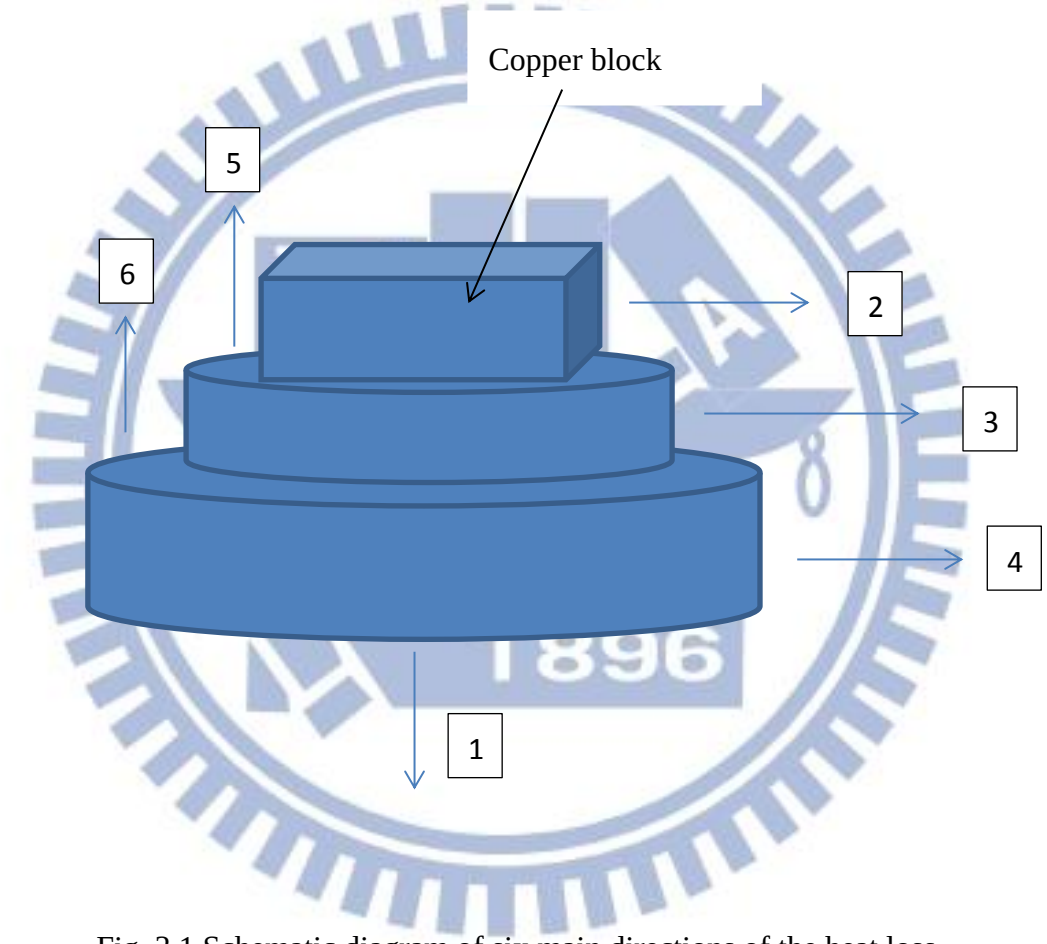

Fig. 3.1 Schematic diagram of six main directions of the heat loss.

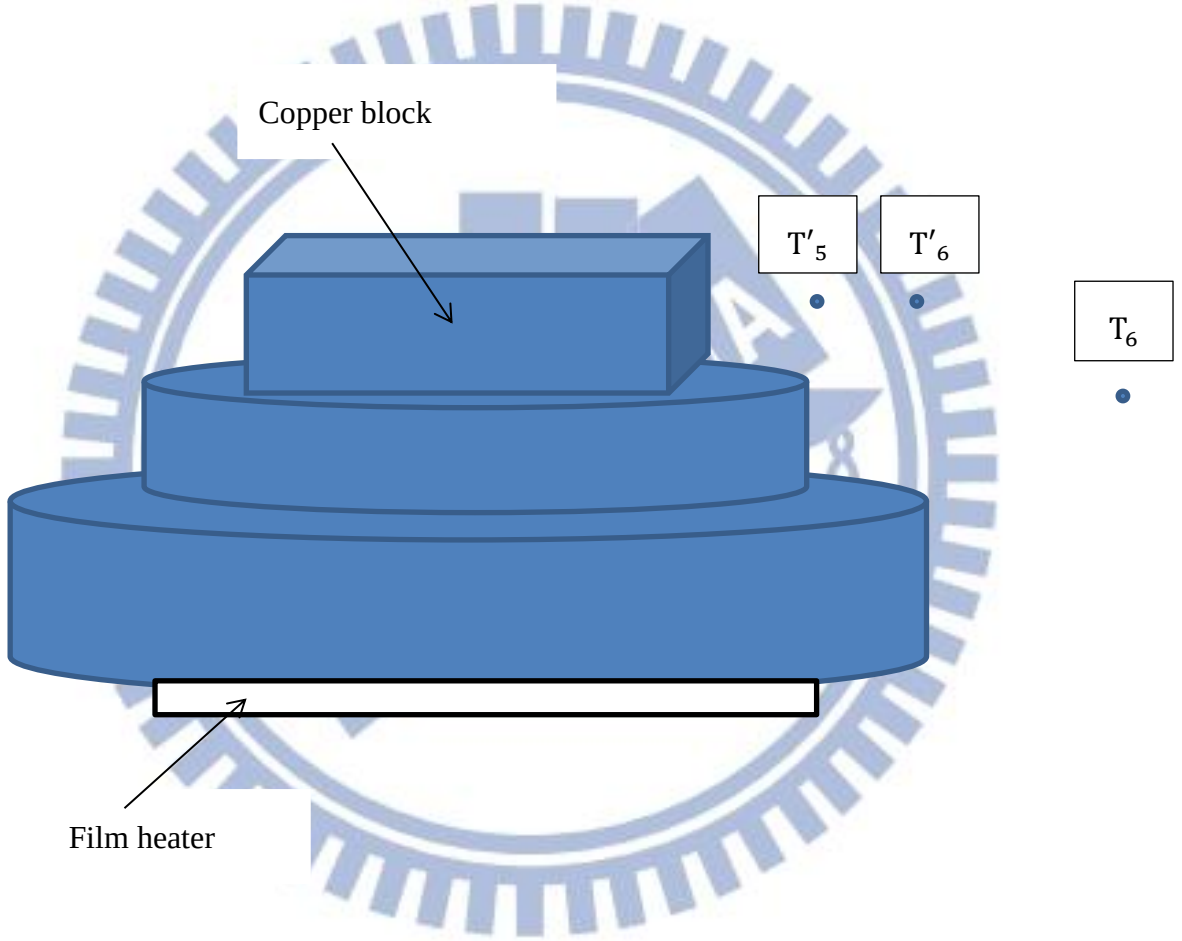

Fig. 3.2 Schematic diagram showing locations for T'$_5$ and T'$_6$

CHAPTER 4

POSSIBLE POOL BOILING HEAT TRANSFER ENHANCEMENT OF FC-72 OVER HEATED COPPER SURFACE

The experimental results to illustrate possible enhancement of saturated pool boiling heat transfer of FC-72 by placing the movable ceramic particles on the heating surface obtained in the present study are presented in this chapter. The present experiments are carried out for the zirconia particles with the diameter of the particles d_p fixed at 1.0 and 1.6 mm and the lighter silicon nitride particles with the diameter of particles fixed at 1.6 and 2.0 mm. The total number of particles N_p placed on the heated surface varied from 100 to 1800 for the zirconia particles with diameter 1.0 mm, from 100 to 700 for the both zirconia and silicon nitride particles with diameter 1.6 mm, and from 100 to 500 for the silicon nitride particles with diameter 2.0 mm. The FC-72 liquid in the test chamber is maintained at saturated liquid state corresponding to the atmospheric pressure. Note that the maximum number of particles forming a single closely packed particle layer over the boiling surface of area $3.0 \times 3.0\ cm^2$ N_{pf} is 900 for the zirconia particles with diameter 1.0 mm, 324 for the both zirconia and silicon nitride particles with diameter 1.6 mm, and 225 for the silicon nitride particles with diameter 2.0 mm. In the experiment tests are also conducted for the total particle number well exceeds N_{pf} and then many particles are on top of the other particles when the lift force from the boiling flow is not high enough to levitate the particles. The measured data are presented in terms of the boiling curves and boiling heat transfer coefficients for various diameters and numbers of the ceramic particles and for a bare heating surface. Effects of the experimental parameters on the possible boiling heat transfer enhancement by the

movable ceramic particles will be examined in detail. Selected data from the present study are presented in the following to illustrate the possible pool boiling heat transfer enhancement by the boiling flow driven ceramic particles.

4.1 Single-phase Natural Convection Heat Transfer

Before conducting the pool boiling heat transfer enhancement experiment, we first measure steady natural convection heat transfer of FC-72 liquid over the heated copper surface without the presence of any ceramic particles which prevails at low imposed heat flux, intending to verify the present experimental setup. The measured data for the natural convection heat transfer coefficient are compared with the empirical correlation of Radziemska and Lewandowski [39] in Fig. 4.1. Their correlation is

$$Nu_L=(2.1e^{-48W}+1.2)Ra_L^{0.2} \tag{4.1}$$

where w is the width of the heating plate (m). The correlation given in Eq.(4.1) is based on the data for a small horizontal plate heated from below for $10^5<Ra_L<10^8$. Note that the characteristic length L used in defining the dimensionless groups in the above equation is chosen to be the ratio of the heated surface area to its perimeter, and the Nusselt and Rayleigh numbers are respectively defined as

$$Nu_L = \frac{hL}{k_\ell} \tag{4.2}$$

and

$$Ra_L = \frac{g\beta(\Delta T_{sat})L^3}{\alpha\nu} \tag{4.3}$$

The results in Fig. 4.1 indicate that our natural convection data are in good agreement with that calculated from Eq. (4.1). Thus the experimental system established here is considered to be suitable for the present study.

4.2 Saturated Pool Boiling on Bare Copper Surface

To further verify the suitability of the present experimental system, the measured boiling curve for saturated pool boiling of liquid FC-72 on the bare heated copper plate is obtained next. These data are compared with that from Rainey and You [22] in Fig. 4.2 for pool boiling of FC-72 on a square copper plate of 5×5 cm^2 in surface area. Note that the present data are in good agreement with theirs.

4.3 Effect of Surface Aging on Boiling over Bare Copper Plate

It is well known that the change of the boiling surface properties with time, the so called "aging effect", can be significant in affecting the boiling heat transfer from a surface after the surface has been used over certain period of time. Obviously, the measured boiling heat transfer data for the cases with and without the presence of the particles on the surface can be meaningfully compared only when the surface aging effect is small. Thus tests are carried out here to investigate the aging effect of FC-72 liquid boiling on the present heated surface. The results show that the boiling curves and heat transfer coefficients measured over a time interval of 6 hours do not differ to a noticeable degree, as seen from Fig. 4.3. But a significant aging effect is found for an interval of 24 hours. Thus in the present experiment the boiling heat transfer data for the corresponding cases with and without the presence of particles on the surface are obtained within 6 hours.

4.4 Effects of Moving Zirconia Particles on Boiling Heat Transfer

Possible boiling heat transfer enhancement by the zirconia particles moving above the heated surface is then examined. Results are presented first for the FC-72 nucleate boiling heat transfer affected by the movable zirconia particles placed freely

on the heated surface by showing the measured heat transfer data for the bare surface and for the surface with zirconia particles on it for various sizes and total numbers of the particles in Figs. 4.4-4.21. The results in Figs. 4.4 and 4.5 for the small zirconia particles with the diameter d_p=1.0 mm and the particle number N_p=100 and 300 indicate that even at a small particle number the boiling heat transfer can be effectively enhanced by the zirconia particles at low wall superheat near the onset of nucleate boiling. The enhancement gets smaller at increasing wall superheat. It is also noted that the moving zirconia particles can also slightly augment in the single-phase convective heat transfer at very low wall superheat and in the fully developed nucleate boiling region at high wall superheat, unlike that for the heavier copper and stainless steel particles [2]. For these heavier particles heat transfer in the single-phase flow and high wall superheat fully-developed nucleate boiling regions is retarded by these particles.

As the total number of the zirconia particles is increased to 500 and 700, significant augmentation in the boiling heat transfer by the zirconia particles appears even at low wall superheat (Figs. 4.6 and 4.7). Besides, the boiling heat transfer is still enhanced at relatively high wall superheat especially for N_p= 500. For a further increase in the number of the zirconia particles to 900, the particles on the heated copper plate are rather crowded. Note that at this high N_p enhancement in the boiling heat transfer by the zirconia particles is even more significant at low ΔT_w (Fig. 4.8), implying strong interactions between the particles and bubbles in the boiling flow already occur at low ΔT_w at this large N_p. Apparently, substantial augmentation in the boiling heat transfer by the zirconia particles also exists at high ΔT_w. It is of interest to realize from the data given in Figs. 4.9-4.12 that even when the total number of the zirconia particles well exceeds N_{pf} for $N_p \geq 1{,}000$ the boiling heat

transfer enhancement by the zirconia particles is even more significant at both low and high ΔT_w. This suggests that the presence of a large number of ceramic particles on top of the other particles dose not lower the boiling heat transfer performance at low wall superheat. However, when the total particle number is very large at $N_p \geq 1600$ the boiling heat transfer is retarded at high ΔT_w by the particles (Figs. 4.11 and 4.12).

To be more quantitative on the boiling heat transfer affected by the small zirconia particles presented above for d_p=1.0 mm, the ratios of the single-phase and boiling heat transfer coefficients for the cases with the presence of the particles to the bare surface h_p/h are shown in Fig. 4.13 for various ΔT_w and N_p. The data given in Figs. 4.4-4.12 clearly show that the presence of the zirconia particles in the boiling flow causes a much earlier onset of nucleate boiling compared with that for a bare surface. Therefore, the results for h_p/h in Fig. 4.13 can be divided into three regions. In region 1 at very low wall superheat single-phase flow prevails and in region 3 at high wall superheat nucleate boiling dominates over the heated surface for cases with and without the presence of the particles. But in region 2 at intermediate wall superheat we have single-phase flow on the bare heated surface and nucleate boiling on the surface with presence of the particles. The data in Fig. 4.13 show that in region 1 the movable ceramic particles on the heated surface slightly enhance the single-phase convective heat transfer for most cases. The enhancement is found to increase at increasing wall superheat. In the region 2 at intermediate ΔT_w the enhancement in the heat transfer from the heated surface is very large obviously due to the earlier onset of boiling on the heated surface. While in region 3 at high wall superheat the boiling heat transfer enhancement is also very large as ΔT_w is slightly highter than that for incipient boiling. But the enhancement decays substantially at

increasing wall superheat. Note that the enhancement in the boiling heat transfer can exceed 300% for N_p ≥300. The best enhancement for these cases can be as high as 550% for N_p=1600 at ΔT_w ≈12.3K. The best enhancement usually occurs at very low ΔT_w near the onset of nucleate boiling. These data also indicate that for N_p ≥300 the enhancement in the boiling heat transfer is rather significant except at high ΔT_w.

Aside from the significant boiling heat transfer enhancement, the above results given in Figs. 4.4-4.12 also show that the presence of the zirconia particles can substantially lower the wall superheat needed for the onset of nucleate boiling for all cases (Table 4.1), as already mentioned above. It is of interest to point out that the reduction in the incipient boiling wall superheat by the movable zirconia particles is more prominent than the metallic particles when the present data are compared with that of Wei [2]. Specifically, the average reduction in the incipient boiling wall superheat by the small ZrO_2 particles is 41% but for the copper particles of the same size the reduction is only 27%. This is also beneficial in electronics cooling by employing movable ceramic particles on the boiling surface.

Next, the measured heat transfer data for the larger zirconia particles with d_p=1.6 mm are given in Figs. 4.14-4.20 for N_p ranging from 100 to 700. By and large, these results are similar to those for the smaller zirconia particles presented above. However, some noted differences do exist. Specifically, the larger particles exhibit more pronounced effects on enhancing and retarding boiling heat transfer. Besides, for the larger particles the onset of nucleate boiling occurs at a higher wall superheat (Fig. 4.1). Checking with the data for h_p/h given in Fig. 4.21 for d_p=1.6 mm indicates that boiling heat transfer coefficient can be increased up to about 300% by placing the larger zirconia particles on the boiling surface for N_p=200 at

$\Delta T_w \approx 13.5$ K. The best boiling heat transfer augmentation can be procured at $N_p = 400$. On the other hand, the reduction in the boiling heat transfer at high wall superheat is more severe for the larger particles, as evident by comparing the data in Fig. 4.21 with Fig. 4.13. Moreover, the heat transfer enhancement is poor at the intermediate wall superheat in region 2 for the larger ZrO_2 particles.

4.5 Effects of Moving Silicon Nitride Particles on Boiling Heat Transfer

Attention is then turned to examining the measured data for the silicon nitride particles, which are much lighter than the zirconia particles. The measured heat transfer data for the small silicon nitride particles with d_p=1.6 mm shown in Figs. 4.22-4.28 qualitatively resemble that for the zirconia particles given in Figs. 4.14-4.20 for the same d_p. But for the lighter silicon nitride particles, the boiling heat transfer augments over a wider range of ΔT_w with the same number of the particles placed on the heated plate. Specifically, the boiling heat transfer enhancement extends to a slightly higher wall superheat. Besides, relatively substantial boiling heat transfer augmentation has been achieved already at N_p=100 for the Si_3N_4 particles. The data in Fig. 4.29 for h_p/h show that the best boiling heat transfer enhancement can be up to 560% for the small silicon nitride particles with N_p=700 at $\Delta T_w \approx 13.2\ K$. It is also noted that the reduction in the boiling heat transfer at rather high wall superheat is much smaller for the Si_3N_4 particles. Moreover, the lighter particles cause slightly earlier onset of nucleate boiling. It is of interest to note from the data for the silicon nitride particles given in Figs. 4.22-4.28 for d_p=1.6 mm and Figs. 4.30-4.34 for d_p=2.0 mm that the resulting boiling heat transfer enhancement is slightly higher when compared with the zirconia particles shown in Figs. 4.4-4.12 for d_p=1.0 mm

and Figs. 4.14-4.20 for d_p=1.6 mm. This can be seen by comparing the data for h_p/h given in Figs. 4.29 and 4.35 for the silicon nitride particles with Figs. 4.13 and 4.21 for the zirconia particles.

4.6 Effects of Particle Material on Boiling Heat Transfer Enhancement

Here we move forward to illustrate the effects of the particle material on the boiling heat transfer enhancement by comparing the present data for the ceramic particles with that of Wei [2] for the metallic particles. The metallic particles are known to be much heavier and the metals have much higher thermal conductivity. At first, we compare the heat transfer data for the small zirconia particles with the small copper particles at the same d_p of 1.0 mm and N_p of 300 in Fig. 4.36. The results clearly show that at N_p=300 for the copper particles the boiling heat transfer enhancement is rather mild over a narrow range of the wall superheat. But for the zirconia particles the enhancement is already very significant at N_p=300 over a wider range of the wall superheat. Besides, slight reduction in the boiling heat transfer at high wall superheat appears for the copper particles. Similar trend is noted as the total number of the particles placed on the boiling surface is increased to 500 and 700 according to the data given in Figs. 4.37 and 4.38. At these higher particle numbers the boiling heat transfer retardation at high wall superheat by the copper particles is more severe. But the boiling heat transfer enhancement by the copper particles is no longer small, although it is still below the zirconia particles. This trend continues for an even higher N_p, as evident from the results shown in Fig. 4.39 for N_p=900. Moreover, we compare the data for h_p/h affected by the particle number in Fig. 4.40 for both zirconia and copper particles at d_p=1.0 mm. The results clearly indicate that the boiling heat transfer is enhanced significantly as N_p is increased from 300 to 500

for the copper particles. But the boiling heat transfer enhancement becomes gradual for a further increase of N_p to 700. However, for the zirconia particles at N_p=300 the enhancement is already rather substantial, as mentioned above. A further increase in N_p only causes a relatively mild increase in the boiling heat transfer enhancement. Obviously, we have much higher best boiling heat transfer enhancement for the zirconia particles.

Next, the effects of the particle material on the heat transfer data for the large particles with d_p=1.5 mm & 1.6 mm are illustrated in Fig. 4.41 for N_p=200 for copper, stainless steel, zirconia and silicon nitride particles. The results manifest that the movable ceramic particles on the heated surface produce a much higher boiling heat transfer enhancement over a wider range of the wall superheat. Note that the retardation of the boiling heat transfer by the metallic particles at high wall superheat is clearly seen. The retardation is more pronounced for the copper particles. At the larger particle number of 400 and 600 the data in Figs. 4.42 and 4.43 show that the boiling heat transfer retardation is more severe for the heavier particles. For the silicon nitride particles, which are lightest among the four particles, the boiling heat transfer retardation is barely seen (Figs. 4.42(d) and 4.43(d)). For the large N_p of 600 the boiling heat transfer retardation is so severe at high ΔT_w that the boiling heat transfer enhancement at low ΔT_w is somewhat overshadowed, except for the silicon nitride particles.

Finally, the effects of the particle material on the boiling heat transfer enhancement for the large particles are summarized in Fig. 4.44 by presenting the data for h_p/h for the four particles at $d_p \approx$1.5 mm. The results indicate that better boiling heat transfer enhancement can be procured by using the zirconia particles with N_p=400. By and large, the movable ceramic particles result in greater boiling heat

transfer enhancement and smaller boiling heat transfer retardation.

4.7 Interactions between Particles and Boiling Flow

To delineate the complicate effects of the movable ceramic particles on the boiling heat transfer, motions of the particles and bubbles in the boiling flow are visualized. The results from this visualization for selected cases are presented in Figs. 4.45-4.61. More specifically, photos taken from the side view of the boiling flow in a small region around the geometric center of the heated surface are shown in these figures for the zirconia and silicon nitride particles with d_p=1.6 mm and 2.0 mm at selected imposed heat fluxes. In these figures, the symbol "t=0" denotes an arbitrary time instant in the statistical state. At high heat flux and large particle number the vigorous motions of the particles and bubbles and their strong interactions are prone to overshadow each other, causing the top view photos to be rather ambiguous. Thus only the side view photos are shown here.

Our flow visualization indicates that when a low heat flux slightly higher than that required for boiling onset is imposed to the heated surface the fast growth of bubbles after their incipience on the heated surface can push the surrounding particles to move away from these original sites horizontally over a short distance for the zirconia particles. On the other hand, the lighter silicon nitride particles can move to a large degree around the heated surface by the nucleated bubbles at the low heat flux. As the particles move on the heated surface, they in turn can push the bubbles along their path to depart from the surface, resulting in earlier bubble departure. Besides, the moving particles can collide with other particles. At higher imposed heat flux more bubbles nucleate from the heated plate and the force resulting from the growth of bubbles can be very strong. Consequently, the particles can be lifted directly up by the

growing bubbles for both zirconia and silicon nitride particles. Many particles are suspended in the boiling flow and are affected by the irregular motion of the bubbles departing from the heated surface, causing the particles to move irregularly up and down, back and forth, and right and left. Later, the ceramic particles may drop back to the plate due to gravity and the surrounding bubbles and liquid can be pushed away. As the particles drop back, they drag some liquid around them towards the boiling surface through the viscous shearing effects. Moreover, collision between the particles is frequent. Furthermore, the silicon nitride particles can be pushed to the edge of the heated plate and hit the acrylic fence by the strong boiling flow. At an even higher imposed heat flux, the ceramic particles move even more violently in the flow. These mutual particle-bubble interactions in the boiling flow schematically shown in Figs. 4.62 and 4.63 get more intense at increasing heat flux, resulting in the three-phase liquid-vapor-particle flow over the heated surface to become highly turbulent and tending to enhance boiling heat transfer over the heated plate.

At a very high heat flux a relatively large number of bubbles nucleate at the heated surface and the presence of a large number of the ZrO_2 particles can impede the bubbles of certain size to grow further and hinder the bubble daparture from the heated surface. The bubbles are then trapped beneath the particles, as schematically illustrated in Fig. 4.64. Besides, the particles can reduce the inrush of the bulk liquid to the heated surface especially at large particle number. Hence, the boiling heat transfer is retarded by the particles. These heat transfer retarding effects are more severe at higher heat flux when more particles are placed on the heated plate. On the other hand, the lighter silicon nitride particles can be fully lift up and move violently by strong boiling flow at high heat flux and the particles do not obstruct the bubbles to escape from the heated surface unless at a much higher heat flux. Thus, the

enhancement in the boiling heat transfer can be extended to a higher heat flux.

It is worth to mention that even at a rather low heat flux the ceramic particles, owing to their low density, can be moved slightly by the single-phase convective flow (Fig. 4.65) and the convective heat transfer can be augmented to some degree, as already noted in the heat transfer data presented above.

4.8 Proposed Correlations

The data for h_p/h presented in Figs. 4.13, 4.21, 4.29 and 4.35 can be correlated empirically as

$$\frac{h_p}{h} = \left\{ A\left(\frac{N_p}{N_{pf}}\right)^2 + B \right\} \cdot \left[\frac{C_{pl}(\Delta T_w - \Delta T_{ONB,b})}{i_{lv}}\right]^{\left[C\left(\frac{N_p}{N_{pf}}\right)^2 + D\right]} \tag{4.4}$$

$$\mathrm{A} = \left[-1409.1864 + 712.4706\left(\frac{\rho_p}{\rho_l}\right)\right] + \left[19.3794 - 9.7934\left(\frac{\rho_p}{\rho_l}\right)\right]\left(d_p/\sqrt{\sigma/g\Delta\rho}\right)$$

$$\mathrm{B} = \left[441.07 - 222.8297\left(\frac{\rho_p}{\rho_l}\right)\right] + \left[-7.378 + 3.7272\left(\frac{\rho_p}{\rho_l}\right)\right]\left(d_p/\sqrt{\sigma/g\Delta\rho}\right)$$

$$\mathrm{C} = \left[-3.9349 + 1.7074\left(\frac{\rho_p}{\rho_l}\right)\right] + \left[0.034 - 0.0195\left(\frac{\rho_p}{\rho_l}\right)\right]\left(d_p/\sqrt{\sigma/g\Delta\rho}\right)$$

$$\mathrm{D} = \left[37.9619 - 19.1121\left(\frac{\rho_p}{\rho_l}\right)\right] + \left[-0.6406 + 0.3221\left(\frac{\rho_p}{\rho_l}\right)\right]\left(d_p/\sqrt{\sigma/g\Delta\rho}\right)$$

The present data for the boiling heat transfer coefficient for the bare surface can be expressed empirically as

$$\begin{cases} \mathrm{h} = 521.458 + 763.855 \cdot (\Delta T_w - \Delta T_{ONB}) & \text{for} \quad 0 < [\Delta T_w - \Delta T_{ONB}] < 1K \\ \mathrm{h} = 57.681 + 1207.547 \cdot (\Delta T_w - \Delta T_{ONB}) & \text{for} \quad 1K < [\Delta T_w - \Delta T_{ONB}] < 4\ K \end{cases} \tag{4.5}$$

The mean absolute error (MAE) for the above correlation for h_p/h when compared with the present data is 23.6%. For the correlation given in Eq. (4.5) for h the mean absolute error is 12.7%.

Finally, we illustrate the ranges of the experimental parameters in which the boiling heat transfer can be enhanced by placing the ceramic particles on the heated surface in Fig. 4.66. The results manifest that the lower bounds of the imposed heat flux for enhancing boiling heat transfer do not significantly vary with the ratio of the particle number placed on the plate to the maximum particle number forming a single particle layer on the plate N_p/N_{pf} and with the particle size and material. However, the lower bounds for the wall superheat with silicon nitride particles at d_p=2.0 mm decrease noticeably with N_p/N_{pf} (Fig. 4.66 (b)). The upper bounds of q and ΔT_w for enhancing boiling heat transfer, nevertheless, show nonmonotonic variations with N_p/N_{pf}, particle size and material. Note that for the silicon nitride particles the retardation of the boiling heat transfer is barely seen.

Table 4.1 Wall superheats at onset of nucleate boiling for zirconia particles

Particle diameter d_p(mm)	N_p	$(\Delta T_w)_{ONB}$ (^{O}C)	$(\Delta T_w)_{ONB}$ (^{O}C) For bare surface
1.0	100	7.0	12.3
	300	8.2	12.6
	500	7.1	12.5
	700	8.2	12.6
	900	7.4	12.8
	1200	7.4	12.7
	1400	7.2	12.5
	1600	7.4	12.3
	1800	7.2	12.5
1.6	100	9.9	13.2
	200	9.2	13.5
	300	9.4	13.3
	400	9.5	13.4
	500	8.7	12.7
	600	9.4	13.4
	700	9.1	13.4

Table 4.2 Wall superheats at onset of nucleate boiling for silicon nitride particles

Particle diameter d_p(mm)	N_p	$(\Delta T_w)_{ONB}$ (^{O}C)	$(\Delta T_w)_{ONB}$ (^{O}C) For bare surface
1.6	100	8.7	13.6
	200	9.5	12.8
	300	7.1	12.4
	400	7.3	13.2
	500	7.0	13.5
	600	7.02	13.1
	700	8.3	13.2
2.0	100	7.7	13.0
	200	7.1	12.6
	300	8.3	13.2
	400	8.7	13.4
	500	8.4	13.7

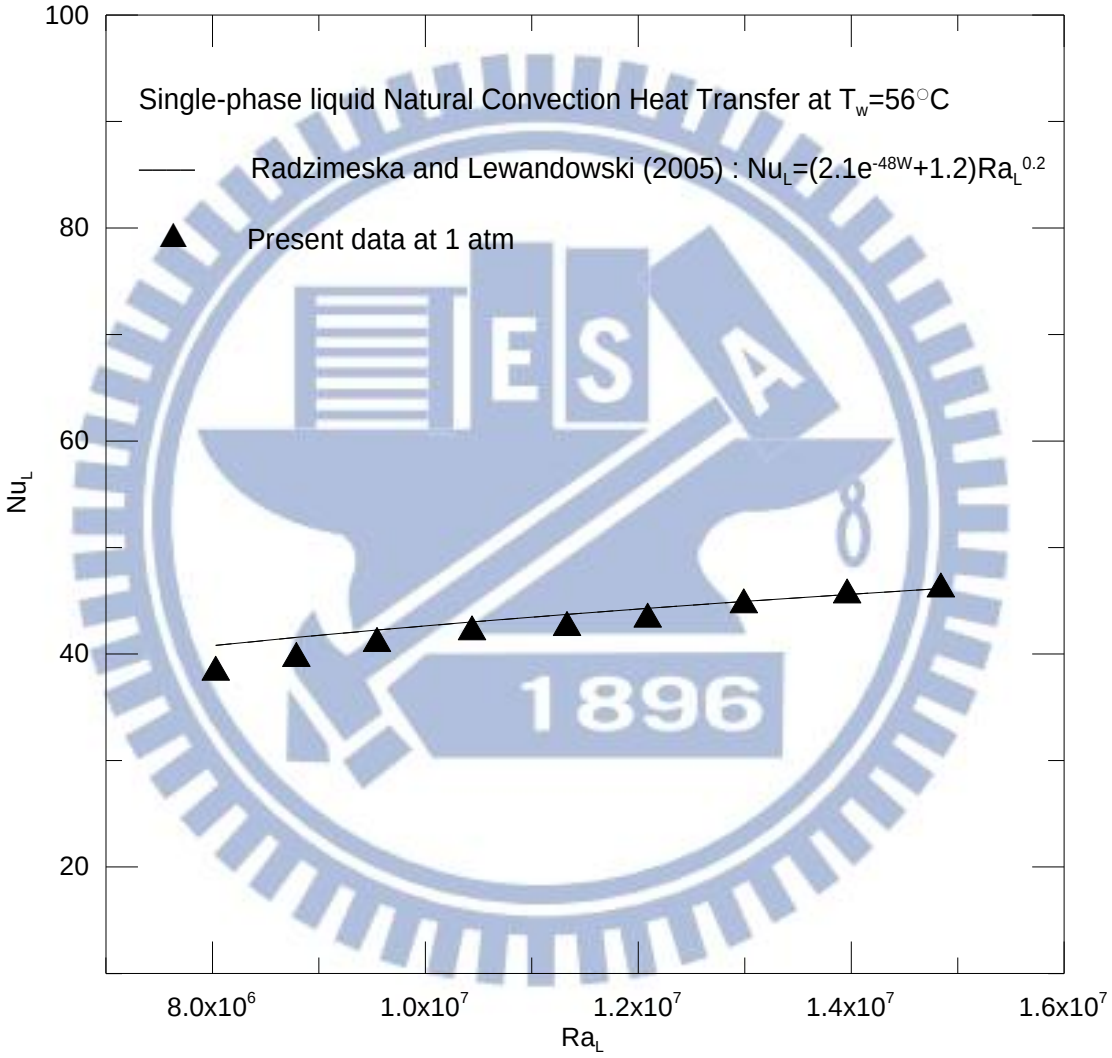

Fig. 4.1 Comparison of the present single-phase natural convection data with the empirical correlation of Radziemska and Lewandowski (2005).

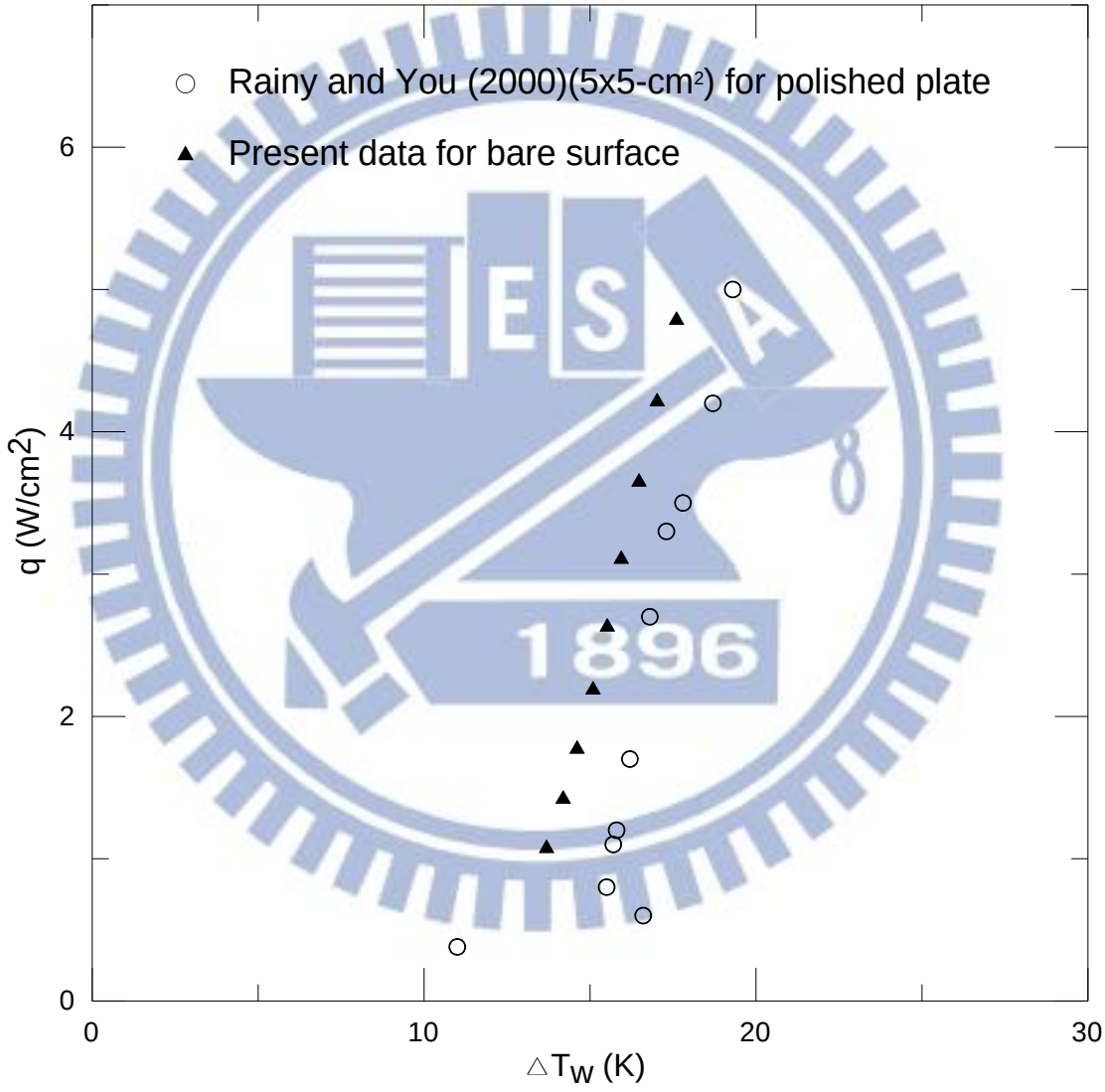

Fig. 4.2 Comparison of the present nucleate boiling heat transfer data for bare surface with Rainy and You (2000).

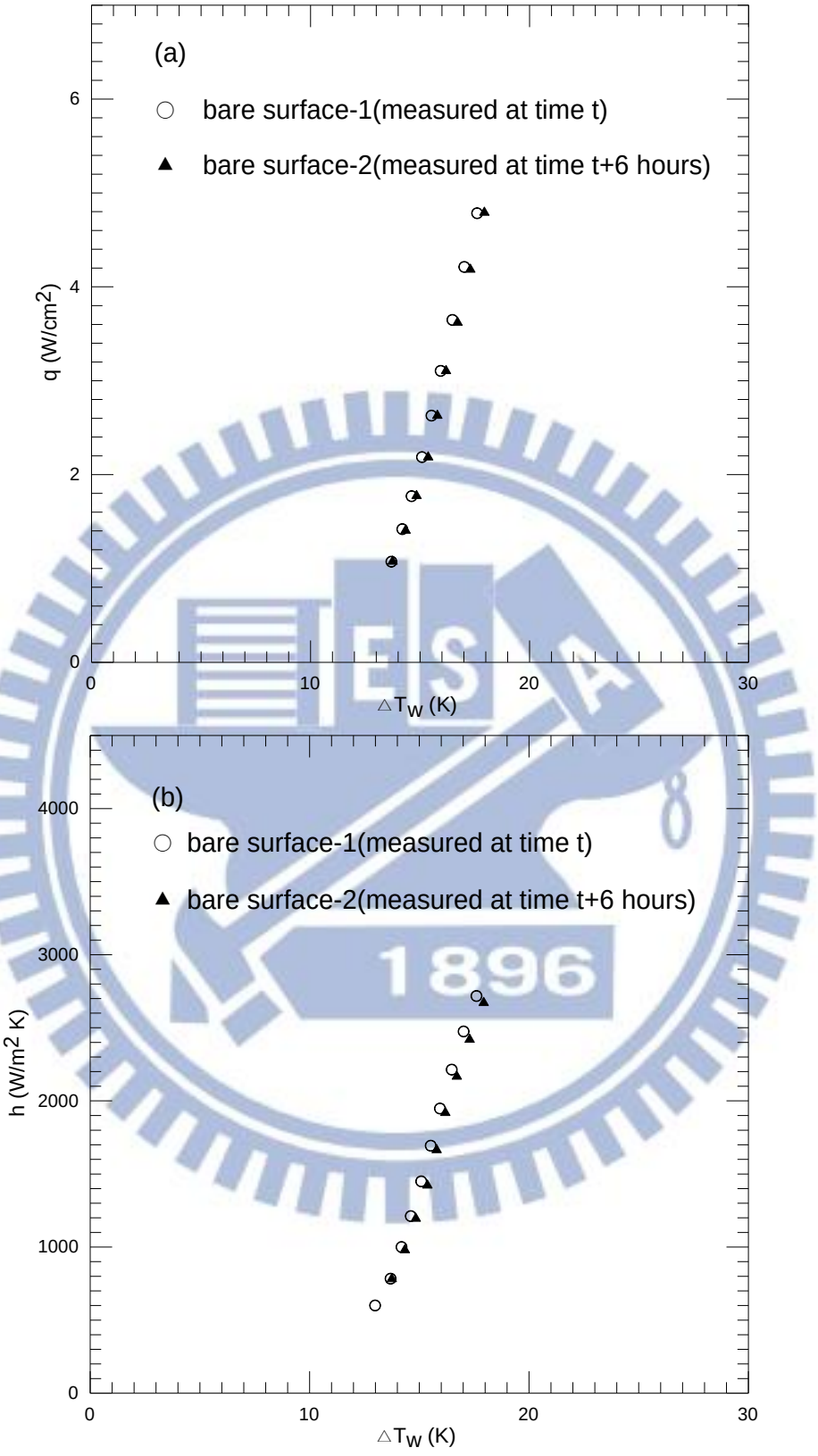

Fig. 4.3 Effects of surface aging on saturated pool boiling curves (a) and boiling heat transfer coefficients (b) for bare surface.

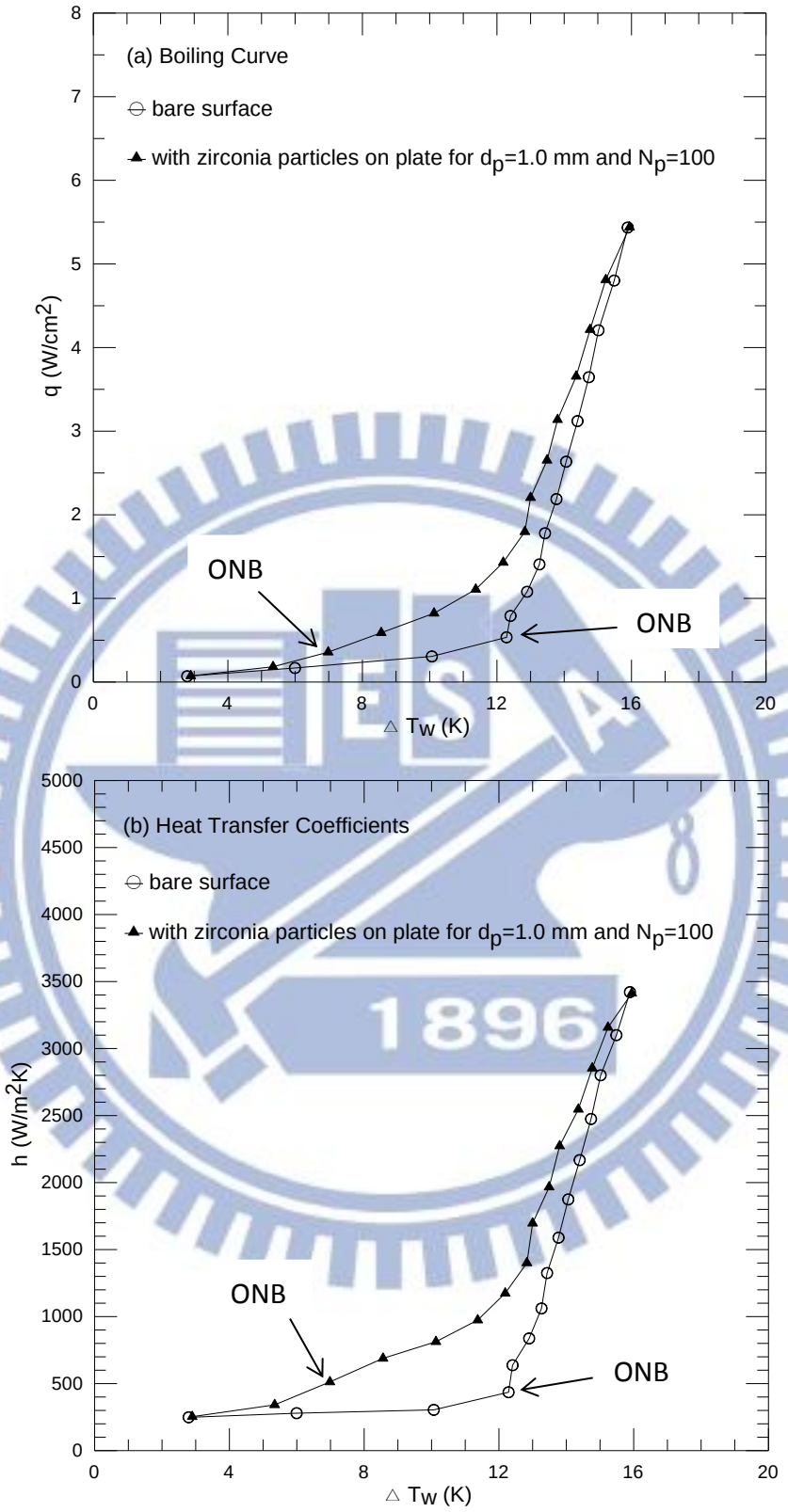

Fig. 4.4 Effects of zirconia particle diameter and number on saturated pool boiling curves (a) and boiling heat transfer coefficients (b) at d_p=1.0 mm and $N_p = 100$.

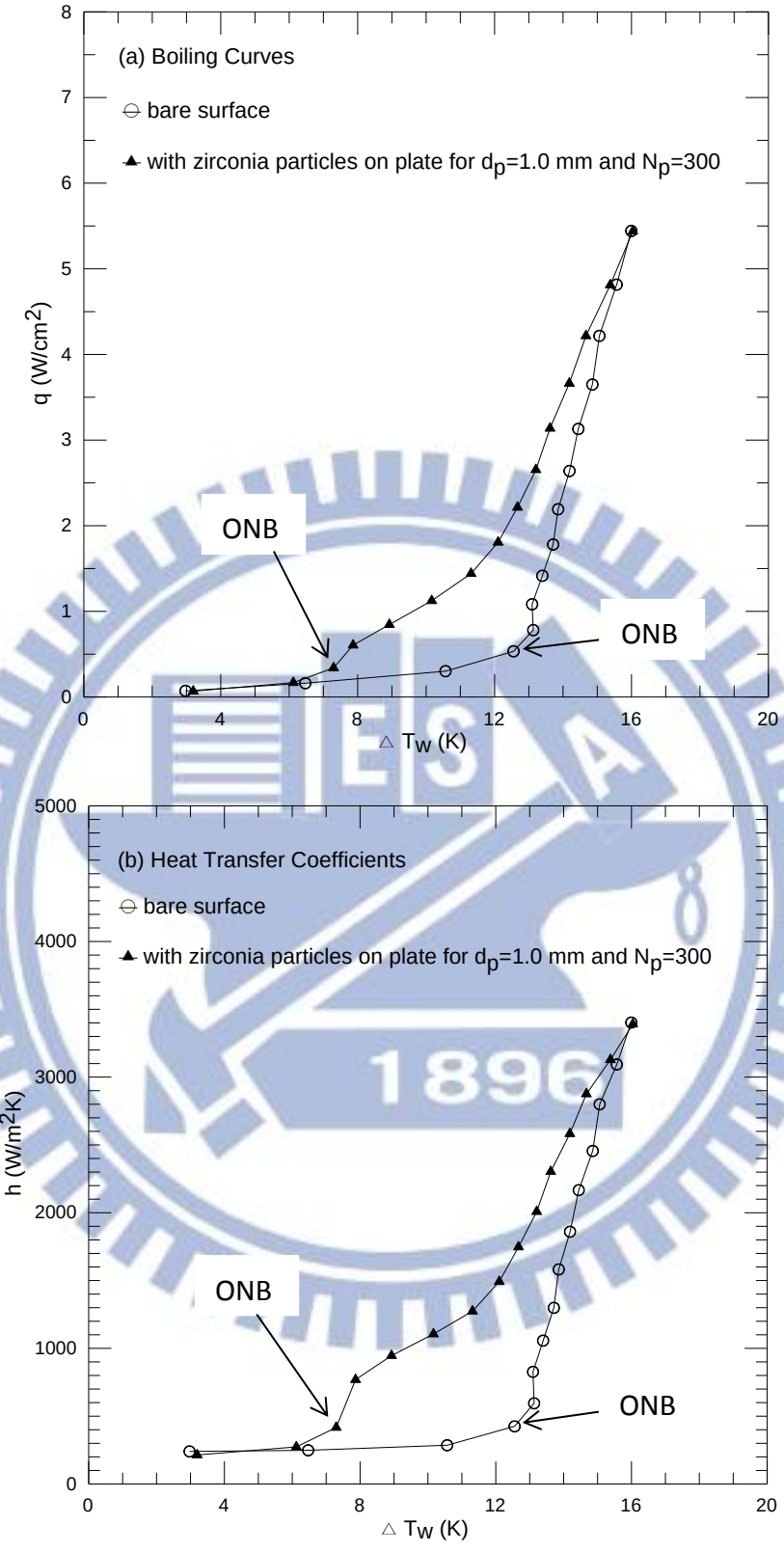

Fig. 4.5 Effects of zirconia particle diameter and number on saturated pool boiling curves (a) and boiling heat transfer coefficients (b) at d_p=1.0 mm and $N_p = 300$.

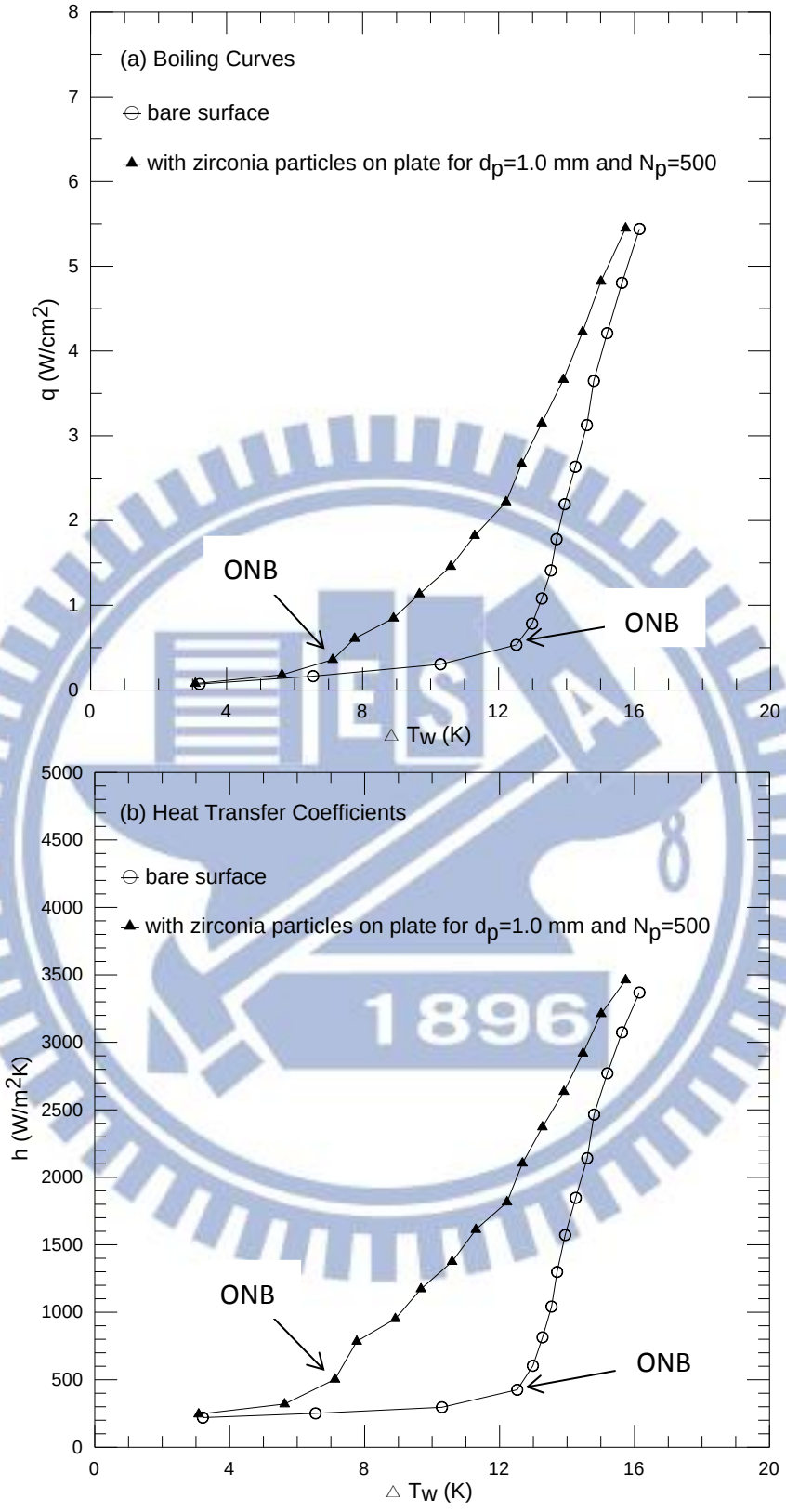

Fig. 4.6 Effects of zirconia particle diameter and number on saturated pool boiling curves (a) and boiling heat transfer coefficients (b) at d_p=1.0 mm and $N_p = 500$.

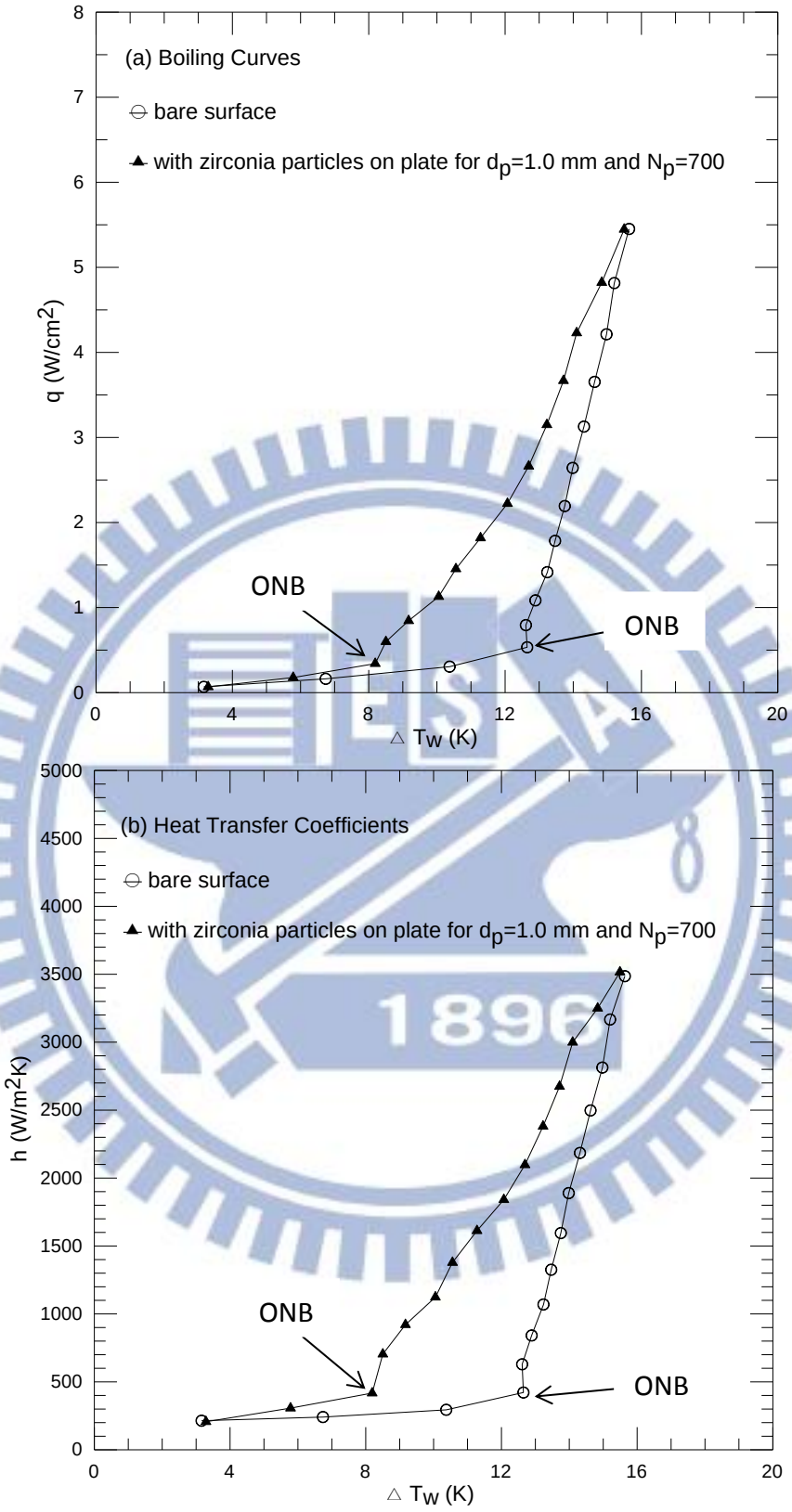

Fig. 4.7 Effects of zirconia particle diameter and number on saturated pool boiling curves (a) and boiling heat transfer coefficients (b) at d_p=1.0 mm and $N_p = 700$.

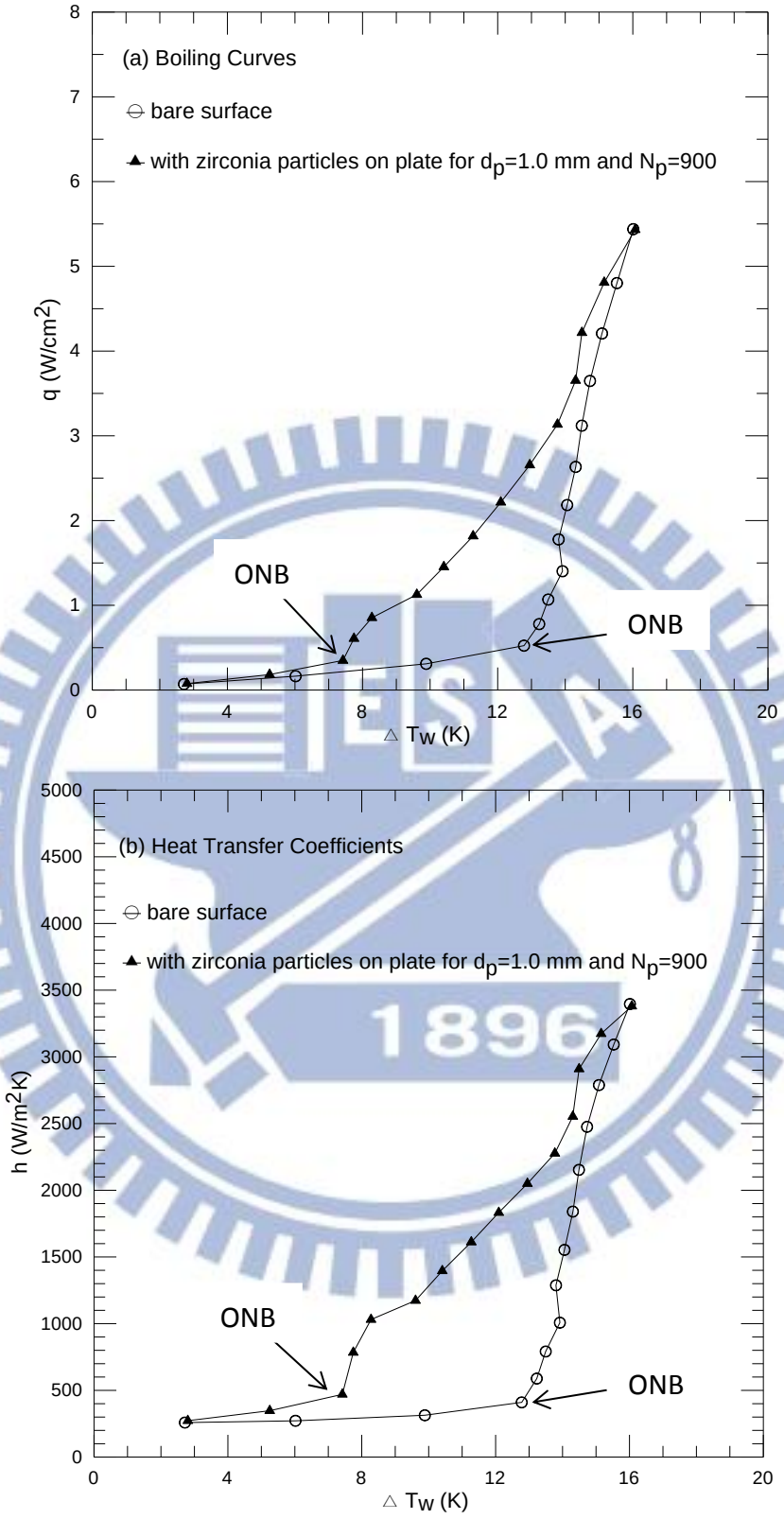

Fig. 4.8 Effects of zirconia particle diameter and number on saturated pool boiling curves (a) and boiling heat transfer coefficients (b) at d_p=1.0 mm and $N_p = 900$.

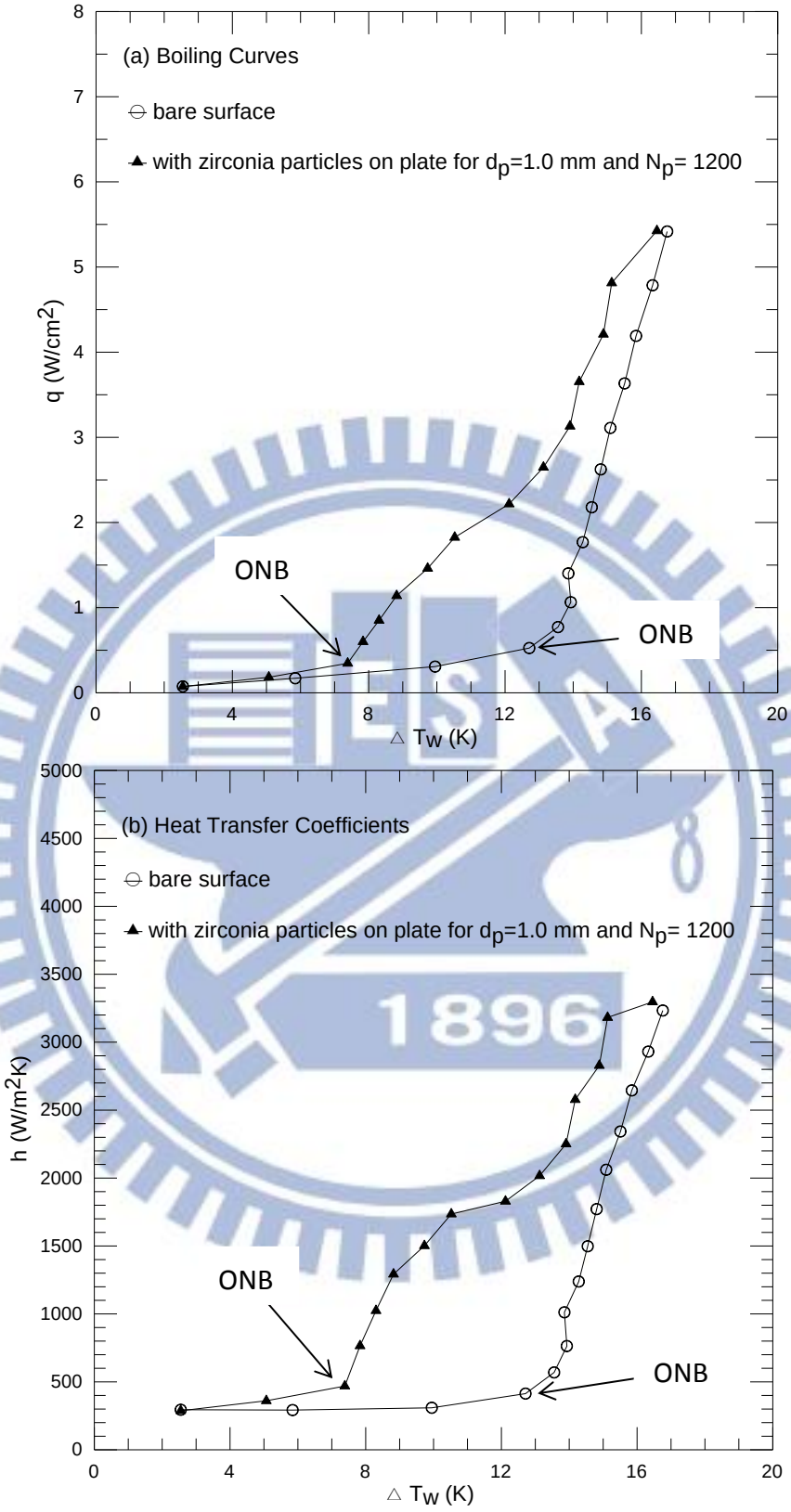

Fig. 4.9 Effects of zirconia particle diameter and number on saturated pool boiling curves (a) and boiling heat transfer coefficients (b) at d_p=1.0 mm and $N_p = 1200$.

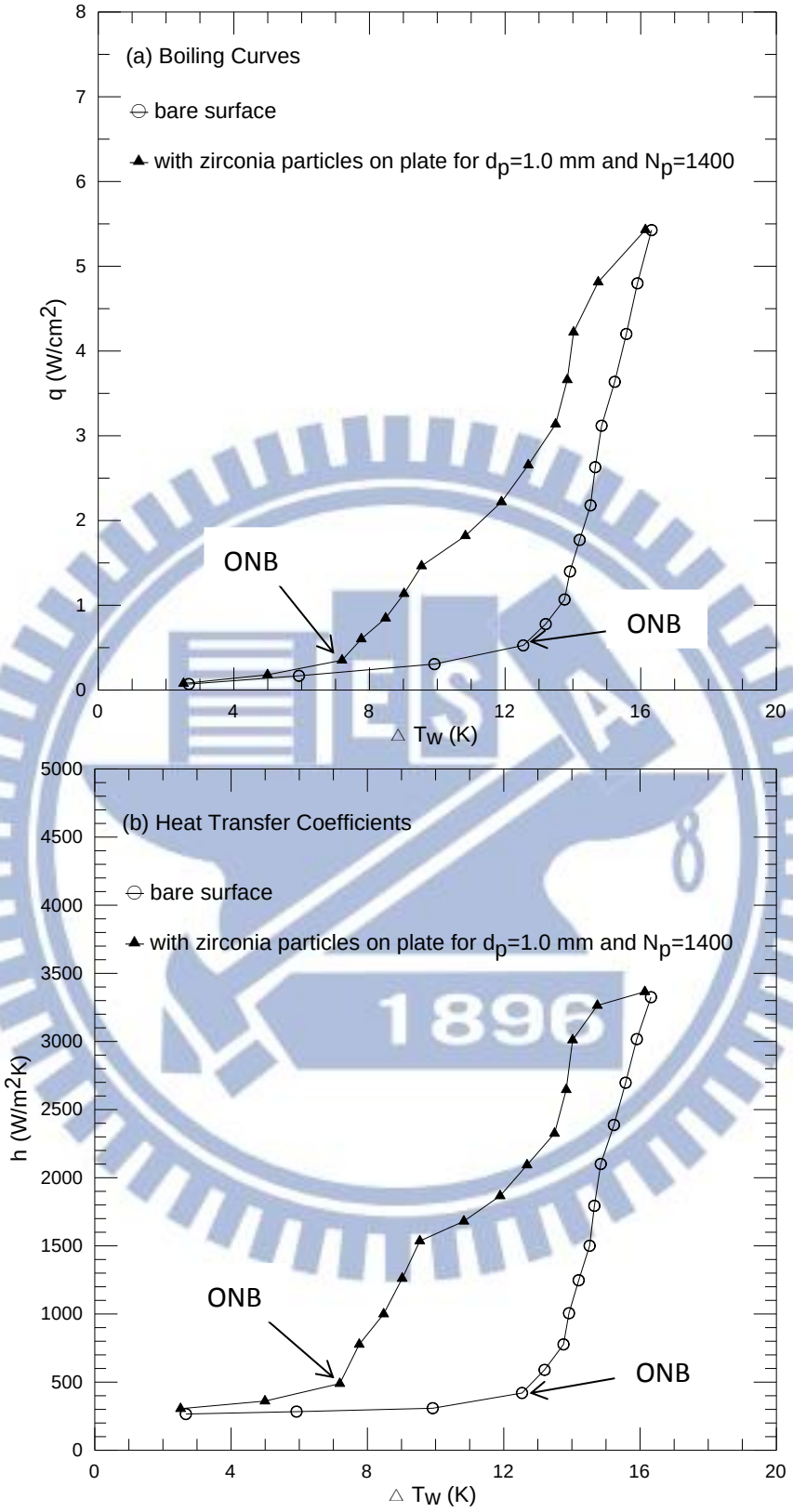

Fig. 4.10 Effects of zirconia particle diameter and number on saturated pool boiling curves (a) and boiling heat transfer coefficients (b) at d_p=1.0 mm and $N_p = 1400$.

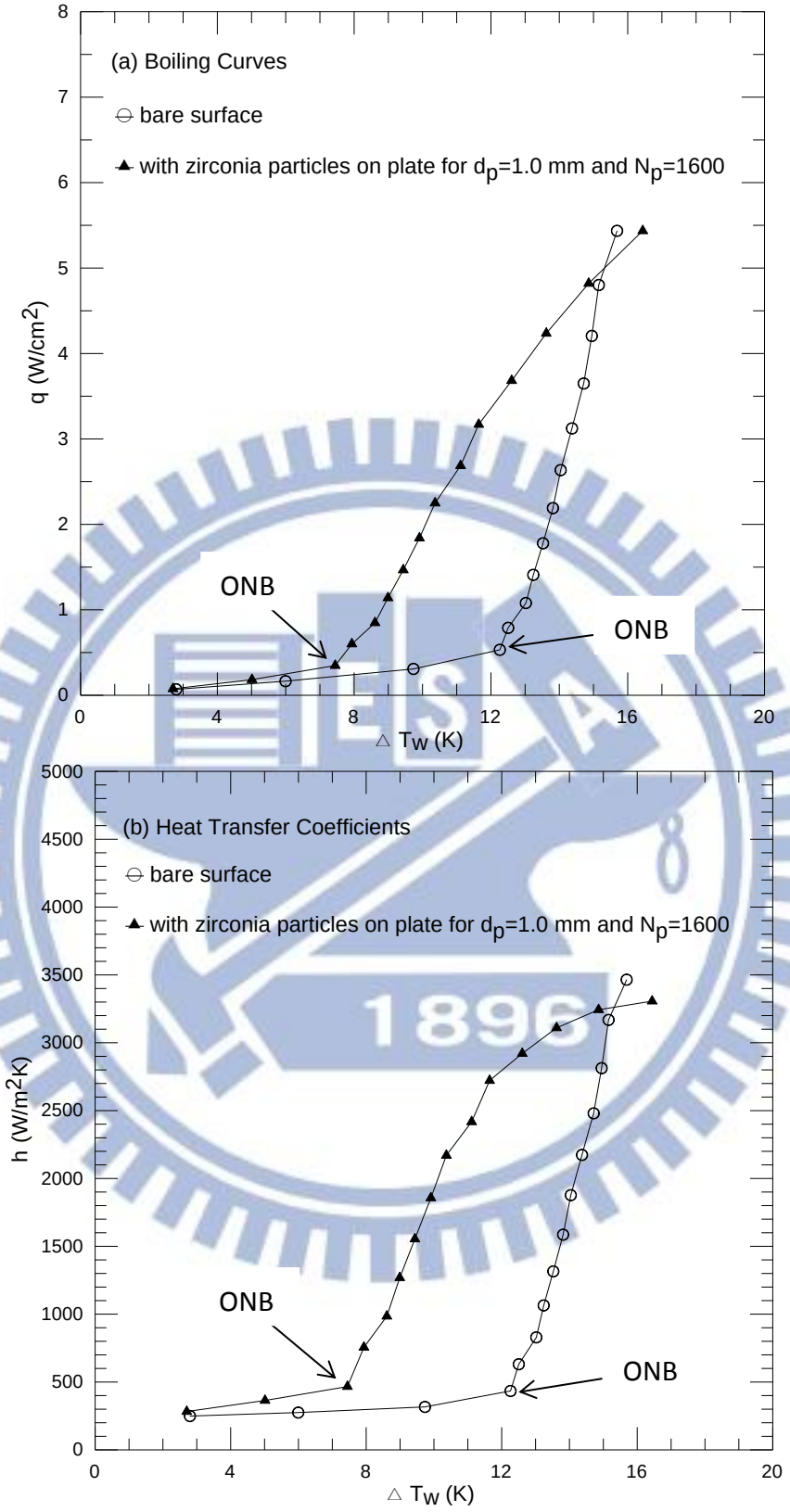

Fig. 4.11 Effects of zirconia particle diameter and number on saturated pool boiling curves (a) and boiling heat transfer coefficients (b) at d_p=1.0 mm and $N_p = 1600$.

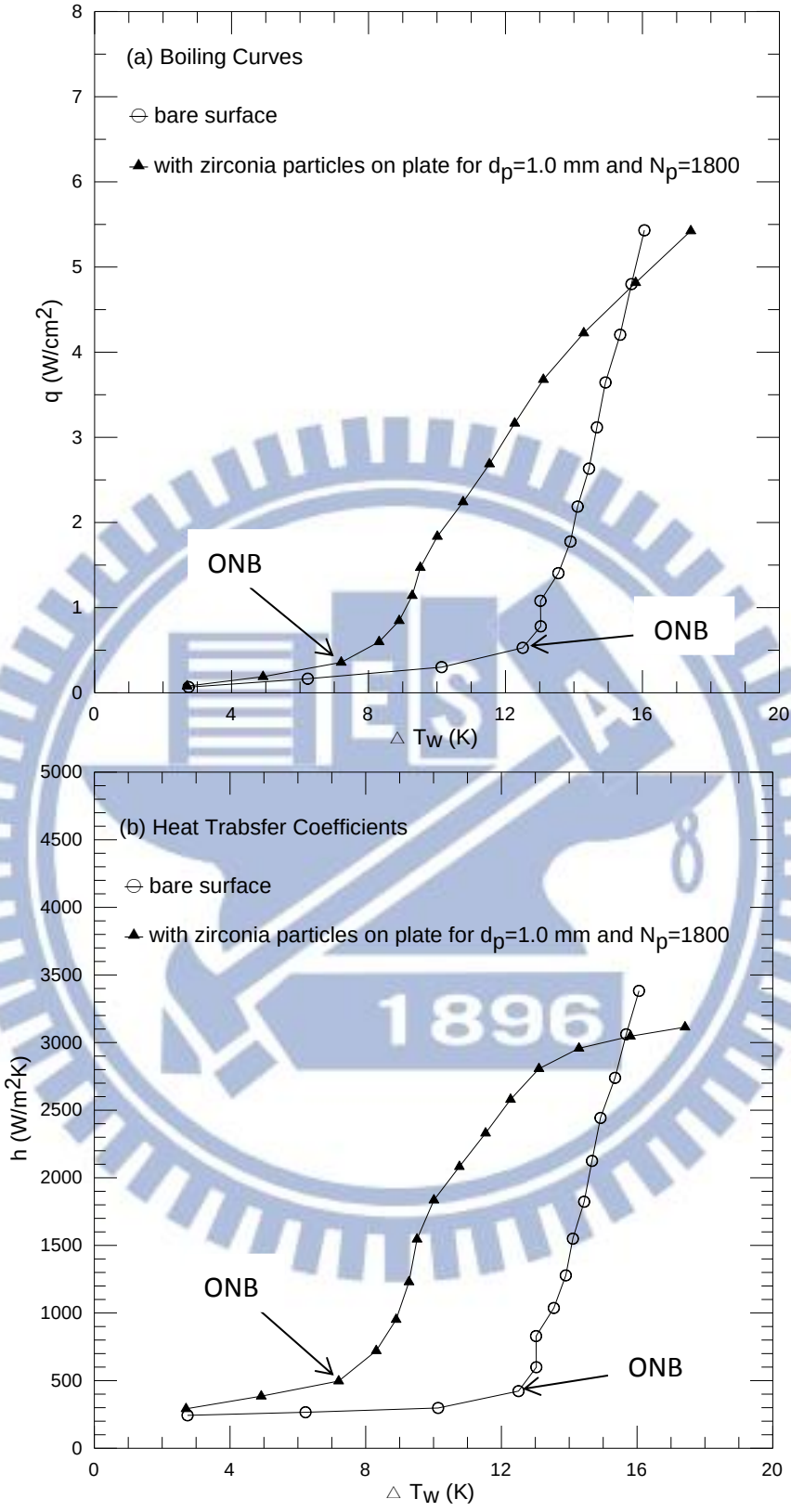

Fig. 4.12 Effects of zirconia particle diameter and number on saturated pool boiling curves (a) and boiling heat transfer coefficients (b) at d_p=1.0 mm and $N_p = 1800$.

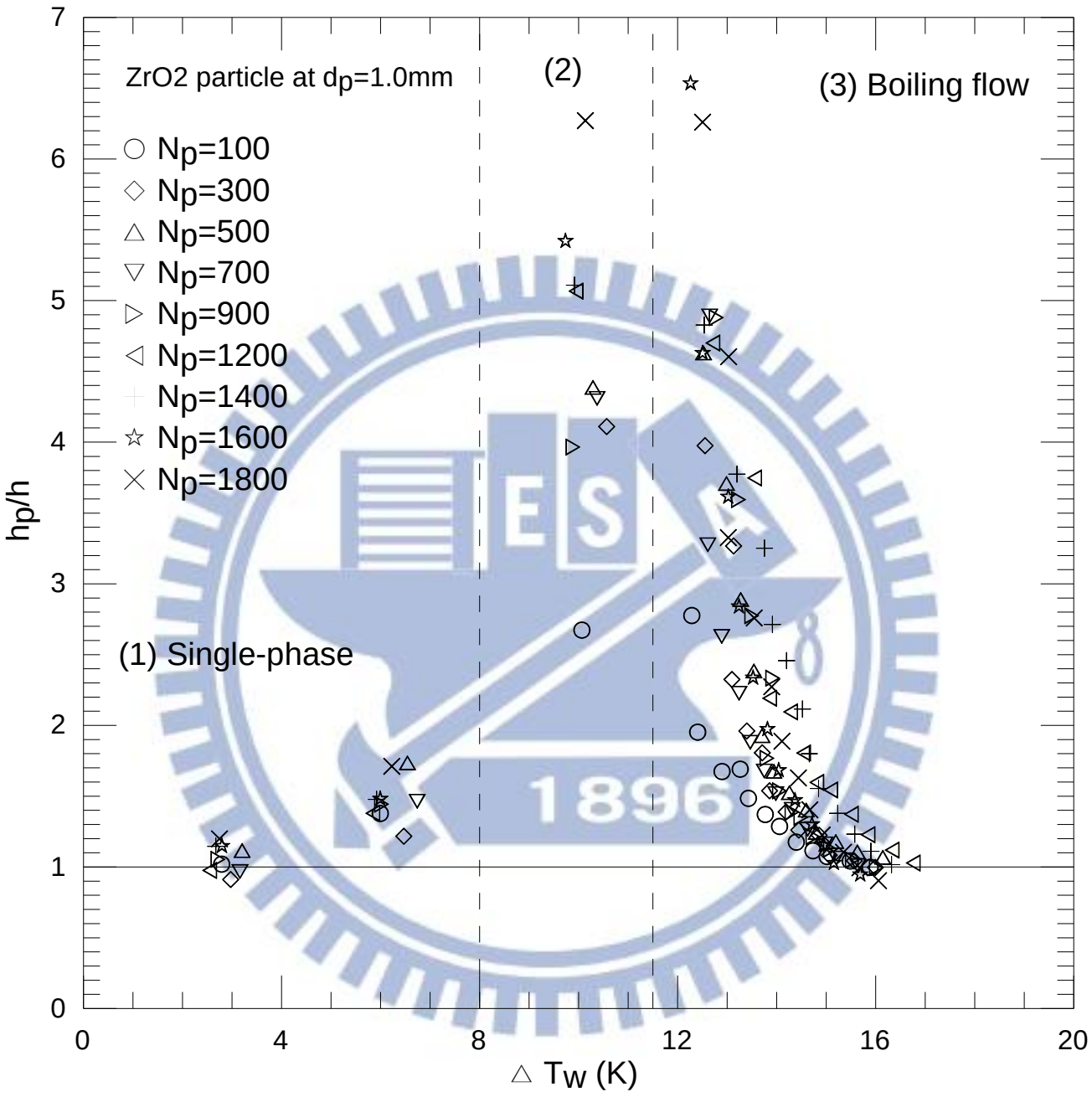

Fig. 4.13 Variations of h_p/h with wall superheat for various zirconia particle numbers at d_p=1.0 mm (the middle area represent single phase for particles on heated plate and boiling for bare surface)

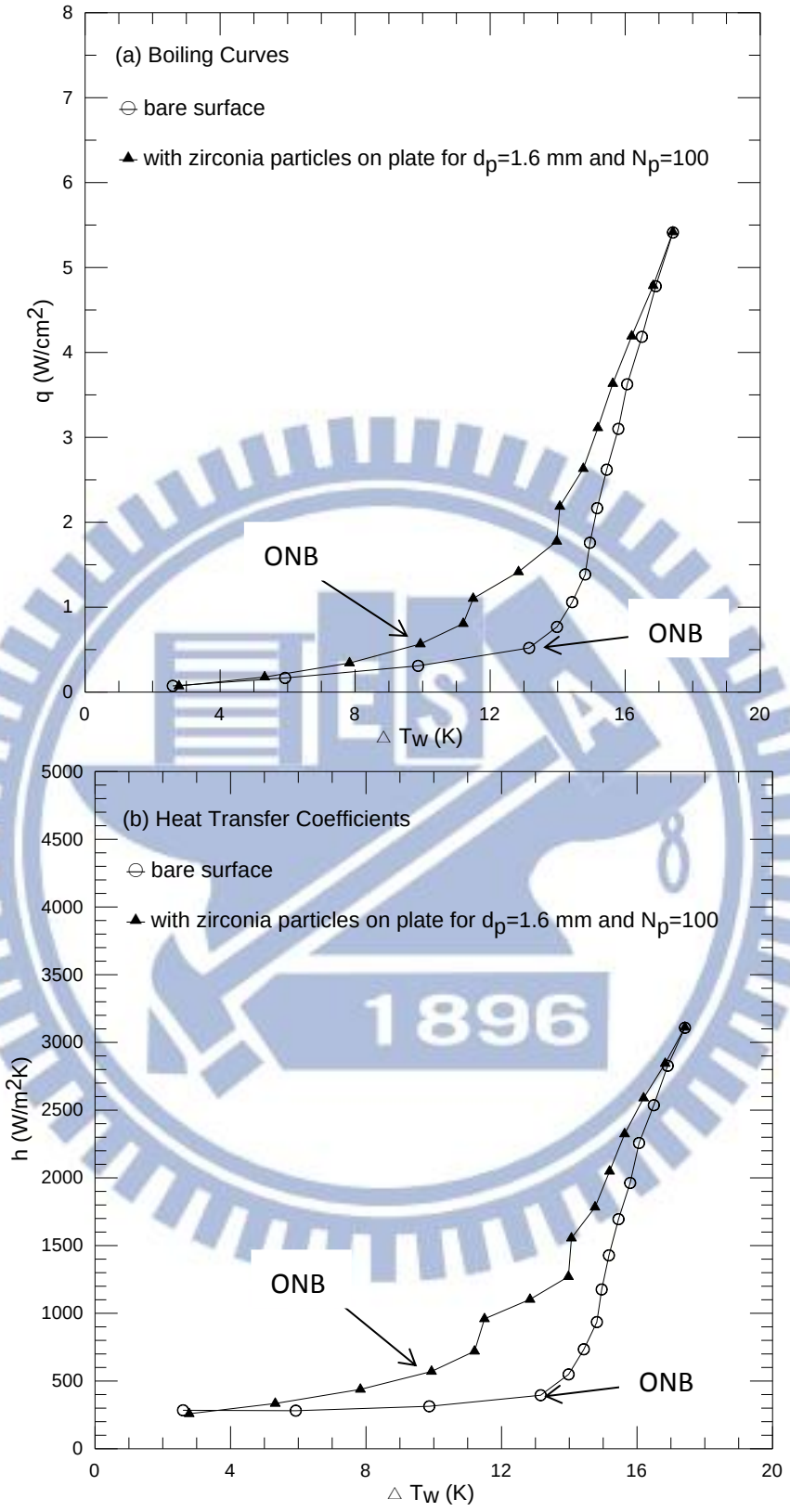

Fig. 4.14 Effects of zirconia particle diameter and number on saturated pool boiling curves (a) and boiling heat transfer coefficients (b) at d_p=1.6 mm and $N_p = 100$.

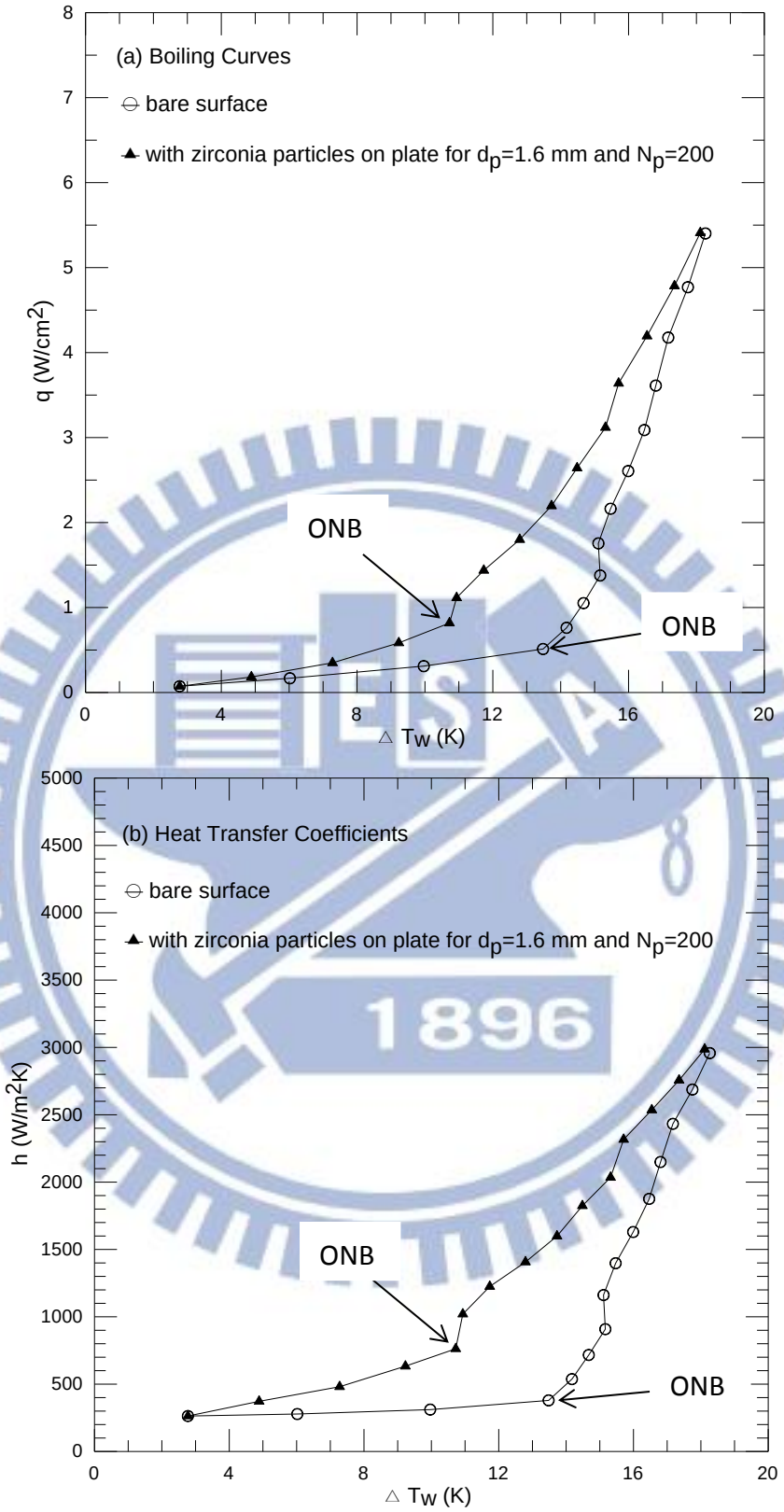

Fig. 4.15 Effects of zirconia particle diameter and number on saturated pool boiling curves (a) and boiling heat transfer coefficients (b) at d_p=1.6 mm and $N_p = 200$.

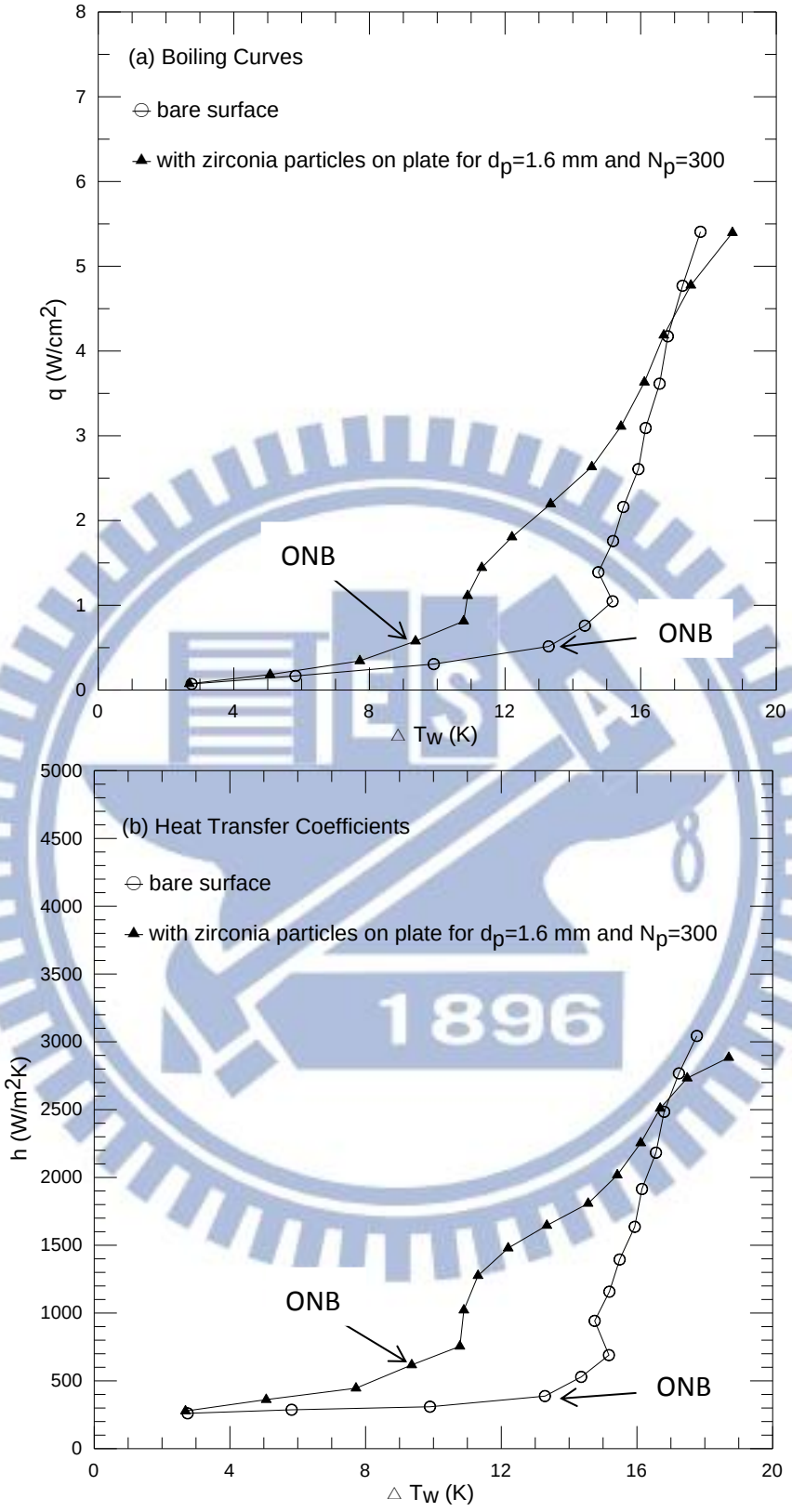

Fig. 4.16 Effects of zirconia particle diameter and number on saturated pool boiling curves (a) and boiling heat transfer coefficients (b) at d_p=1.6 mm and $N_p = 300$.

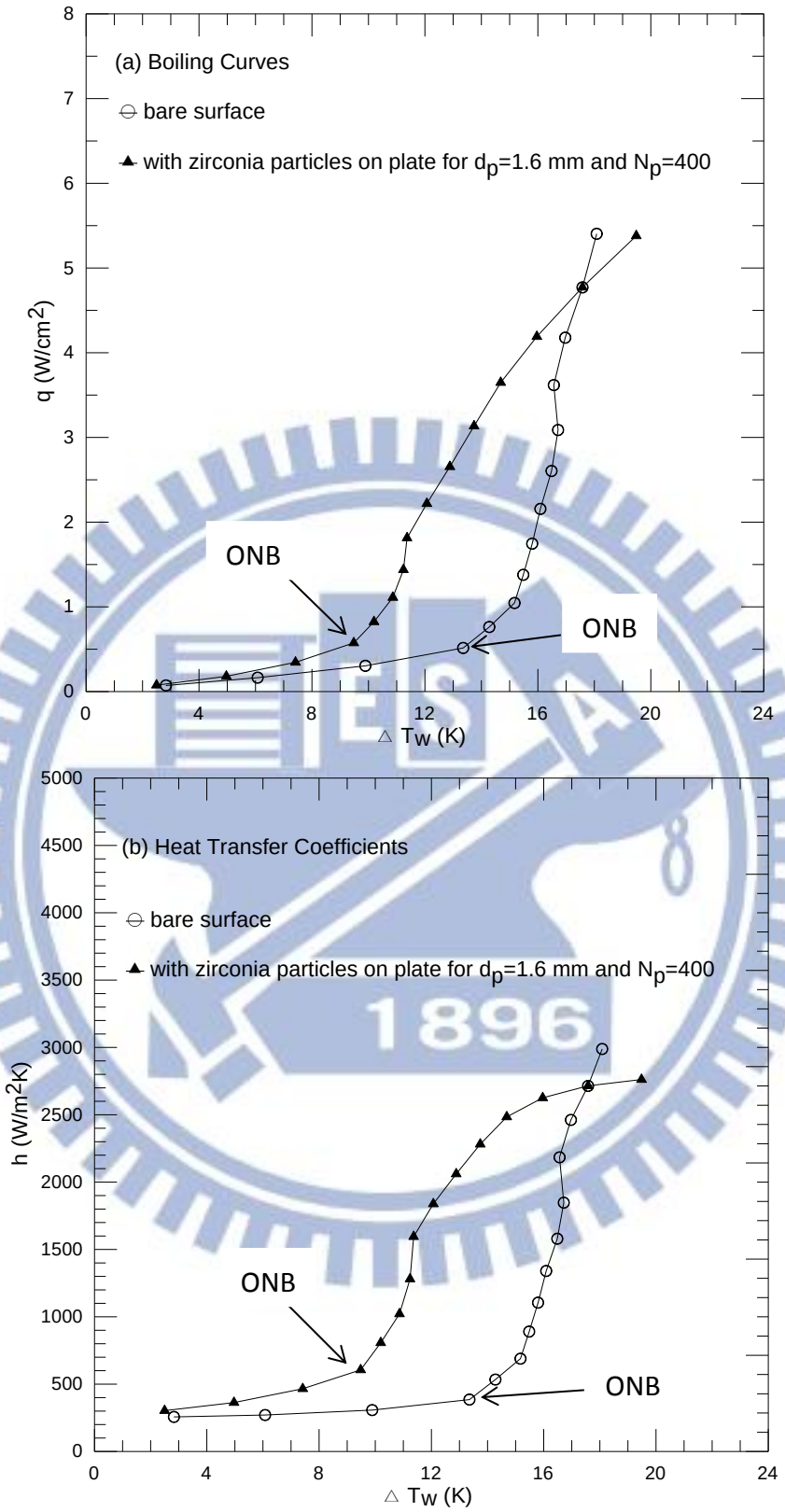

Fig. 4.17 Effects of zirconia particle diameter and number on saturated pool boiling curves (a) and boiling heat transfer coefficients (b) at d_p=1.6 mm and $N_p = 400$.

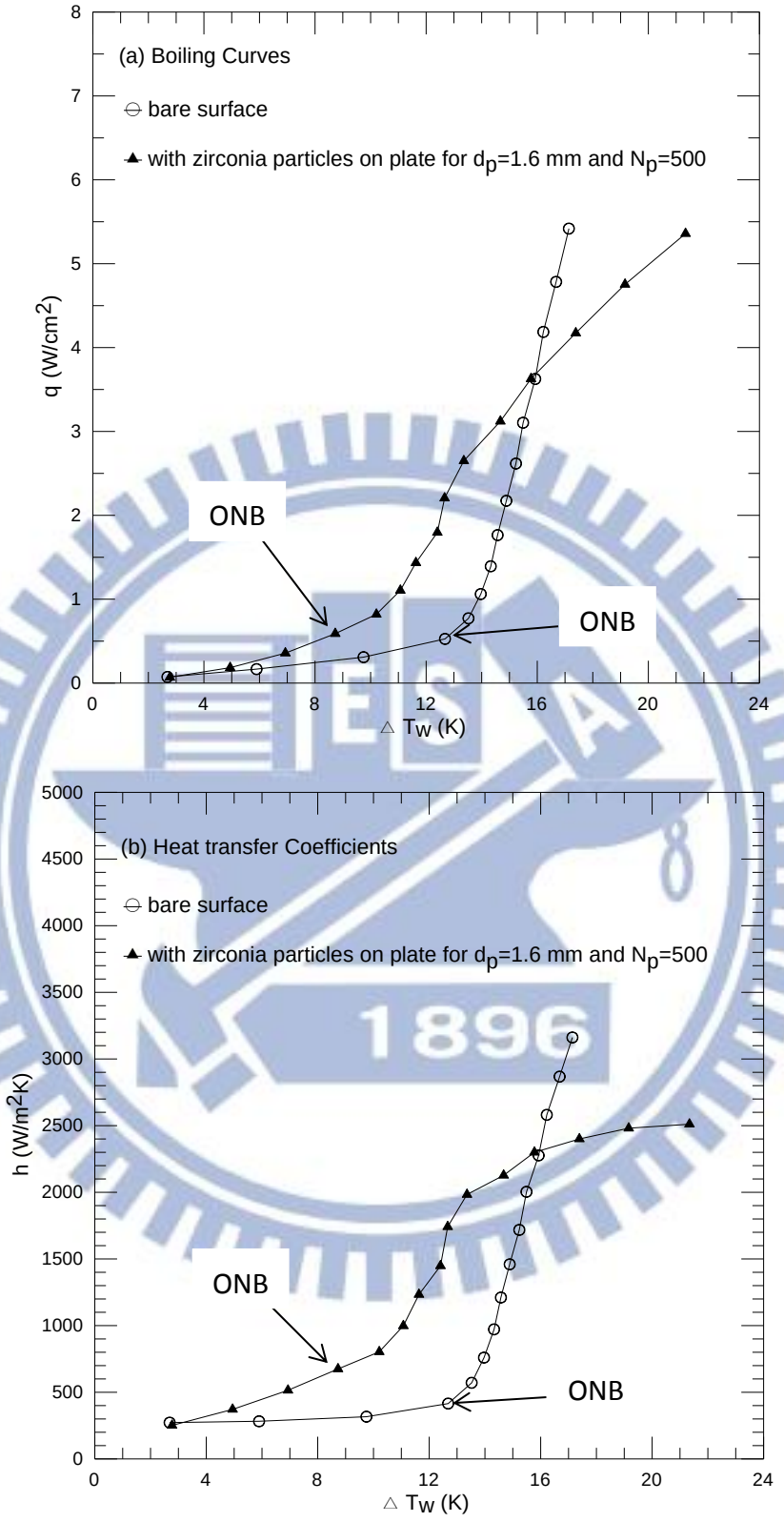

Fig. 4.18 Effects of zirconia particle diameter and number on saturated pool boiling curves (a) and boiling heat transfer coefficients (b) at d_p=1.6 mm and $N_p = 500$.

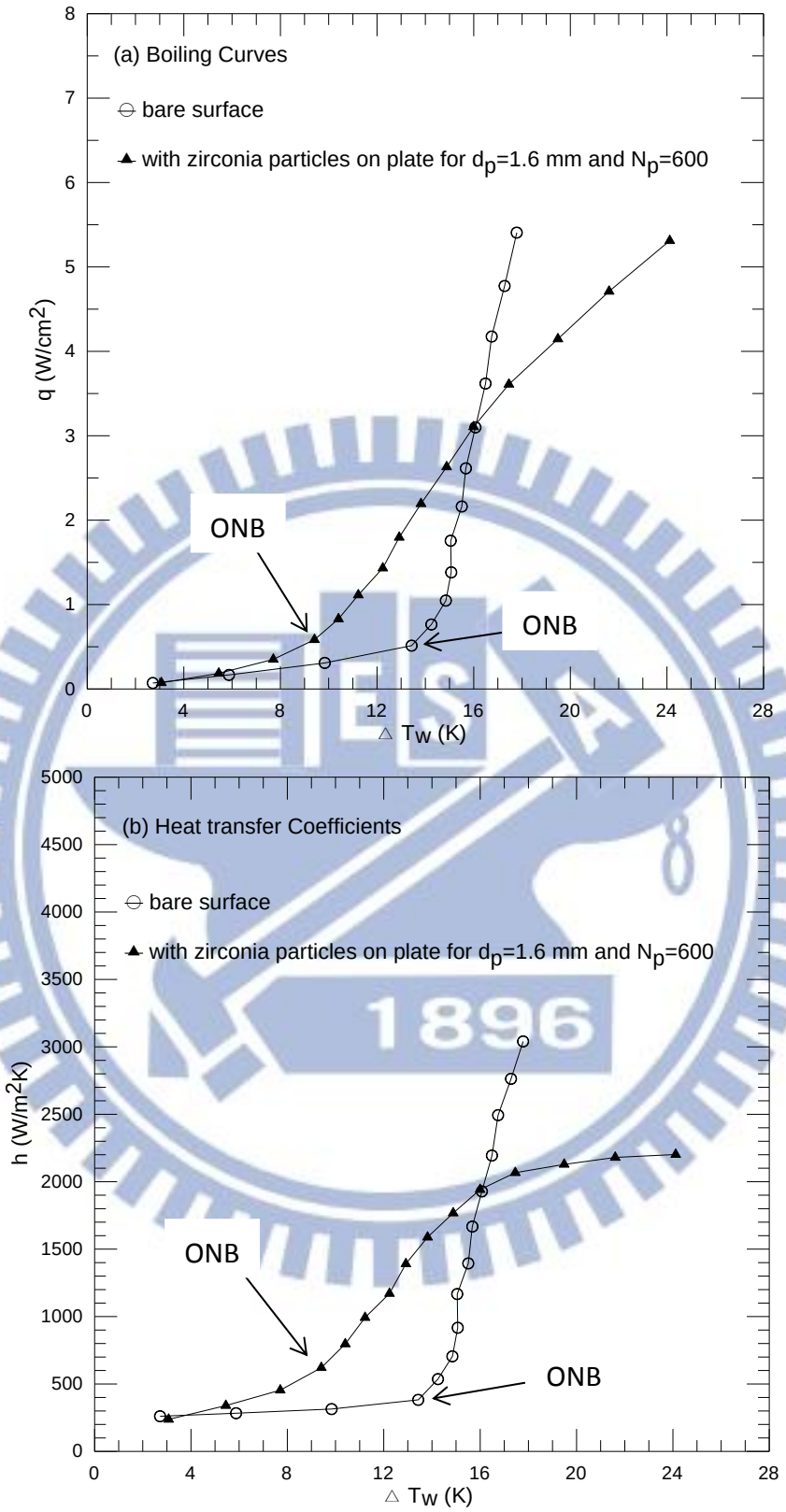

Fig. 4.19 Effects of zirconia particle diameter and number on saturated pool boiling curves (a) and boiling heat transfer coefficients (b) at d_p=1.6 mm and $N_p = 600$.

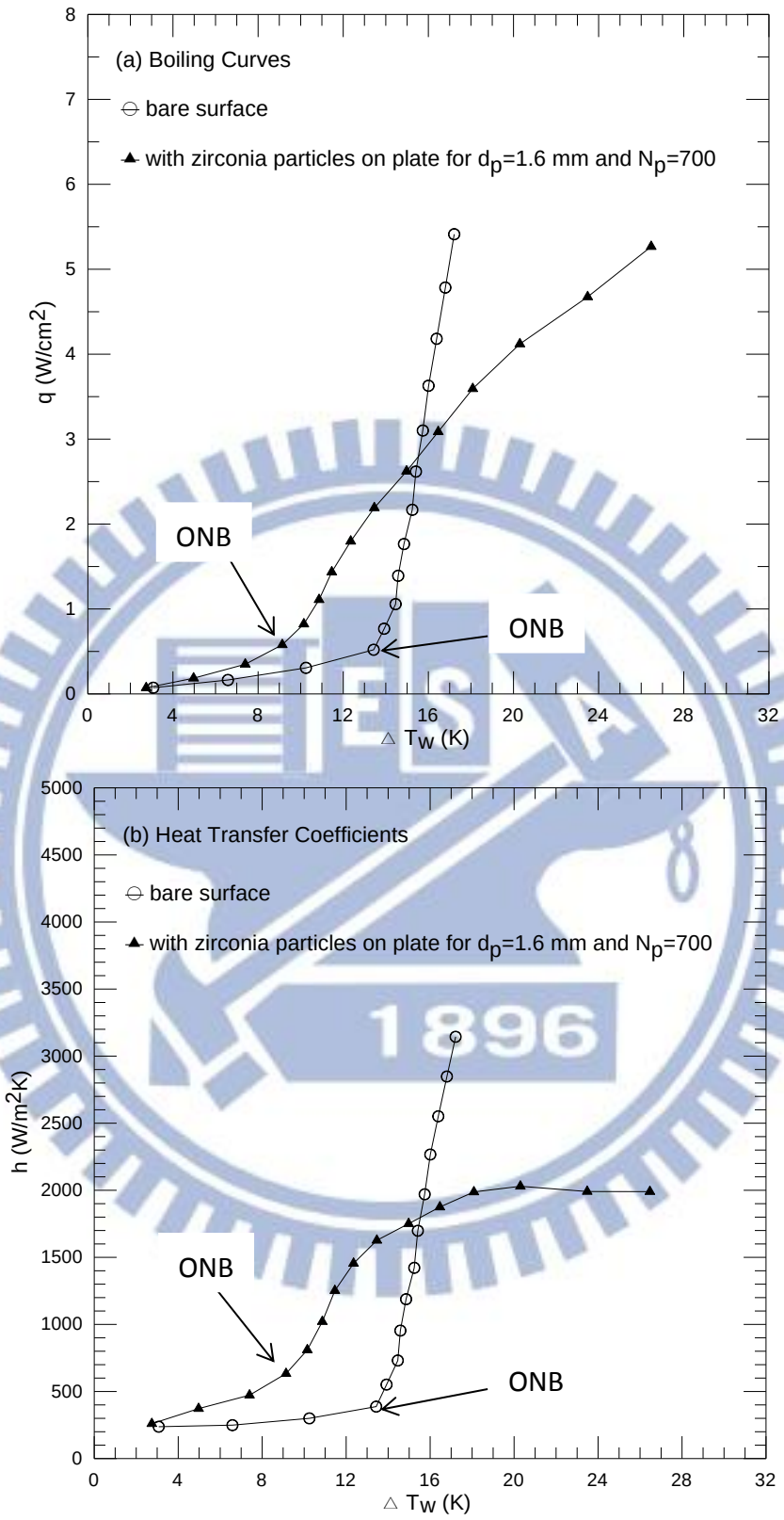

Fig. 4.20 Effects of zirconia particle diameter and number on saturated pool boiling curves (a) and boiling heat transfer coefficients (b) at d_p=1.6 mm and $N_p = 700$.

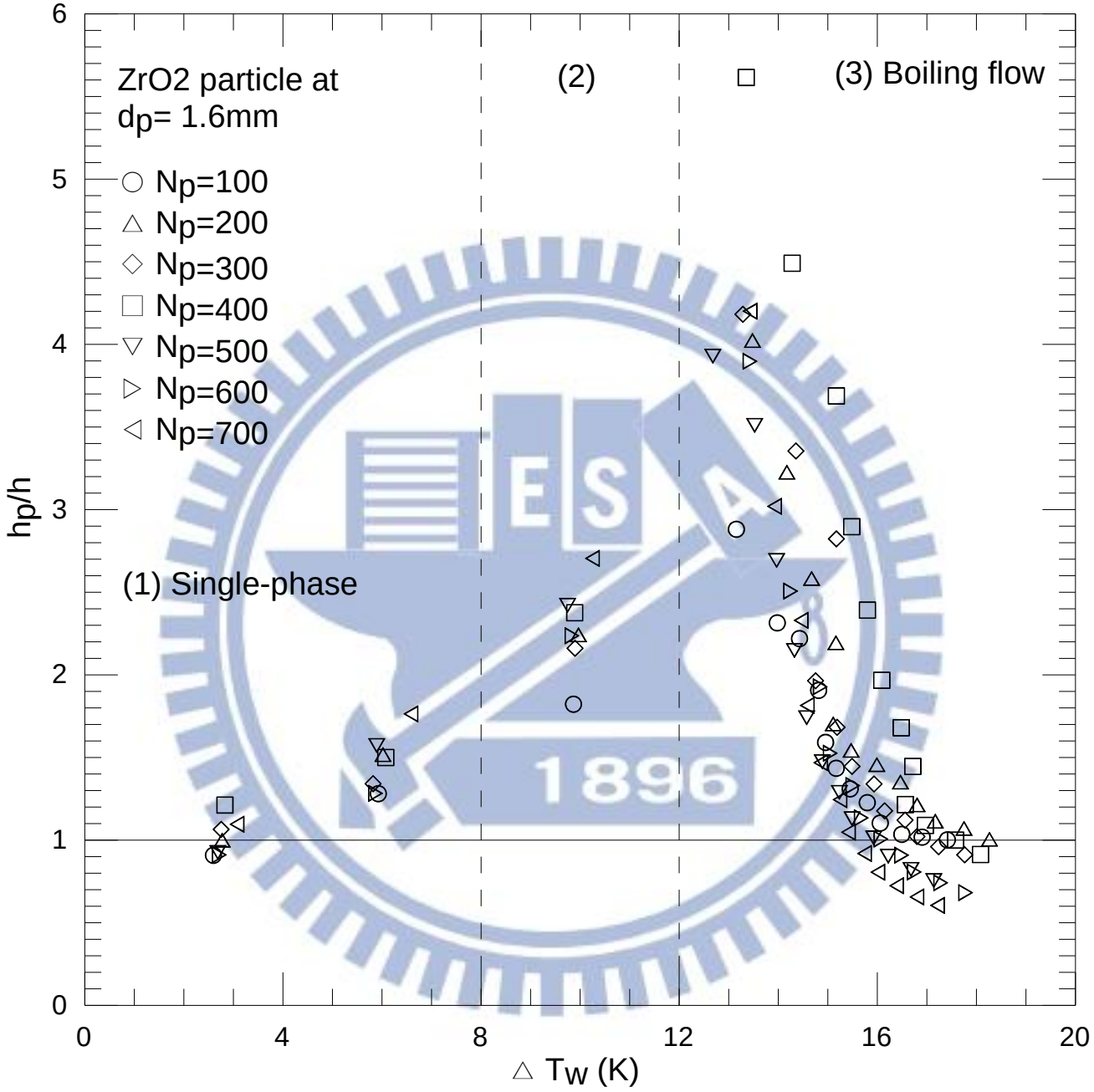

Fig. 4.21 Variations of h_p/h with wall superheat for various zirconia particle numbers at d_p=1.6 mm (the middle area represent single phase for particles on heated plate and boiling for bare surface)

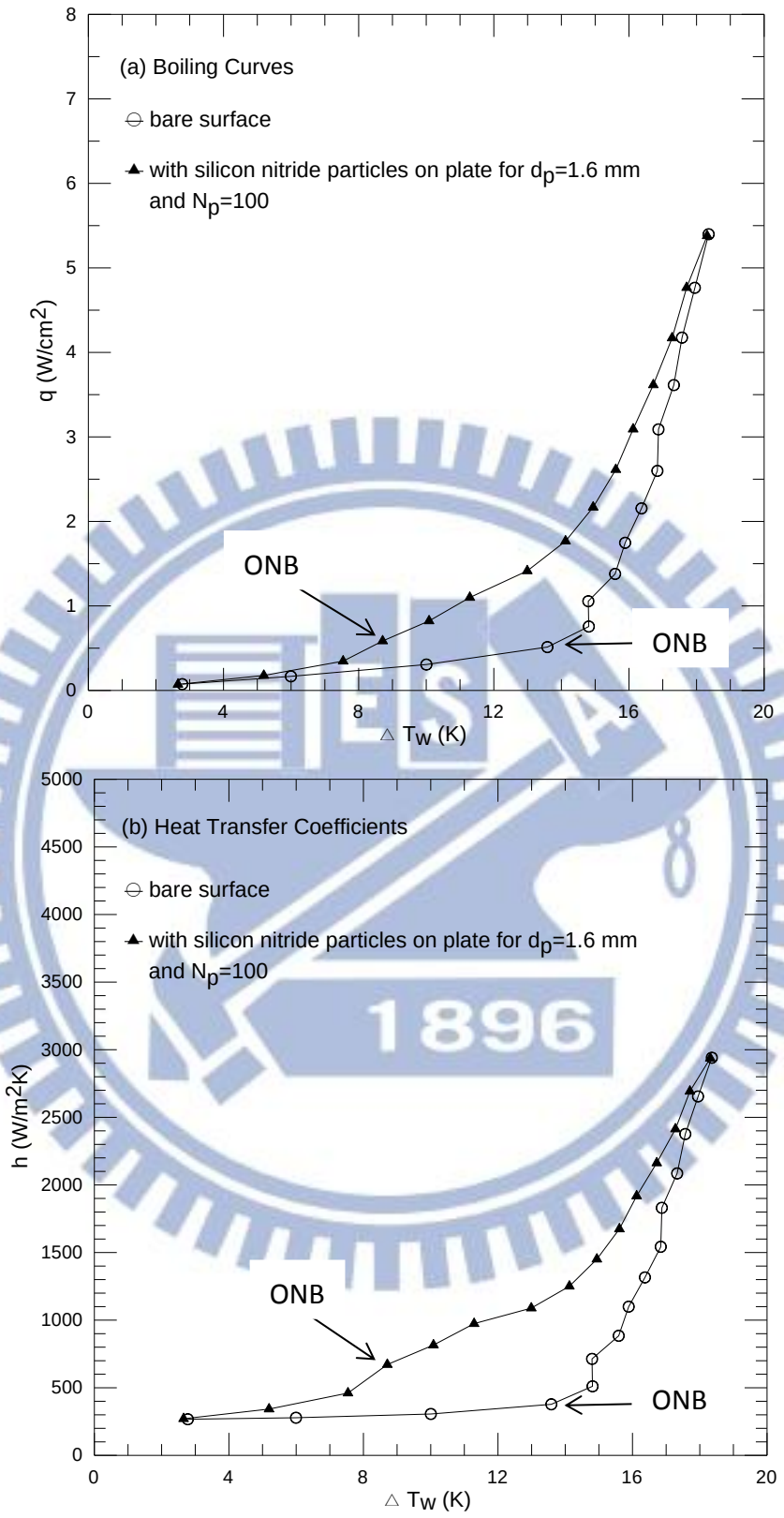

Fig. 4.22 Effects of silicon nitride particle diameter and number on saturated pool boiling curves (a) and boiling heat transfer coefficients (b) at d_p=1.6 mm and $N_p = 100$.

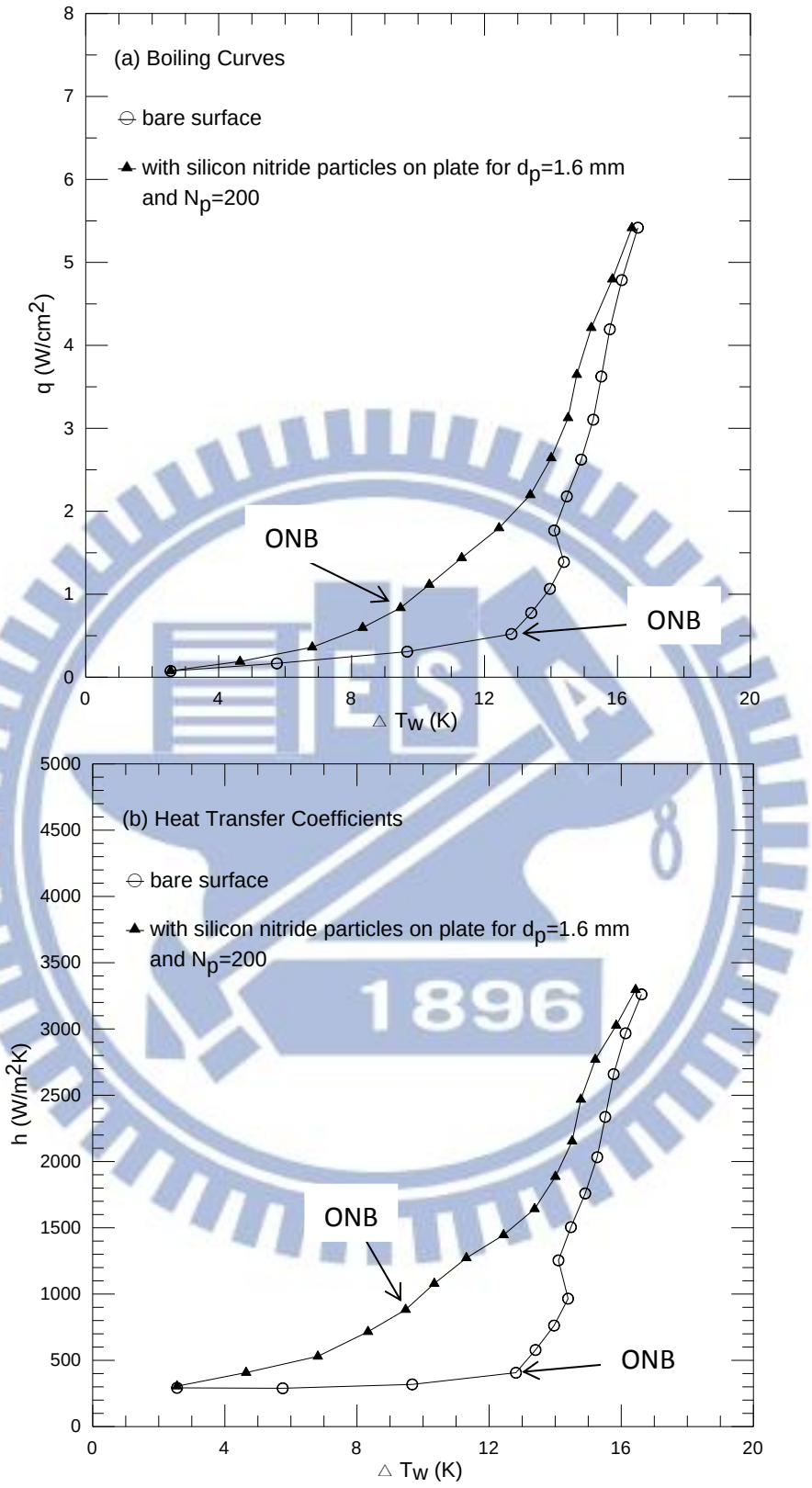

Fig. 4.23 Effects of silicon nitride particle diameter and number on saturated pool boiling curves (a) and boiling heat transfer coefficients (b) at d_p=1.6 mm and $N_p = 200$.

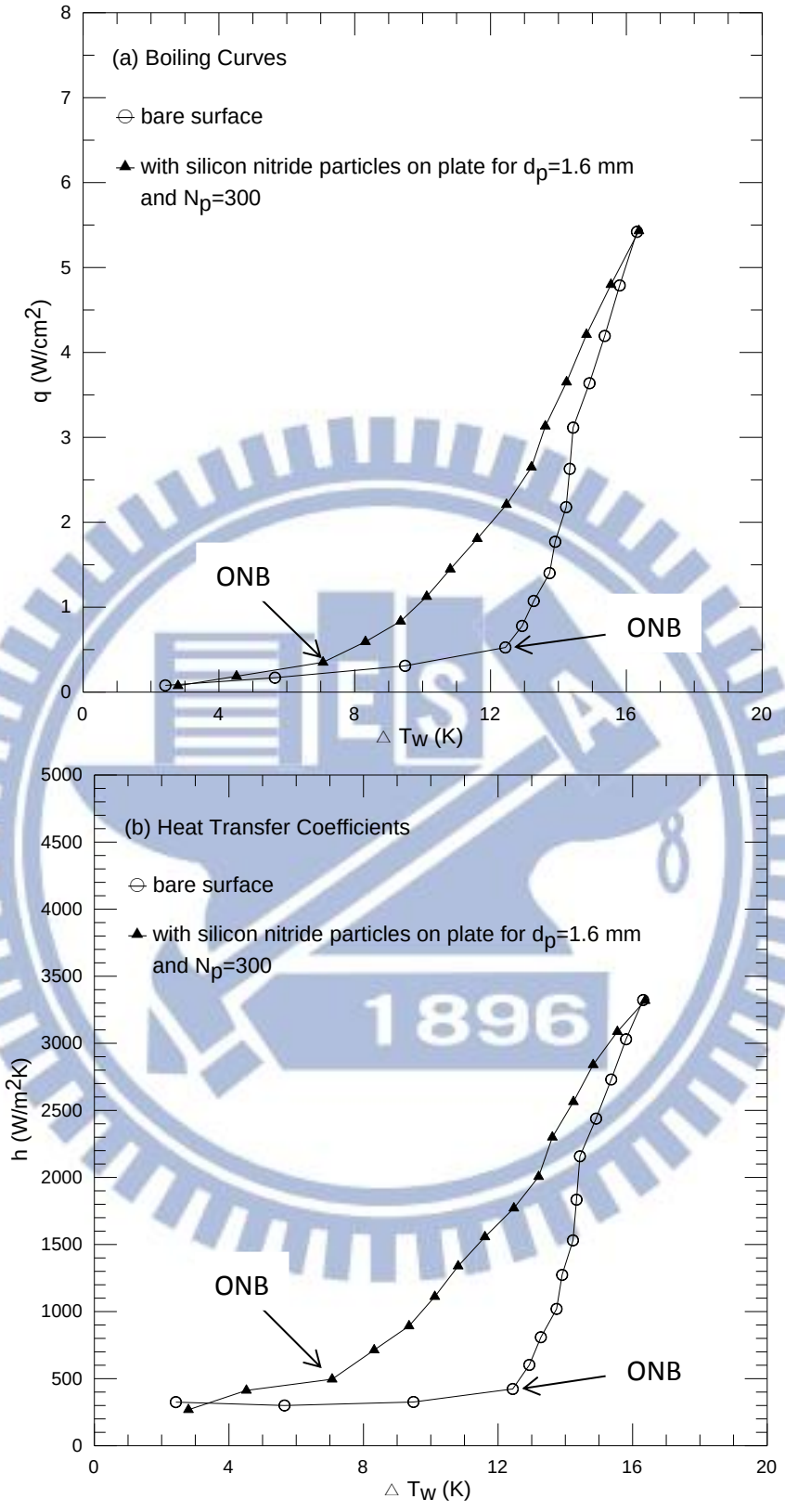

Fig. 4.24 Effects of silicon nitride particle diameter and number on saturated pool boiling curves (a) and boiling heat transfer coefficients (b) at d_p=1.6 mm and $N_p = 300$.

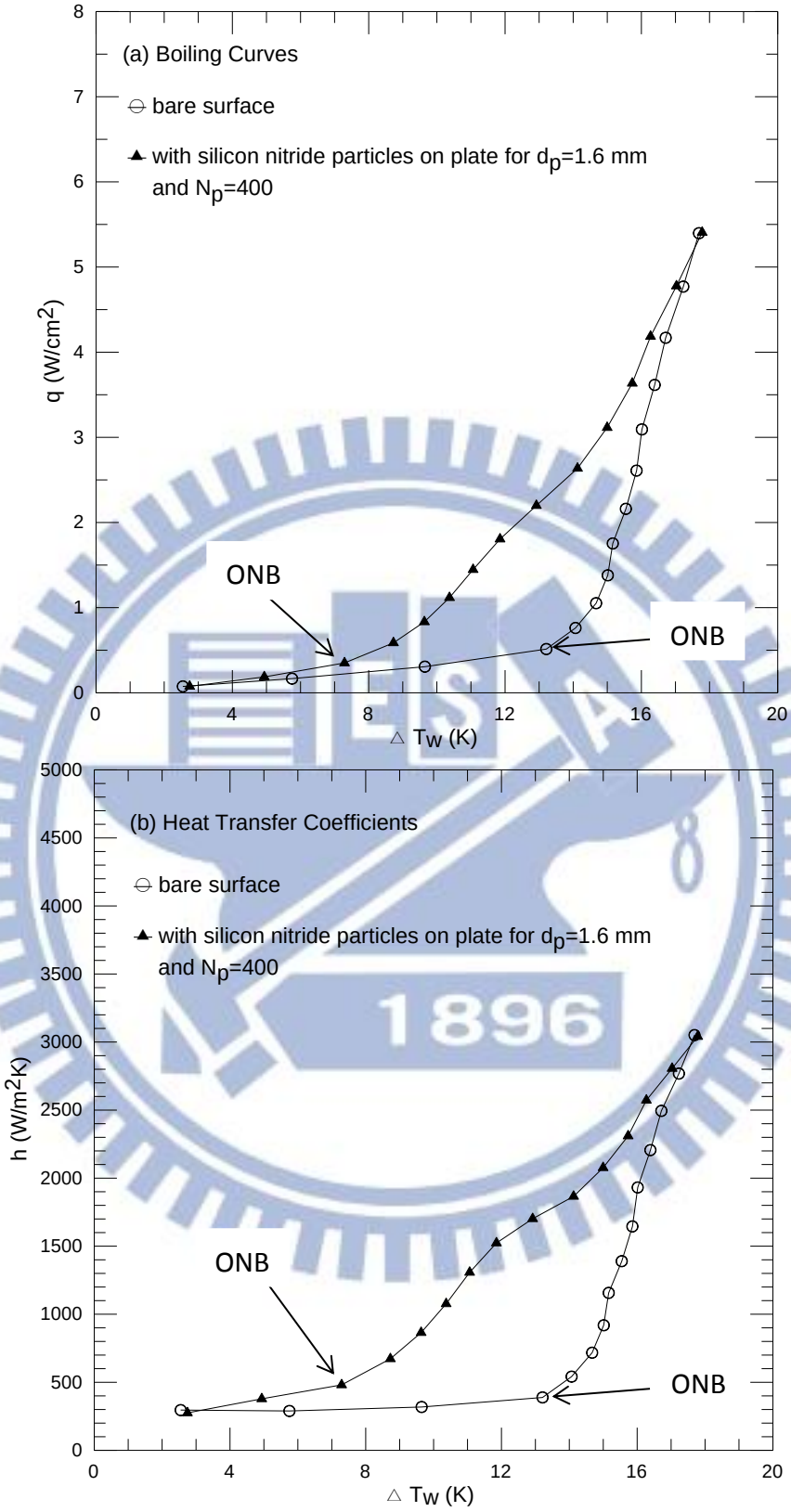

Fig. 4.25 Effects of silicon nitride particle diameter and number on saturated pool boiling curves (a) and boiling heat transfer coefficients (b) at d_p=1.6 mm and $N_p = 400$.

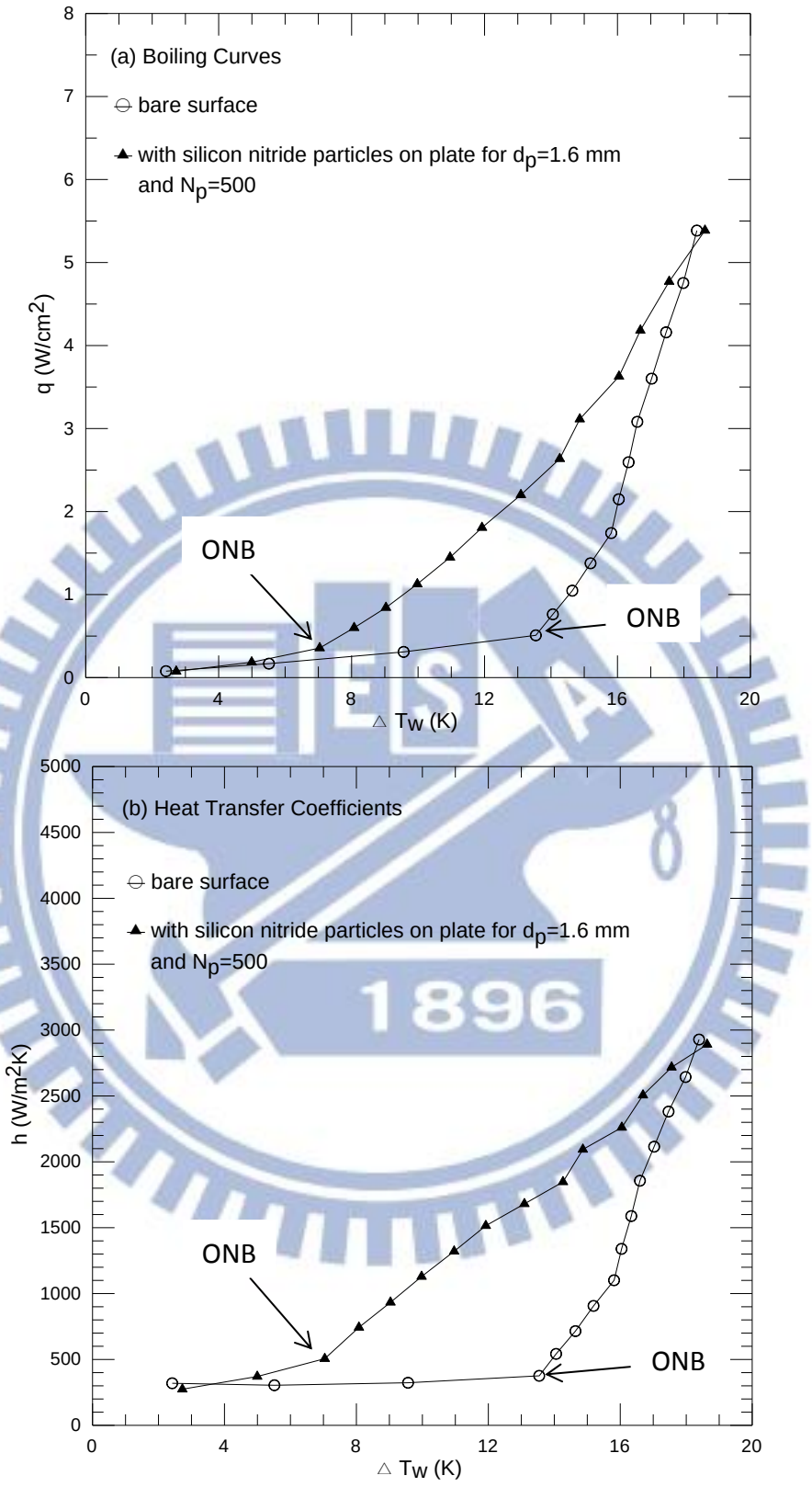

Fig. 4.26 Effects of silicon nitride particle diameter and number on saturated pool boiling curves (a) and boiling heat transfer coefficients (b) at d_p=1.6 mm and $N_p = 500$.

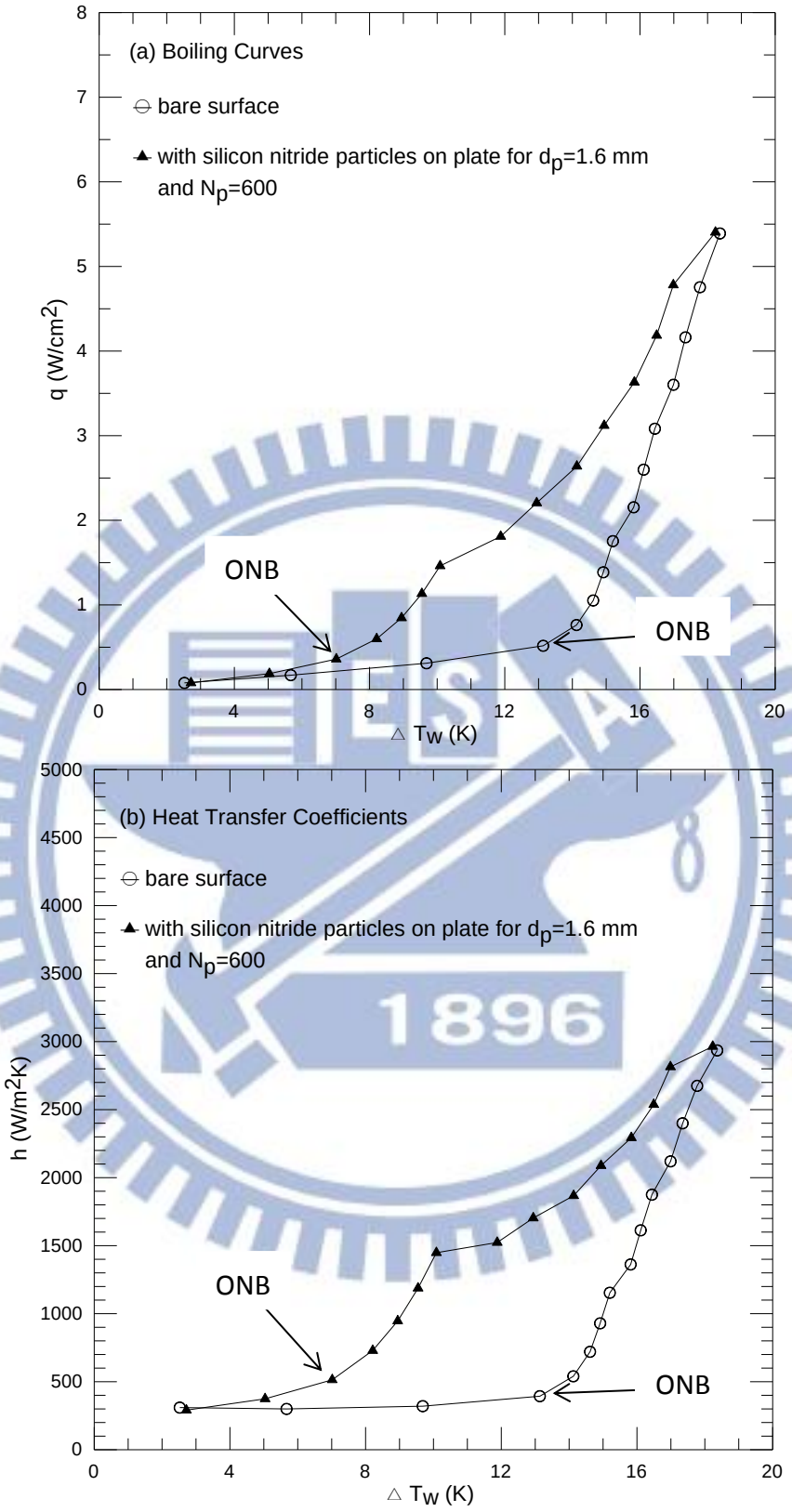

Fig. 4.27 Effects of silicon nitride particle diameter and number on saturated pool boiling curves (a) and boiling heat transfer coefficients (b) at d_p=1.6 mm and $N_p = 600$.

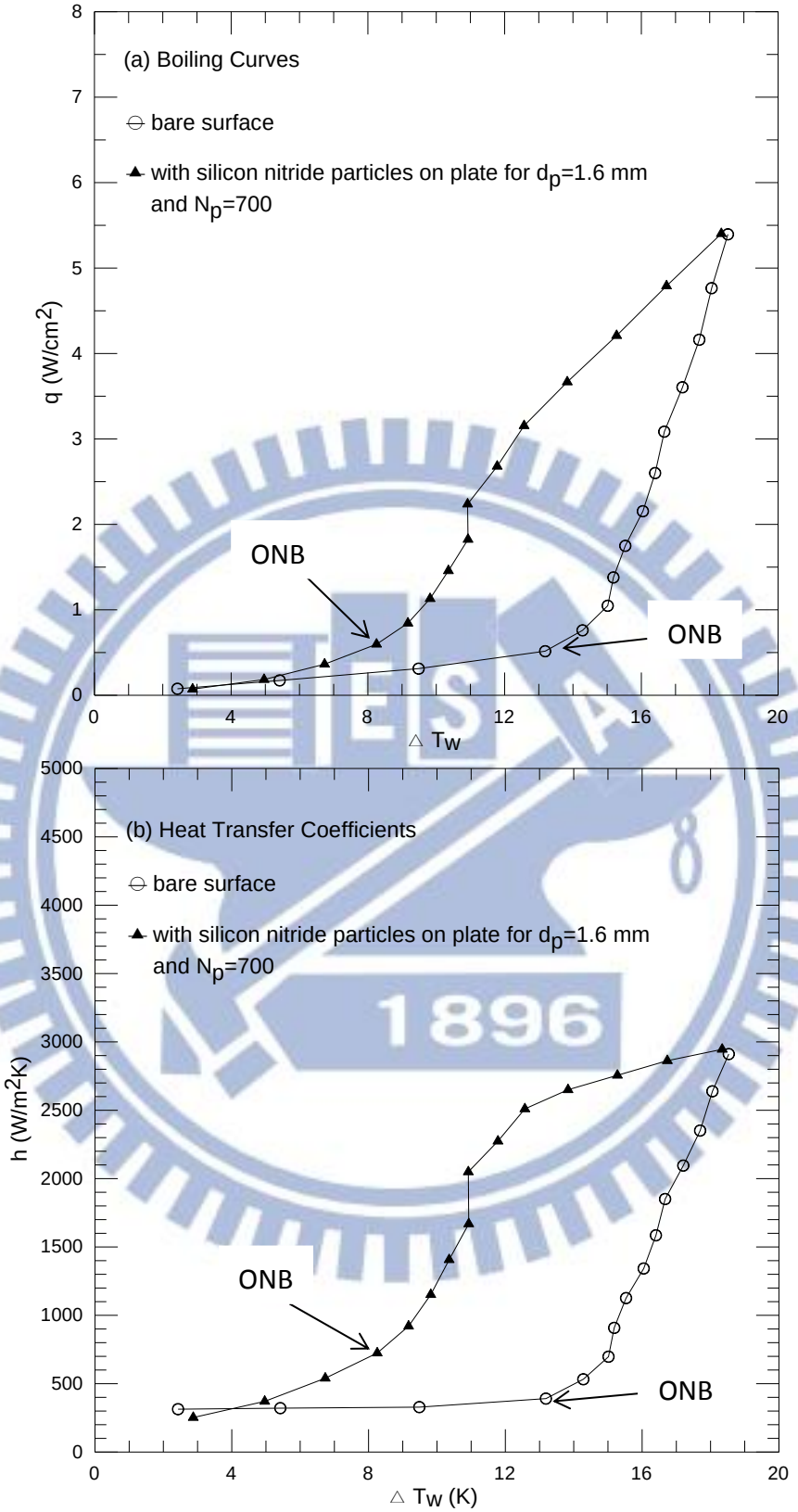

Fig. 4.28 Effects of silicon nitride particle diameter and number on saturated pool boiling curves (a) and boiling heat transfer coefficients (b) at d_p=1.6 mm and $N_p = 700$.

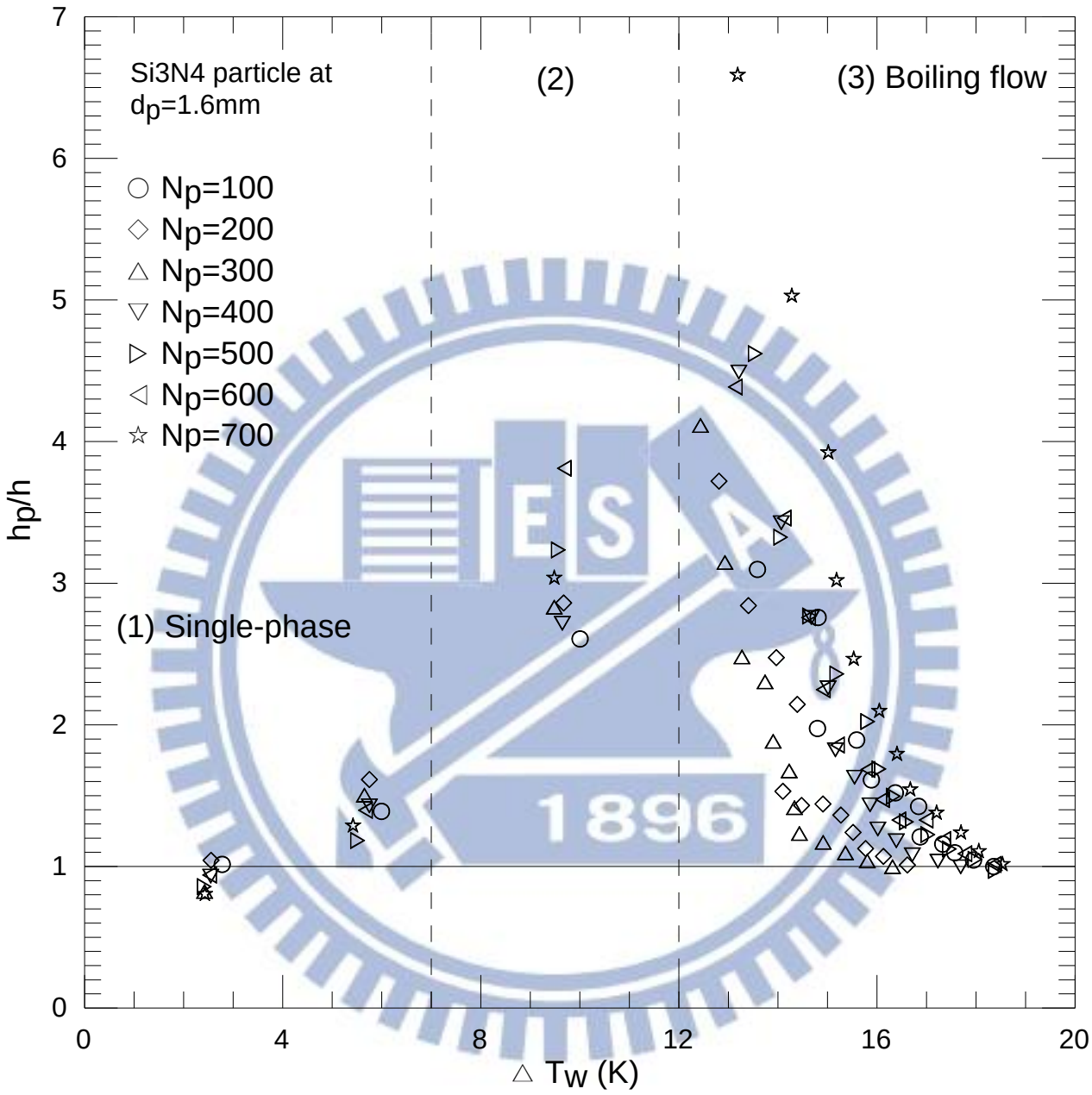

Fig. 4.29 Variations of h_p/h with wall superheat for various silicon nitride particle numbers at d_p=1.6 mm (the middle area represent single phase for particles on heated plate and boiling for bare surface)

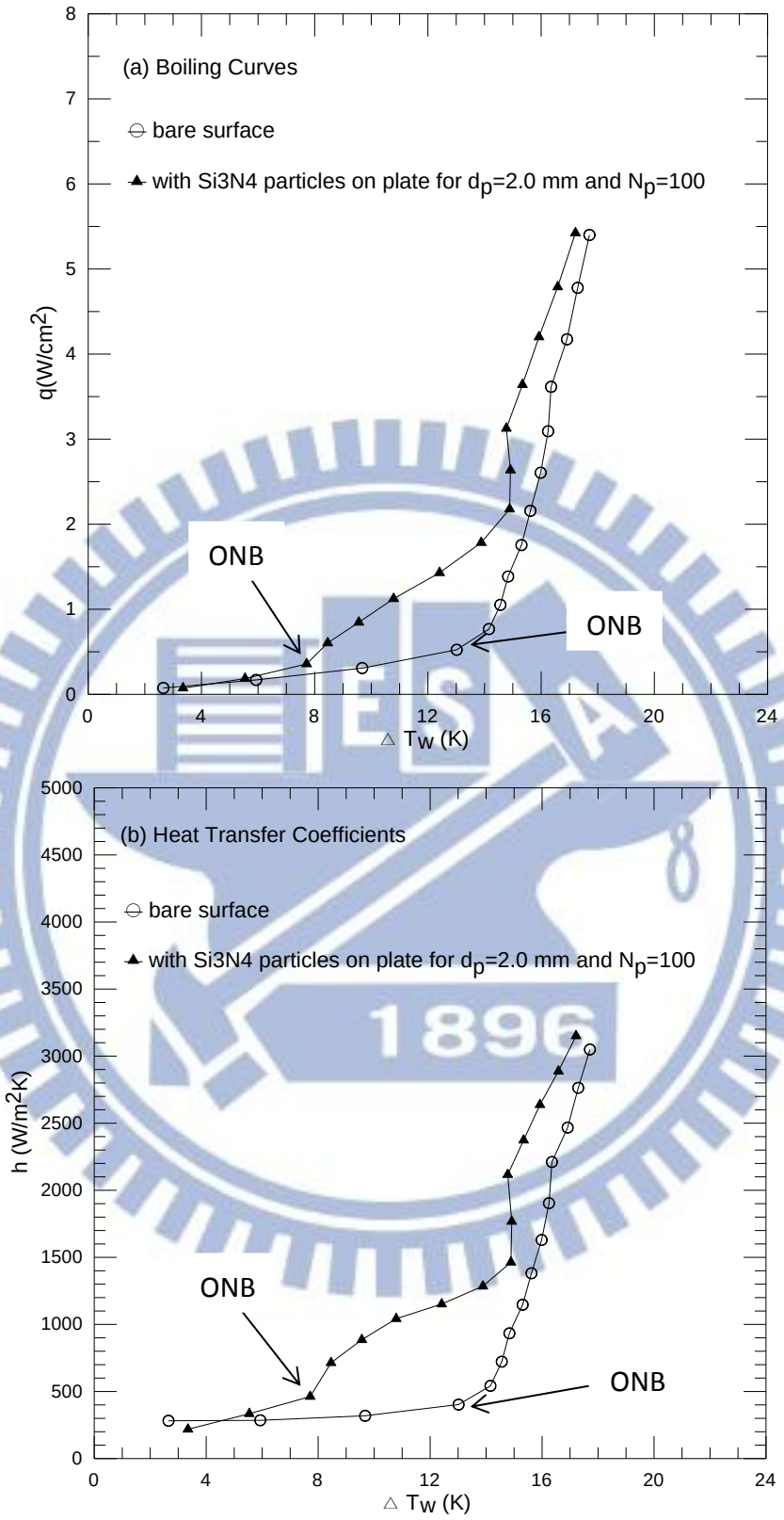

Fig. 4.30 Effects of silicon nitride particle diameter and number on saturated pool boiling curves (a) and boiling heat transfer coefficients (b) at d_p=2.0 mm and $N_p = 100$.

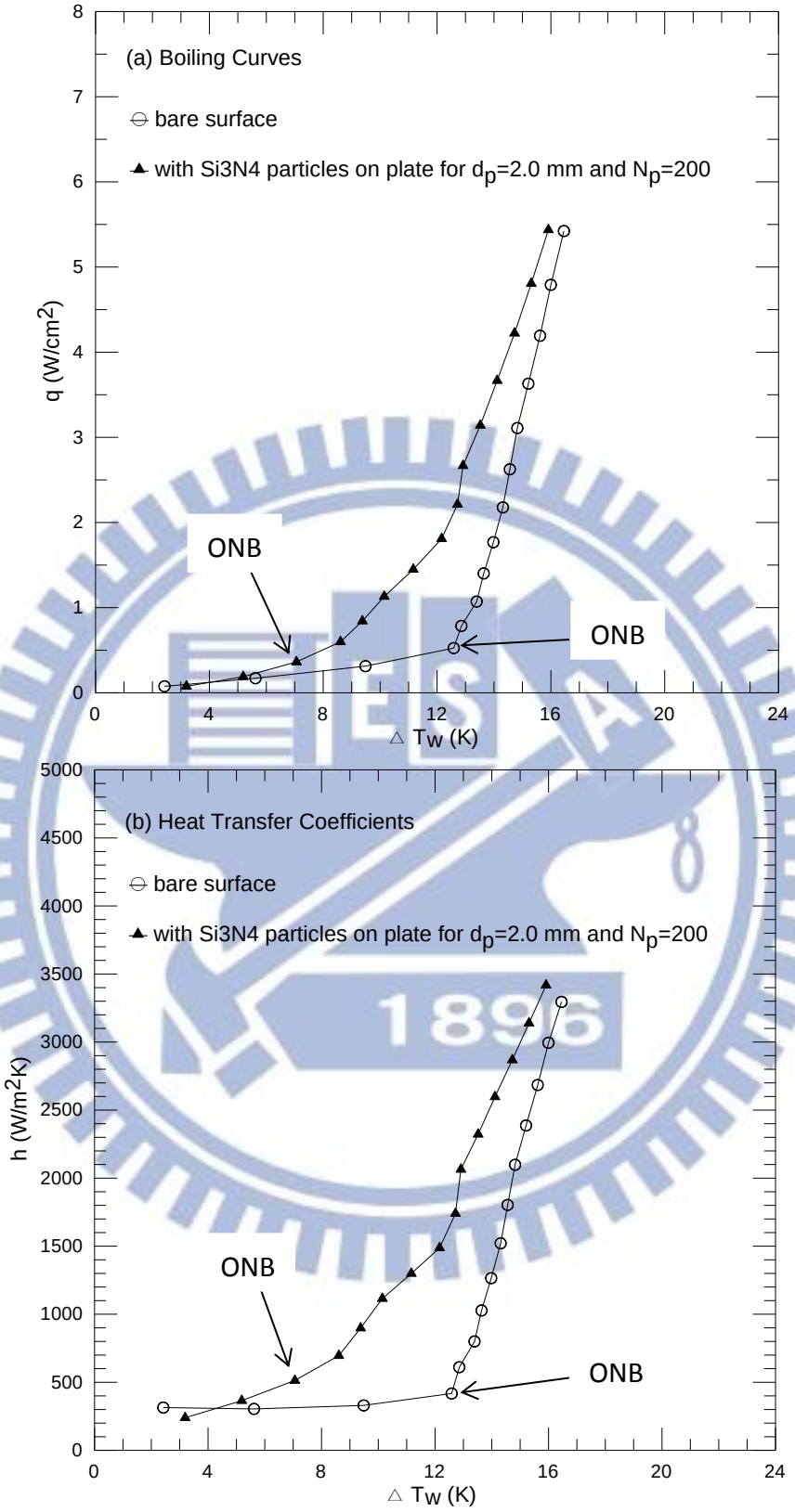

Fig. 4.31 Effects of silicon nitride particle diameter and number on saturated pool boiling curves (a) and boiling heat transfer coefficients (b) at d_p=2.0 mm and $N_p = 200$.

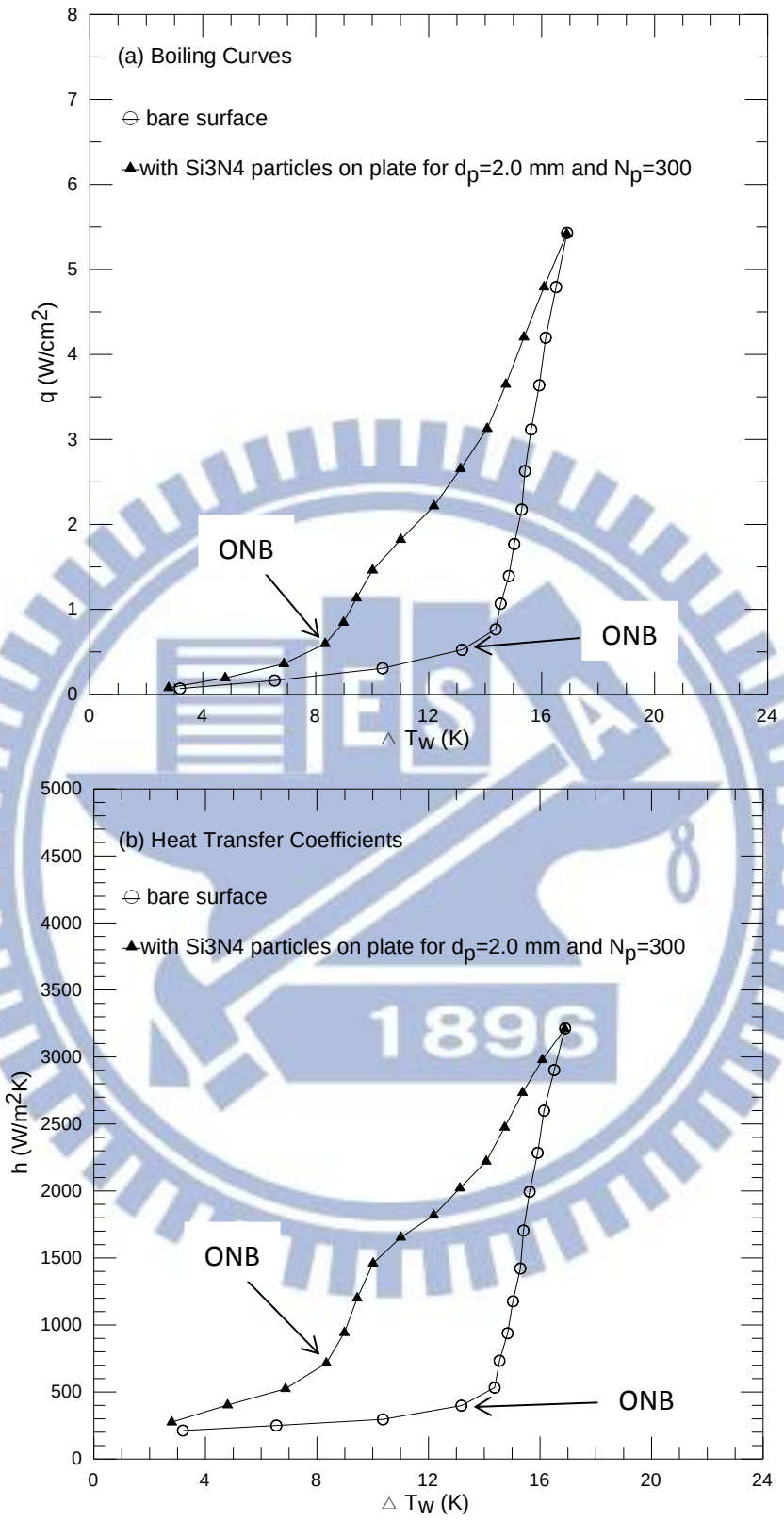

Fig. 4.32 Effects of silicon nitride particle diameter and number on saturated pool boiling curves (a) and boiling heat transfer coefficients (b) at d_p=2.0 mm and $N_p = 300$.

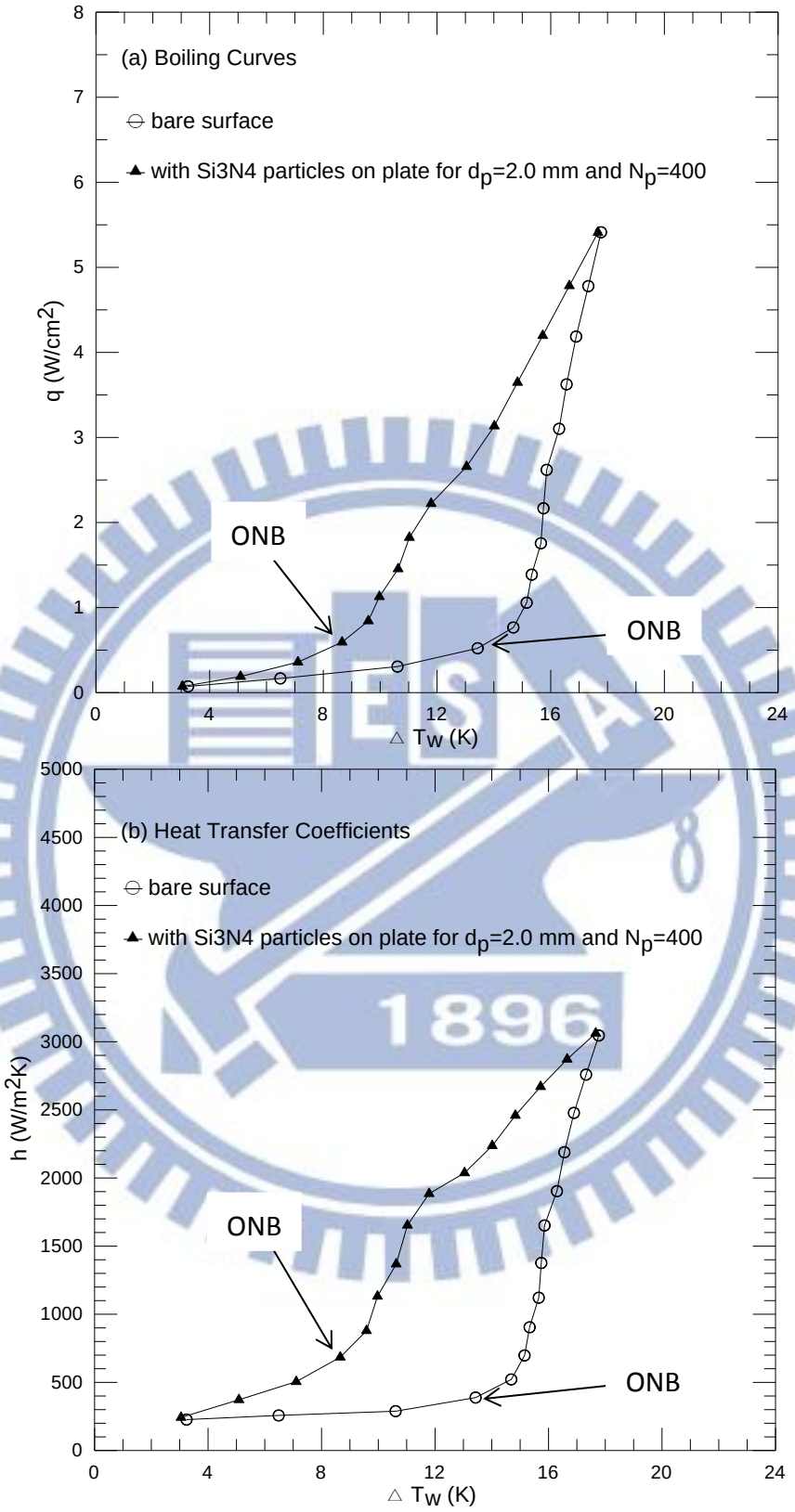

Fig. 4.33 Effects of silicon nitride particle diameter and number on saturated pool boiling curves (a) and boiling heat transfer coefficients (b) at d_p=2.0 mm and $N_p = 400$.

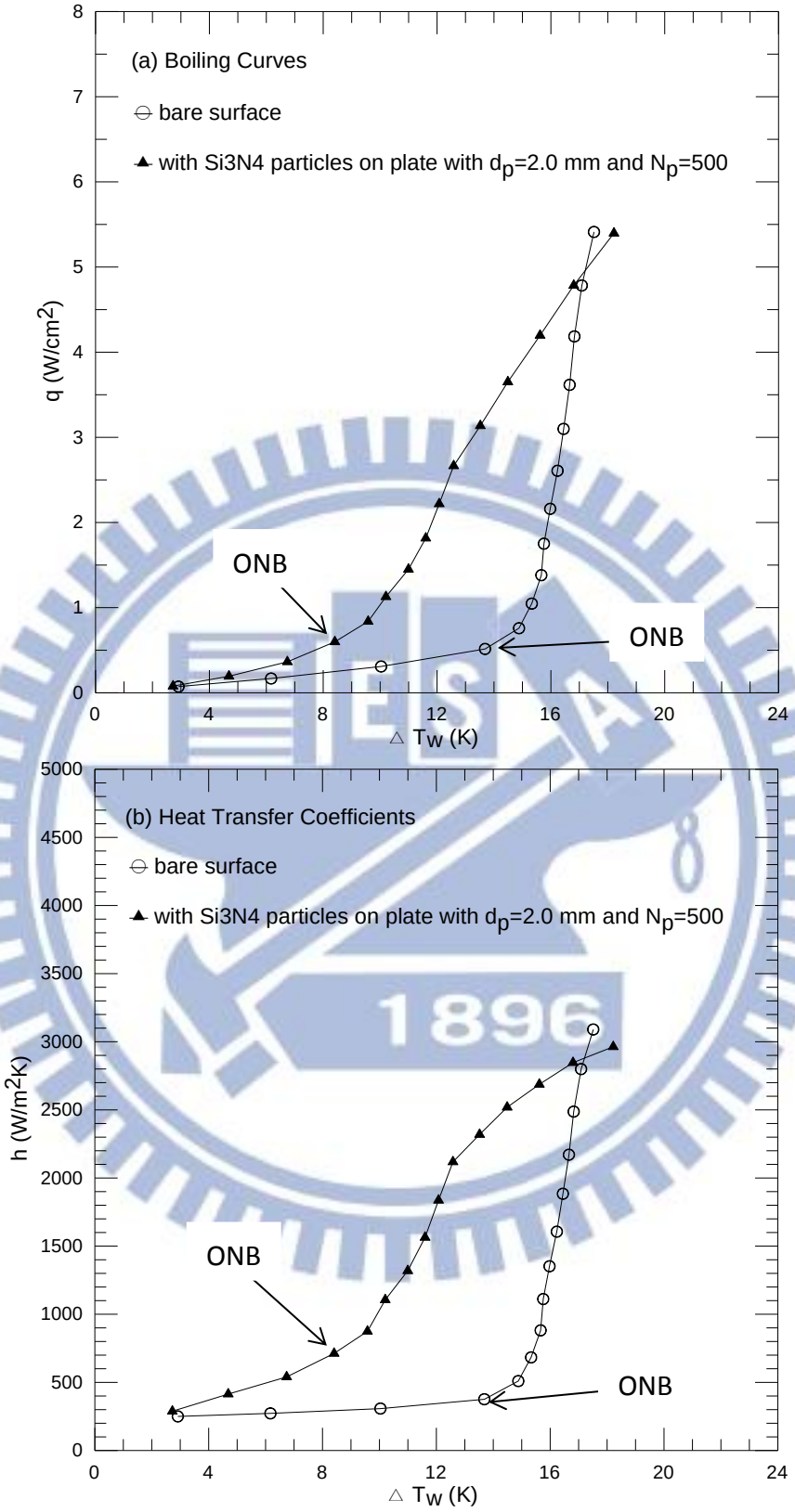

Fig. 4.34 Effects of silicon nitride particle diameter and number on saturated pool boiling curves (a) and boiling heat transfer coefficients (b) at d_p=2.0 mm and $N_p = 500$.

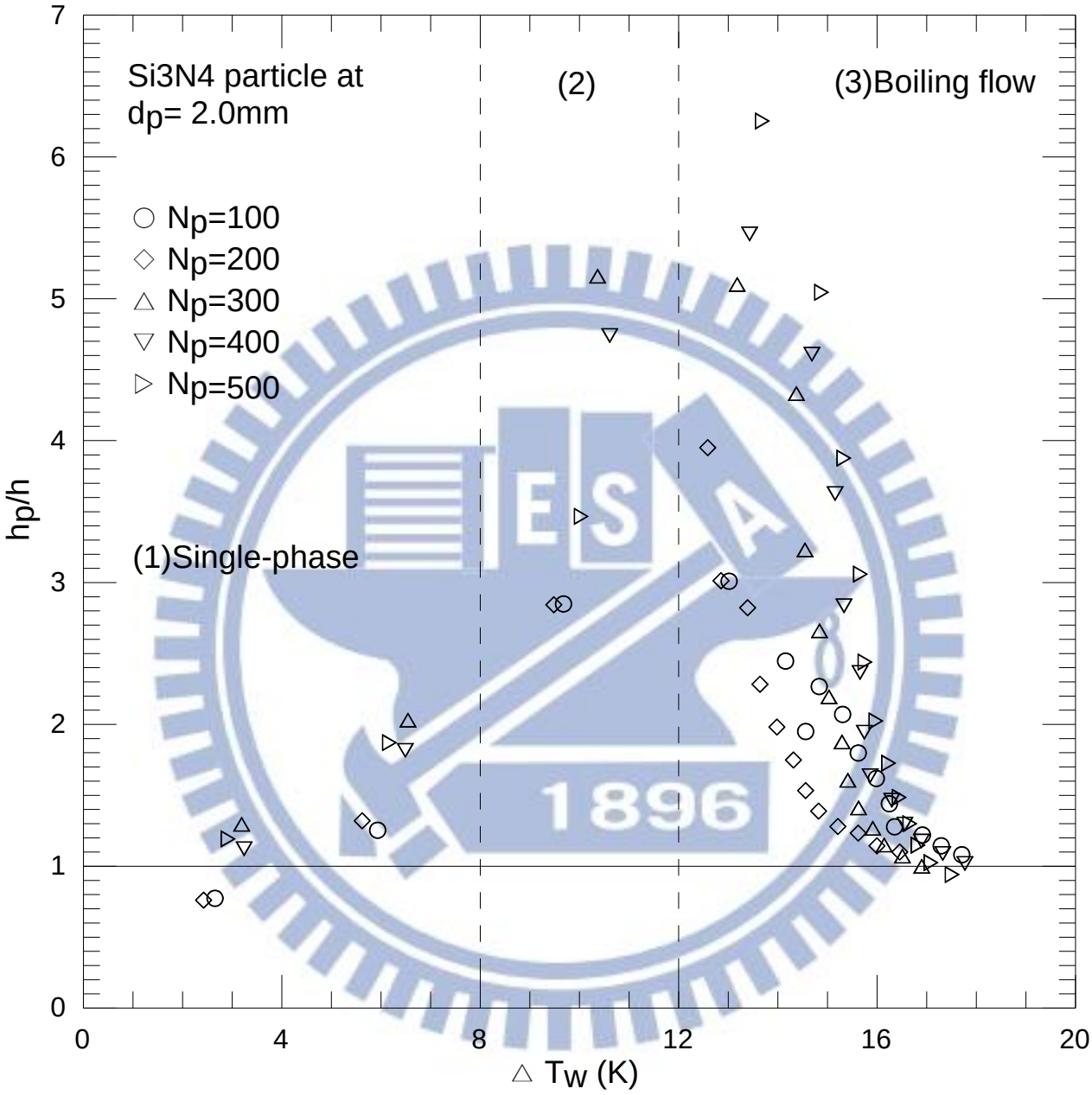

Fig. 4.35 Variations of h_p/h with wall superheat for various silicon nitride particle numbers at d_p=2.0 mm (the middle area represent single phase for particles on heated plate and boiling for bare surface)

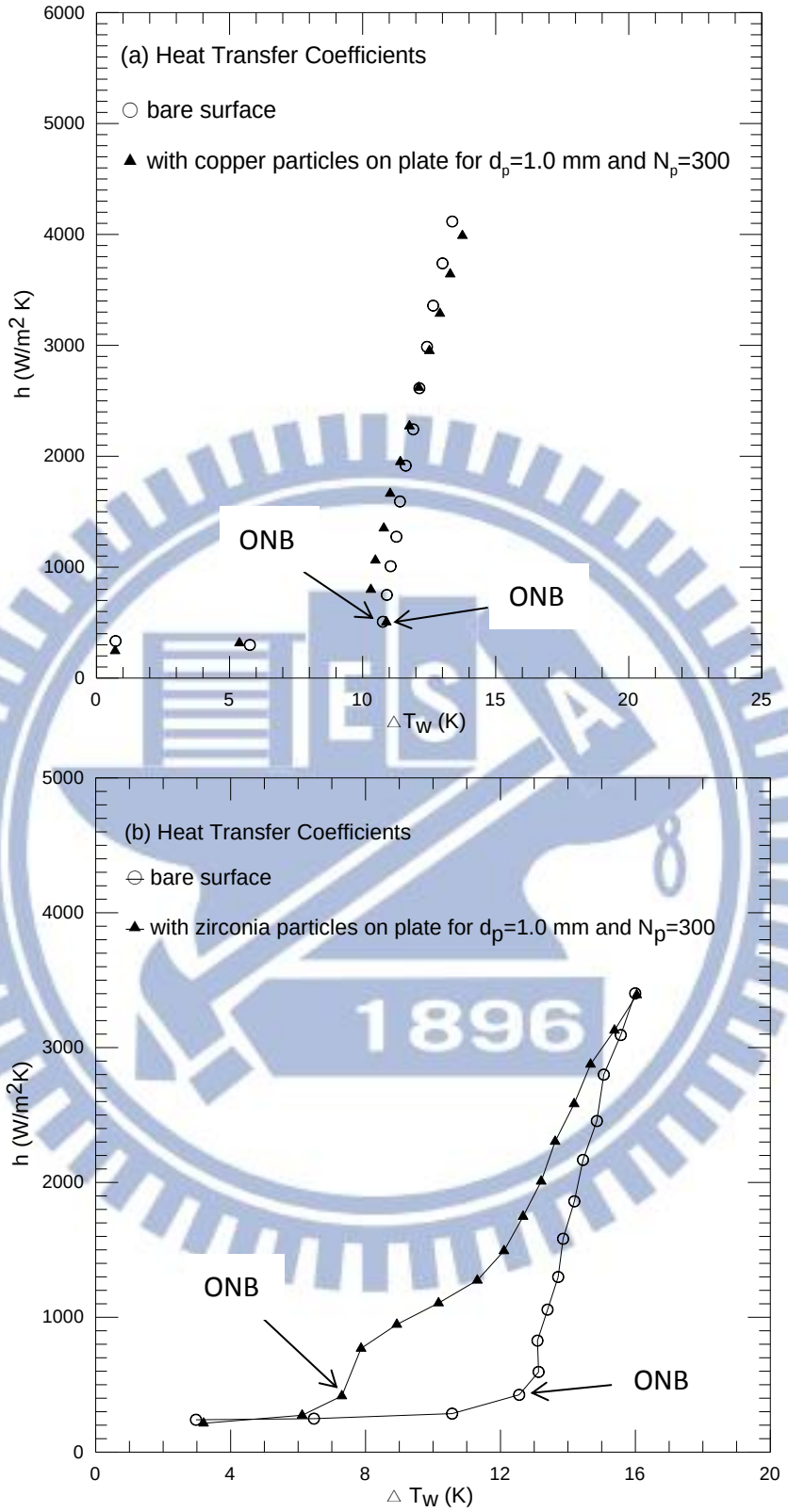

Fig. 4.36 Effects of particle material on boiling heat transfer coefficients for (a) copper particles and (b) zirconia particles at d_p=1.0 mm and $N_p = 300$.

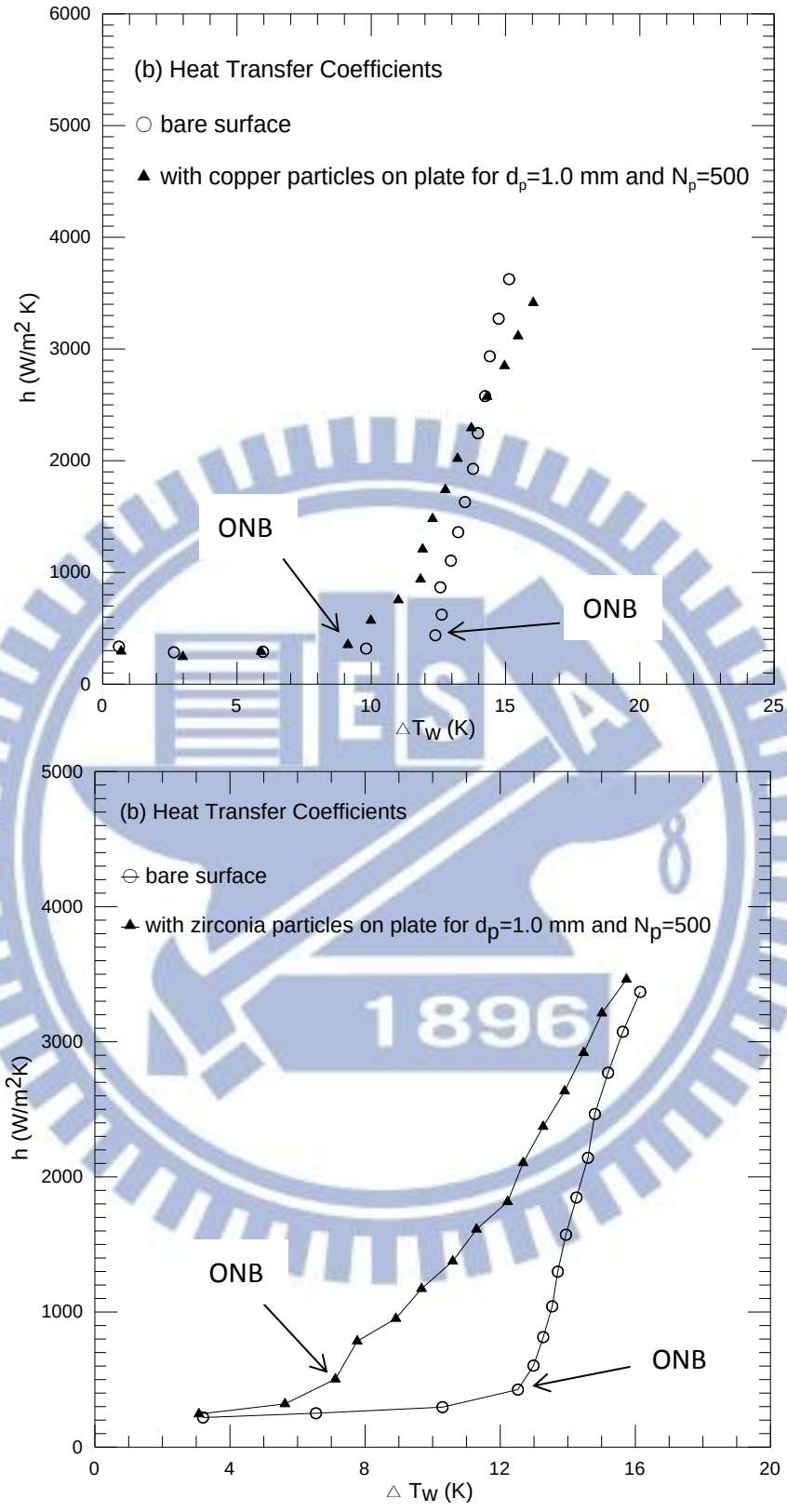

Fig. 4.37 Effects of particle material on boiling heat transfer coefficients for (a) copper particles and (b) zirconia particles at d_p=1.0 mm and $N_p = 500$.

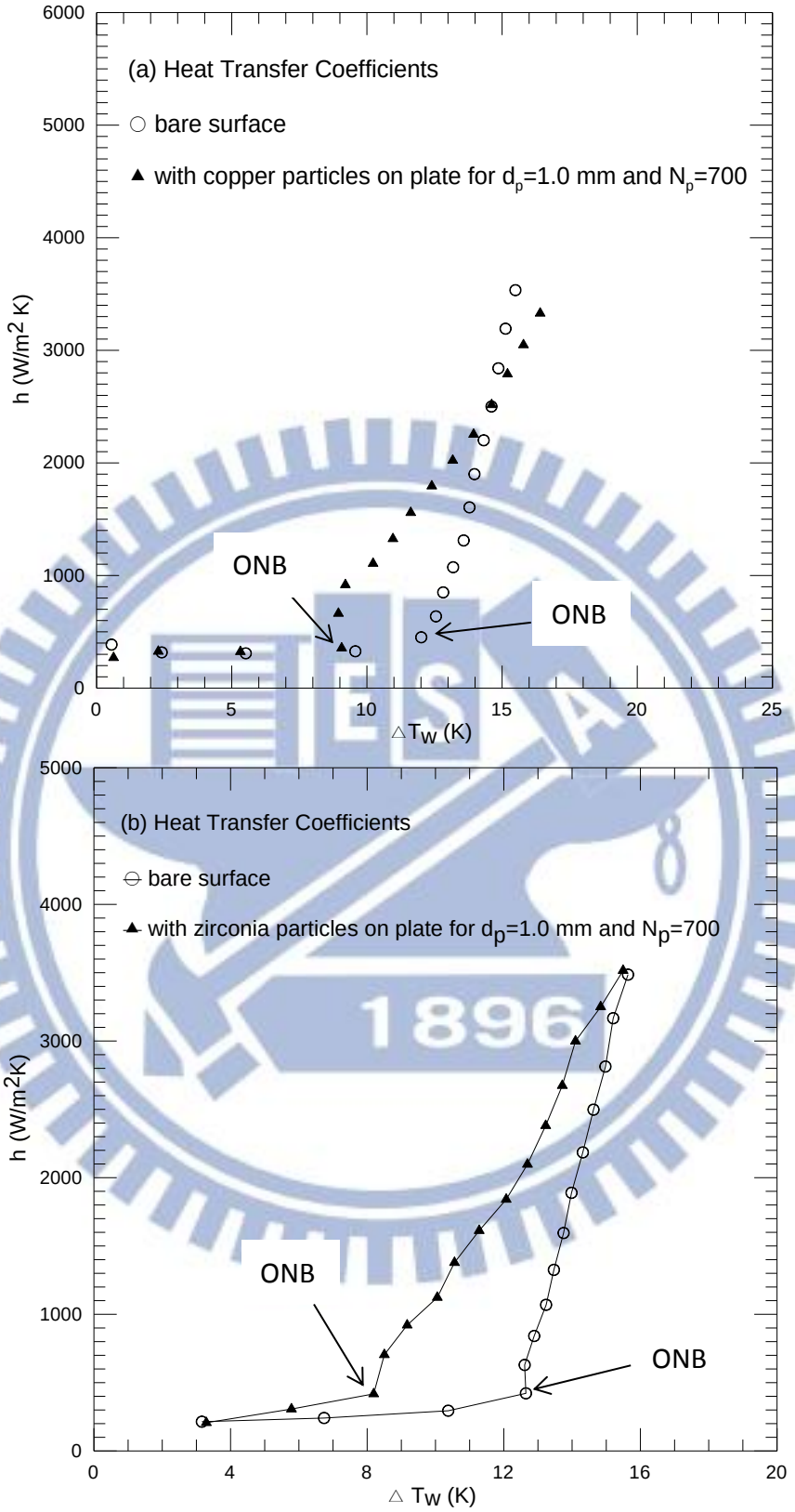

Fig. 4.38 Effects of particle material on boiling heat transfer coefficients for (a) copper particles and (b) zirconia particles at d_p=1.0 mm and $N_p = 700$.

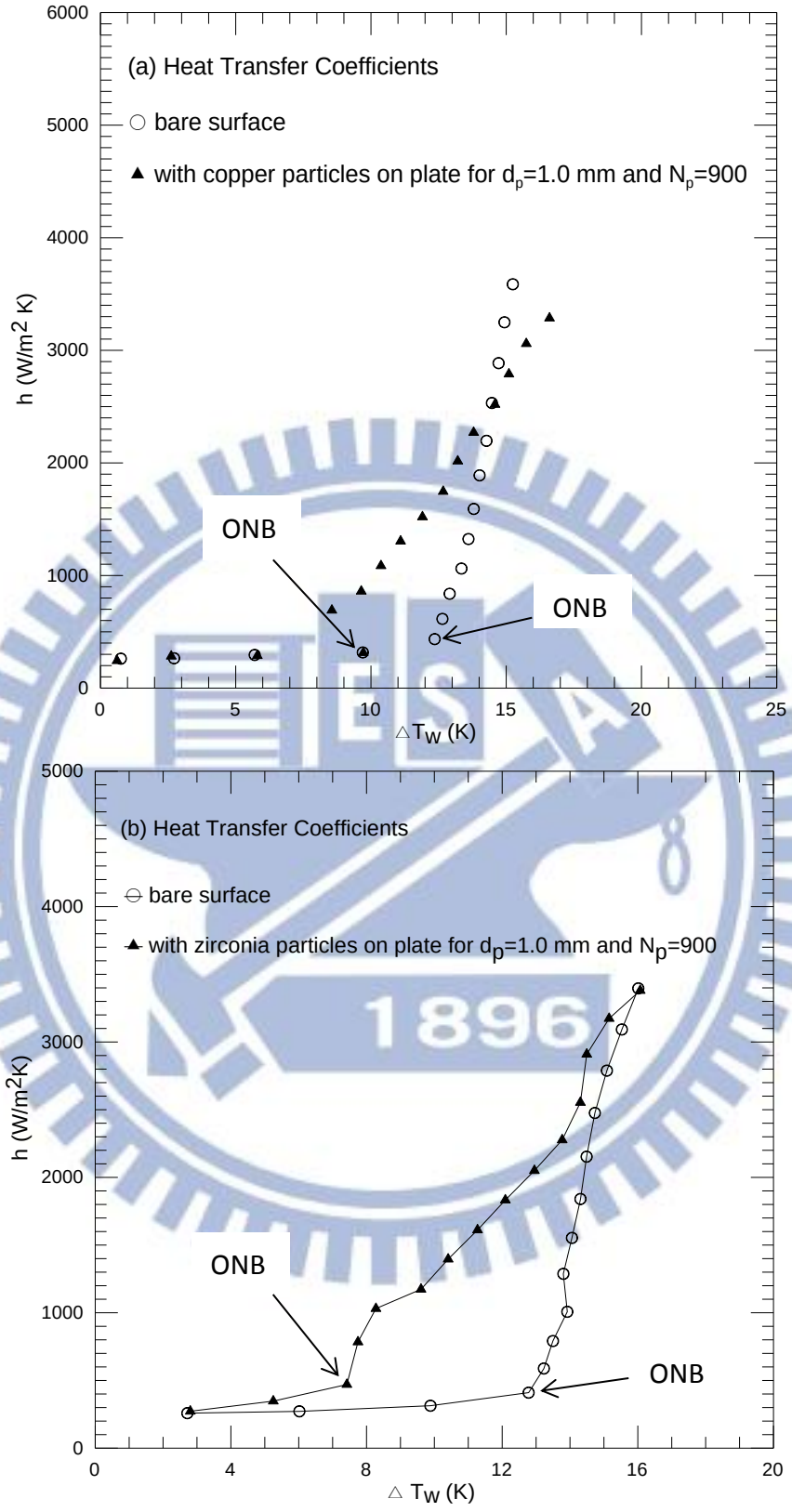

Fig. 4.39 Effects of particle material on boiling heat transfer coefficients for (a) copper particles and (b) zirconia particles at d_p=1.0 mm and $N_p = 900$.

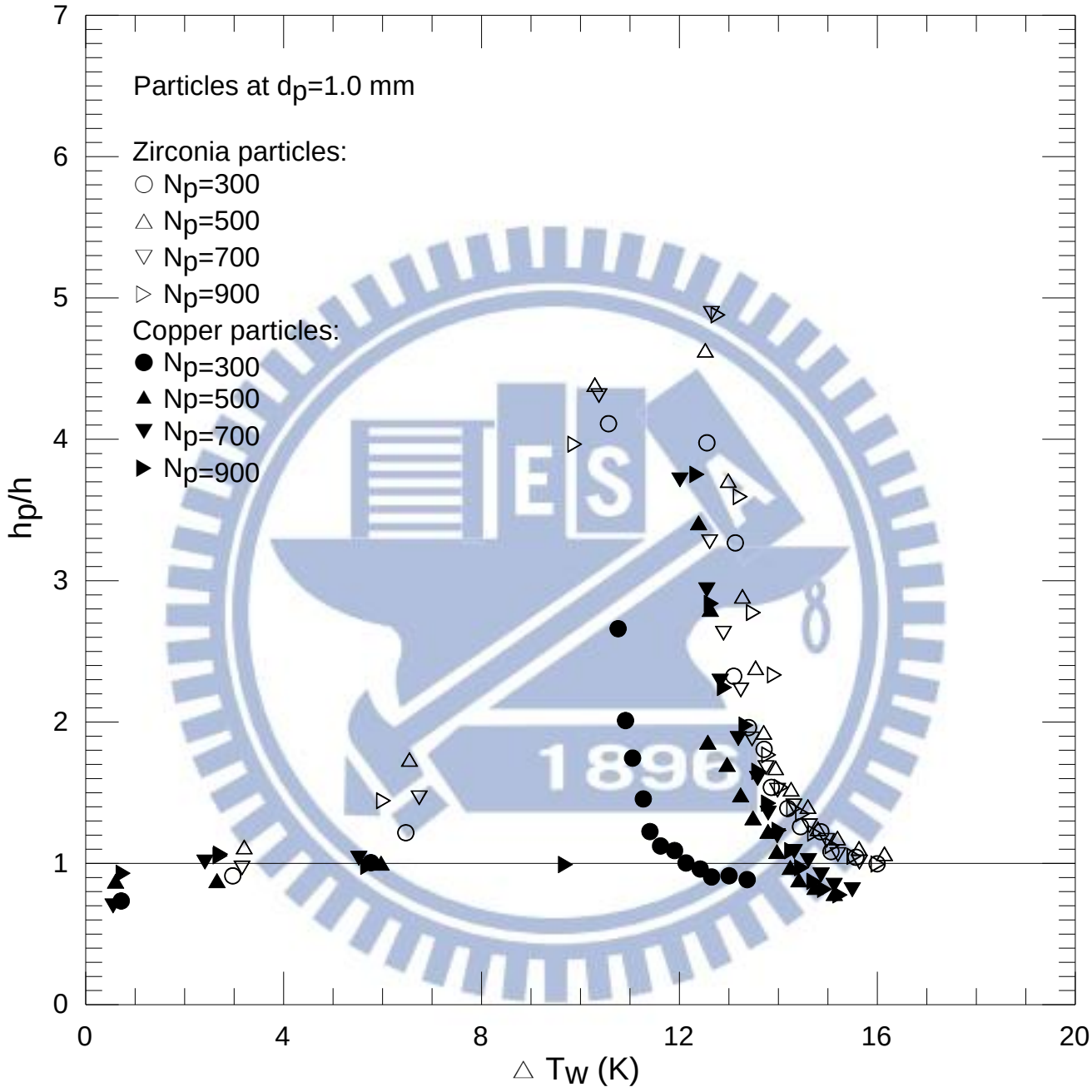

Fig. 4.40 Variations of h_p/h with wall superheat for zirconia and copper particles for various N_p at d_p=1.0 mm. (solid and empty symbols denote data for copper particles and zirconia particles, respectively)

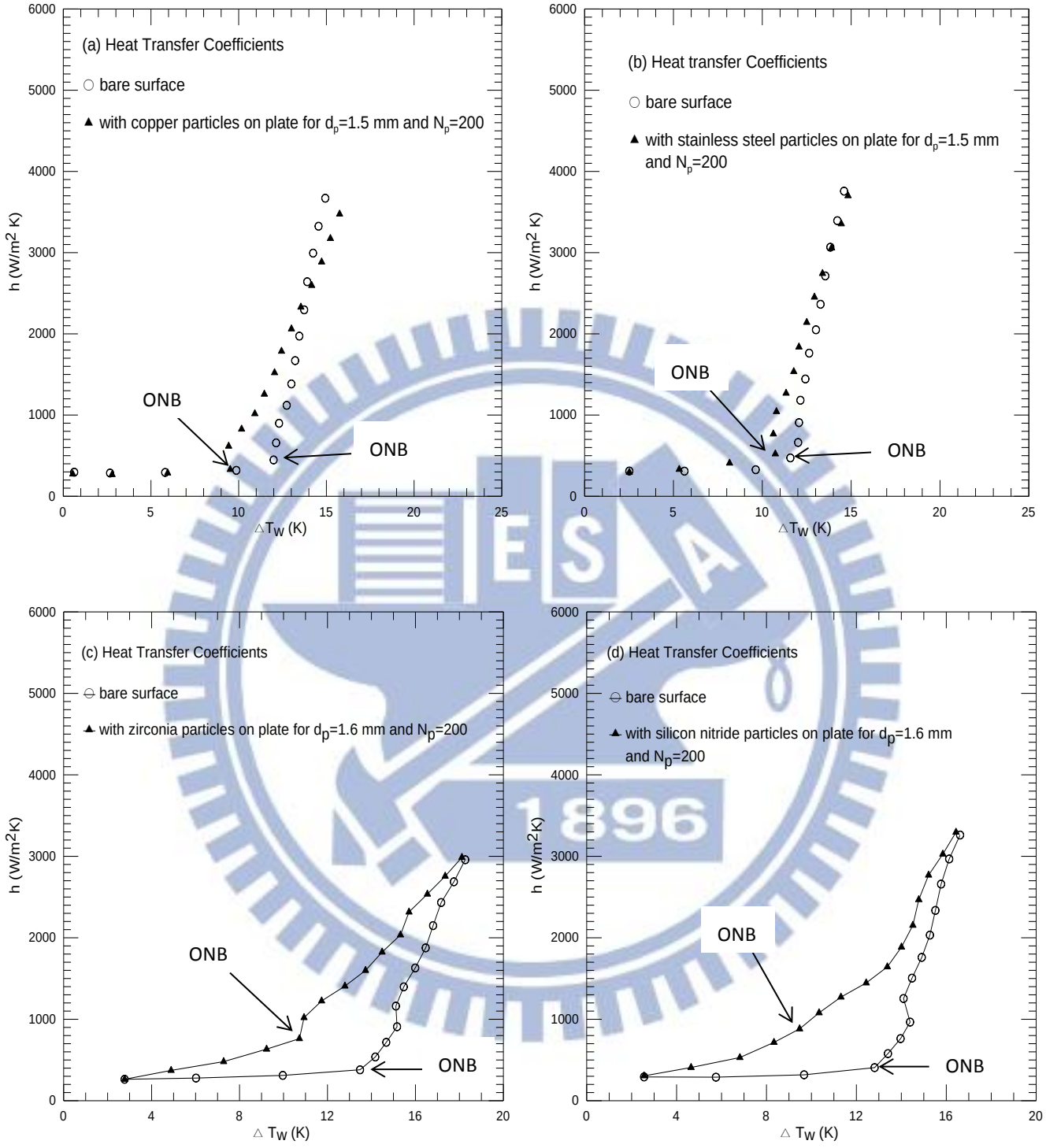

Fig. 4.41 Effects of particle material on boiling heat transfer coefficients for (a) copper particles, (b) stainless steel particles, (c) zirconia particles, and (d) silicon nitride particles at d_p=1.5 & 1.6 mm and $N_p = 200$.

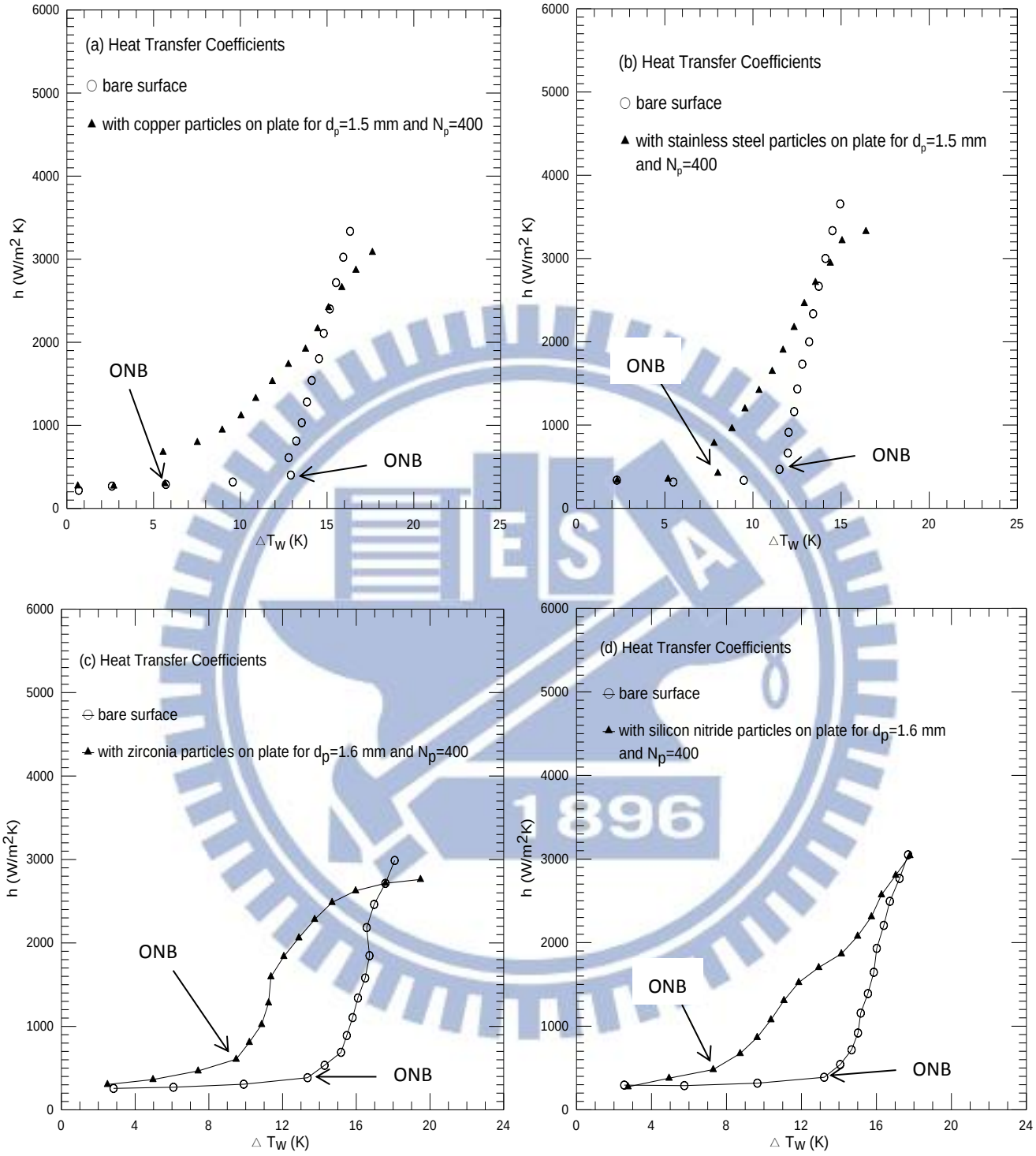

Fig. 4.42 Effects of particle material on boiling heat transfer coefficients for (a) copper particles, (b) stainless steel particles, (c) zirconia particles, and (d) silicon nitride particles at d_p=1.5 & 1.6 mm and $N_p = 400$.

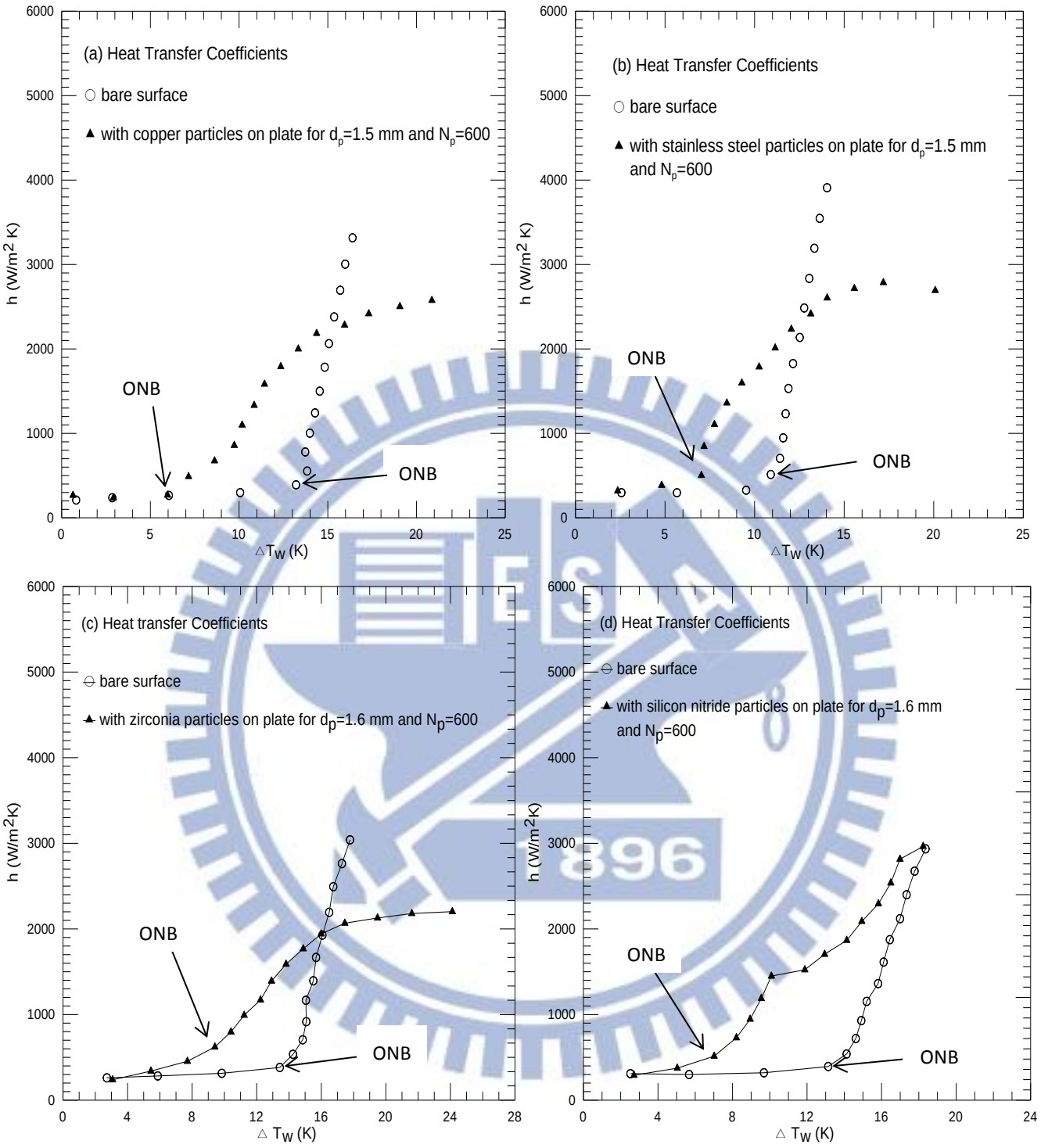

Fig. 4.43 Effects of particle material on boiling heat transfer coefficients for (a) copper particles, (b) stainless steel particles, (c) zirconia particles, and (d)silicon nitride particles at d_p=1.5 & 1.6 mm and $N_p = 600$.

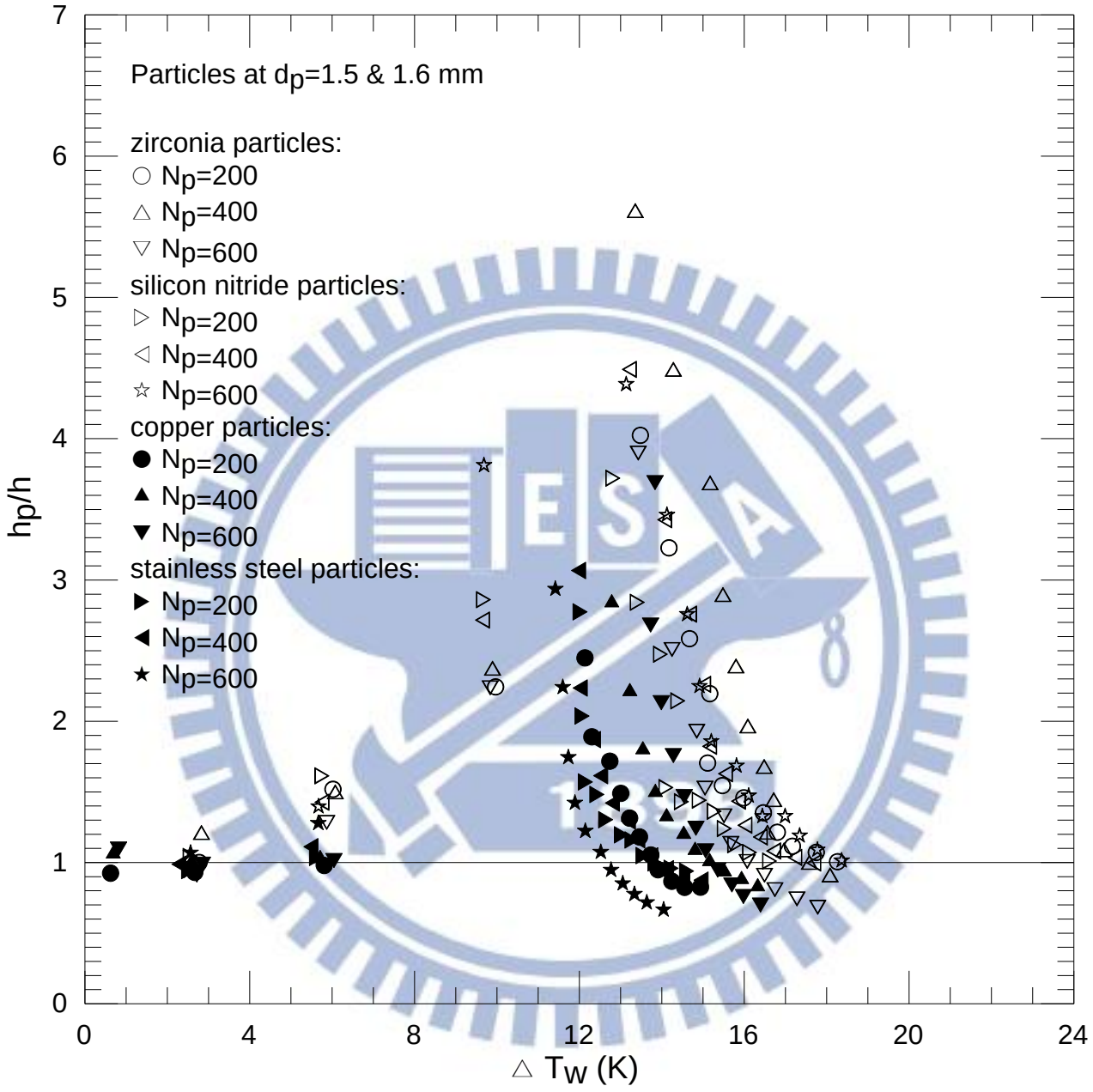

Fig. 4.44 Variations of h_p/h with wall superheat for zirconia, silicon nitride, copper, and stainless steel particles for various N_p at d_p=1.5 & 1.6 mm (solid symbols denote copper and stainless steel particles)

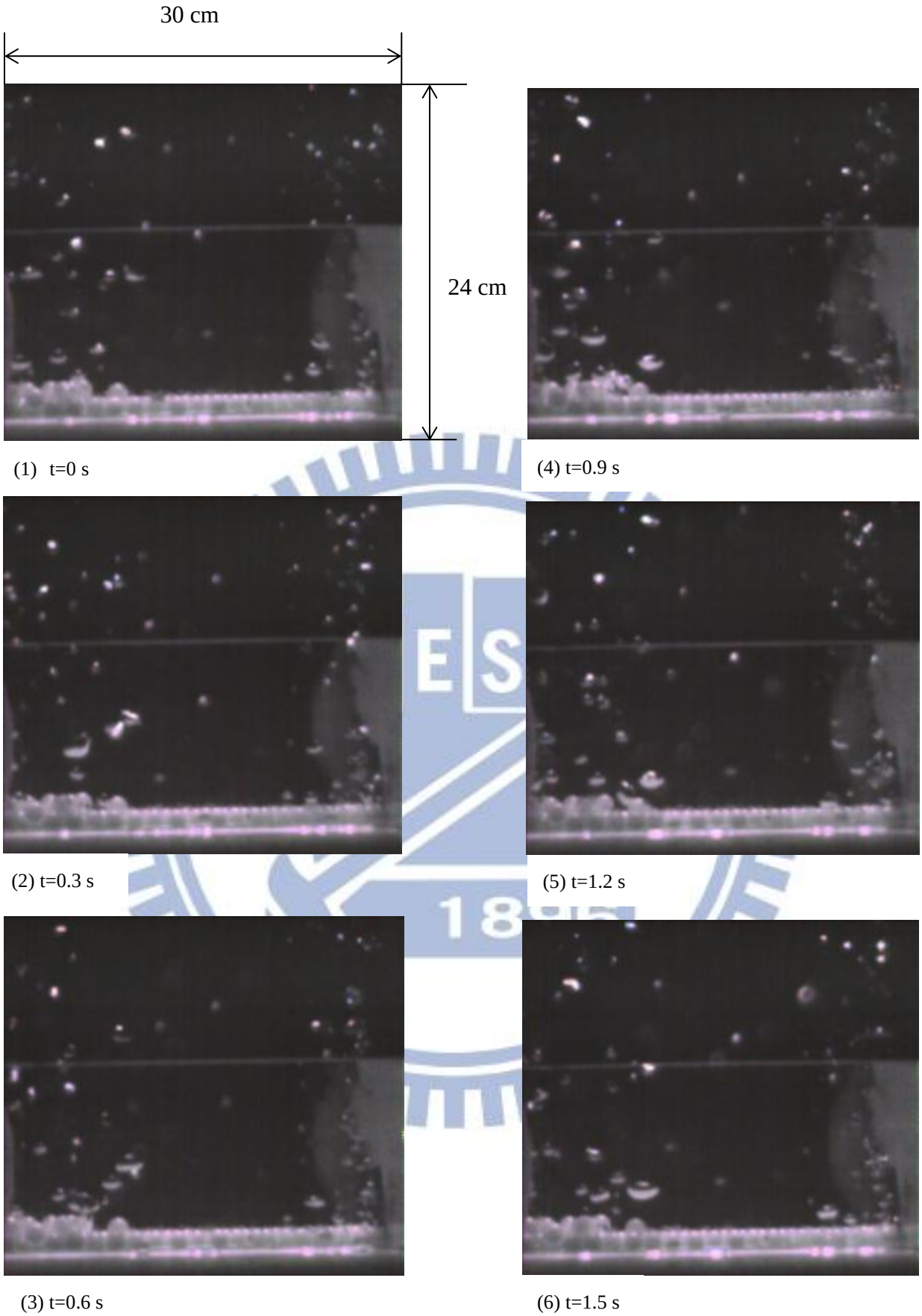

Fig. 4.45 Photos taken from side view of boiling flow at selected time instants for q= 0.39 W/ m^2 with zirconia particles on heated surface at d_p=1.6 mm and $N_p = 250$

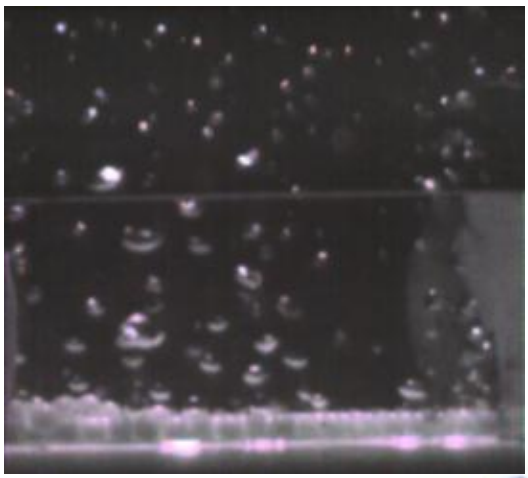

(1) t=0 s

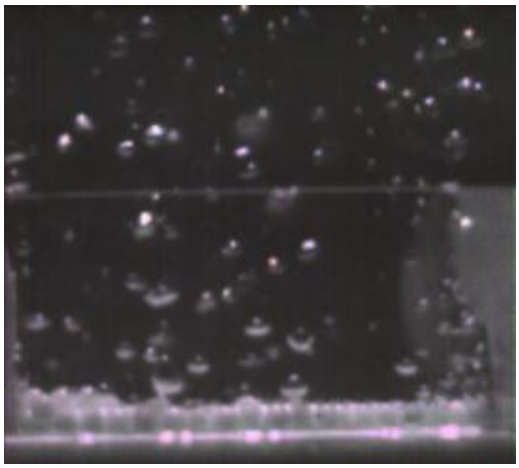

(4) t=1.2 s

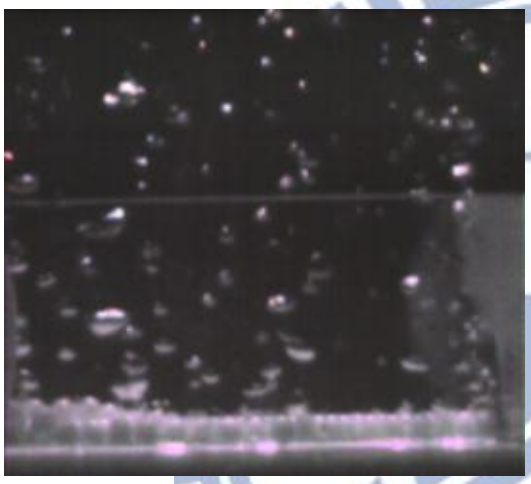

(2) t=0.4 s

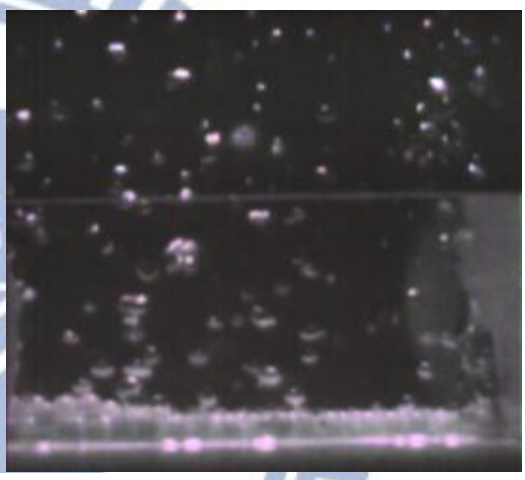

(5) t=1.6 s

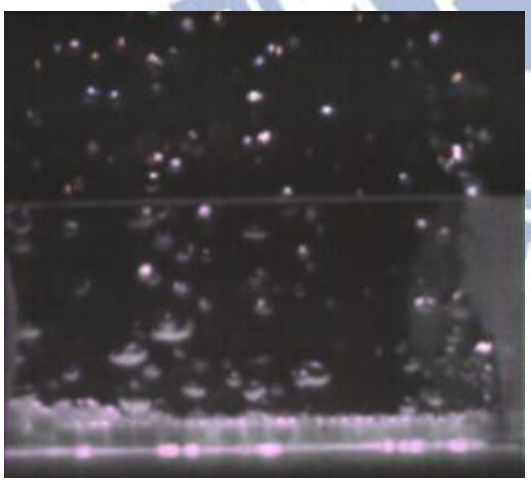

(3) t=0.8 s

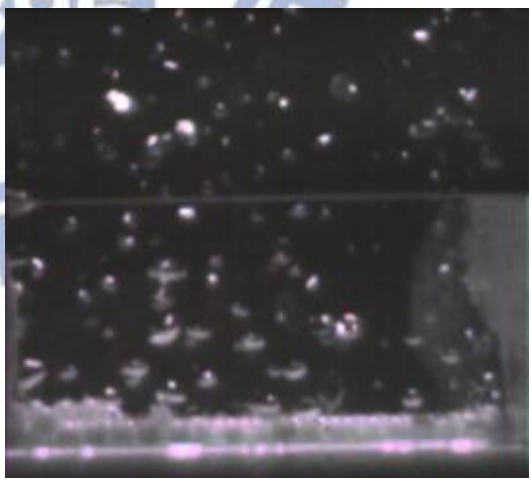

(6) t=2.0s

Fig. 4.46 Photos taken from side view of boiling flow at selected time instants for q= 0.61 W/ m^2 with zirconia particles on heated surface at d_p=1.6 mm and $N_p = 250$

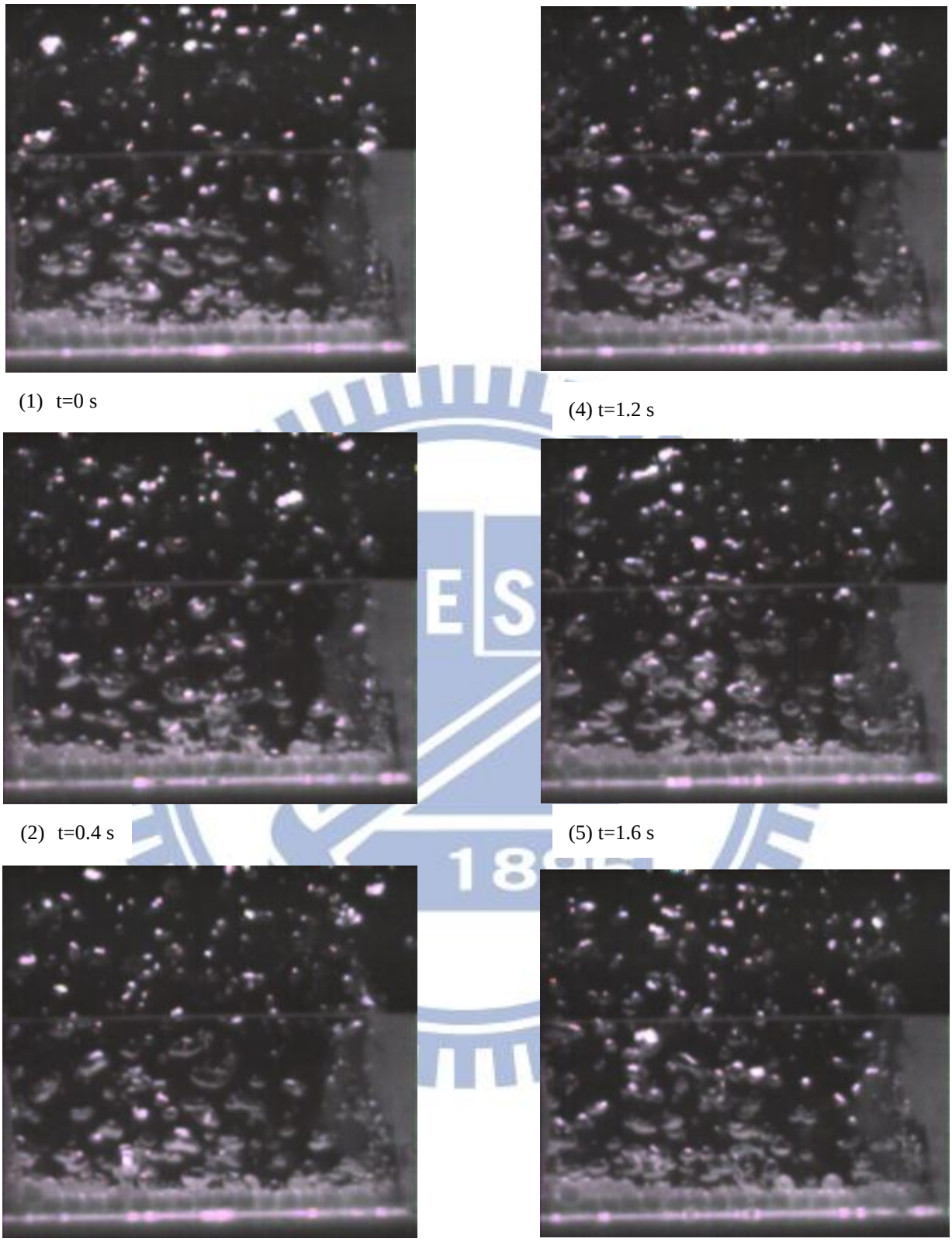

(1) t=0 s (4) t=1.2 s

(2) t=0.4 s (5) t=1.6 s

(3) t=0.8 s (6) t=2.0 s

Fig. 4.47 Photos taken from side view of boiling flow at selected time instants for q= 1.11 W/ m^2 with zirconia particles on heated surface at d_p=1.6 mm and $N_p = 250$

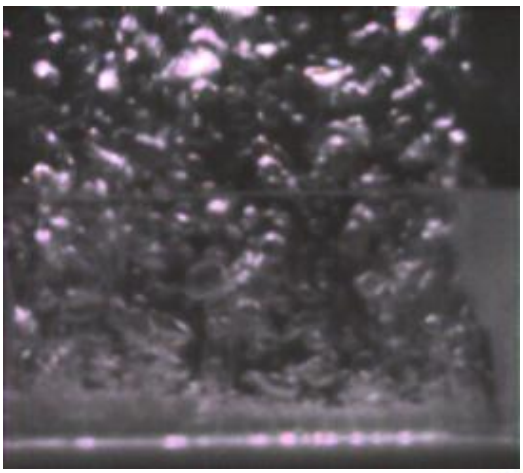

(1) t=0 s

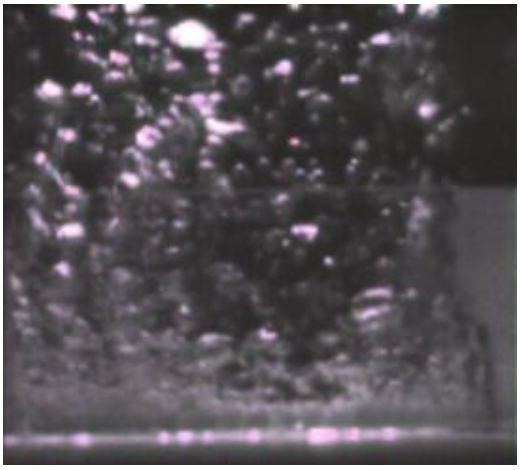

(4) t=1.2 s

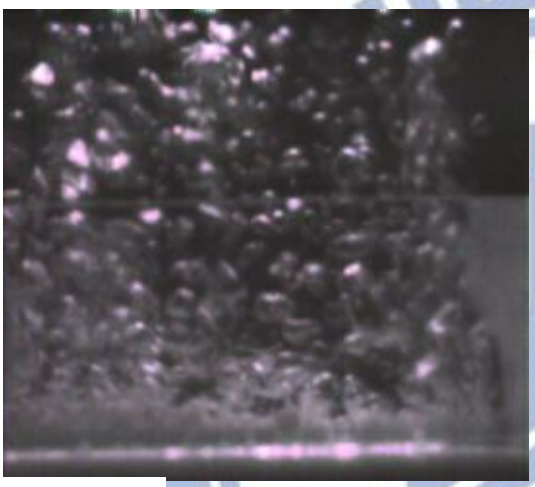

(2) t=0.4 s

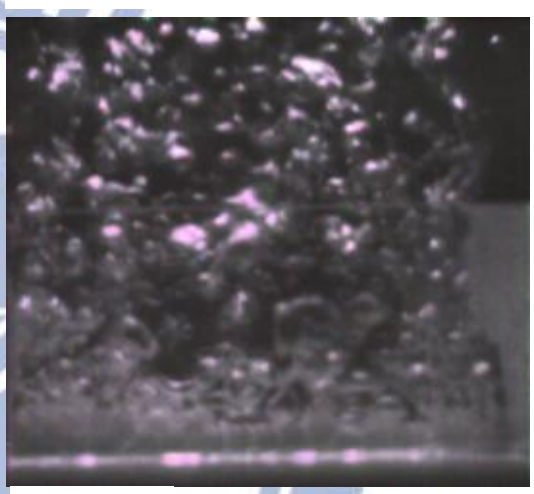

(5) t=1.6 s

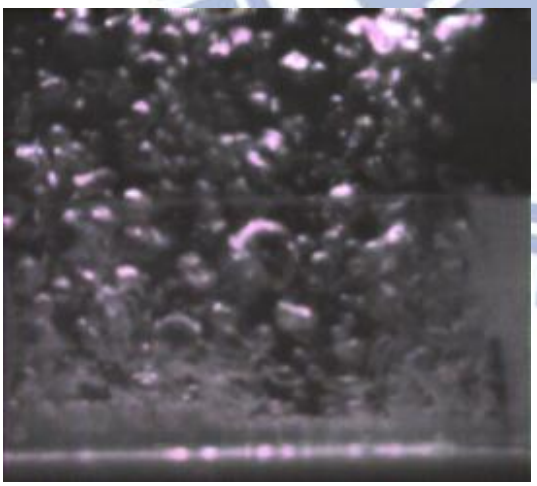

(3) t=0.8 s

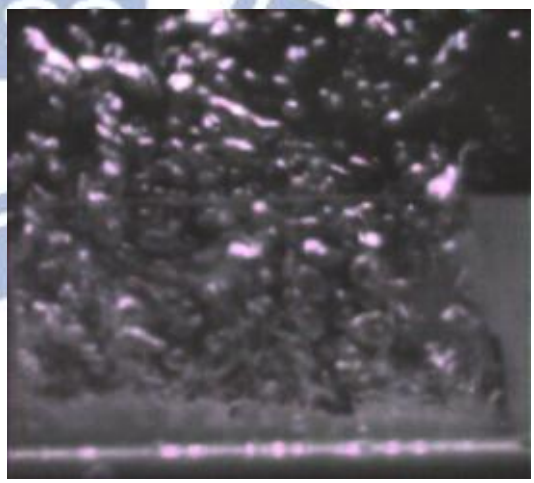

(6) t=2.0 s

Fig. 4.48 Photos taken from side view of boiling flow at selected time instants for q= 2.67 W/ m^2 with zirconia particles on heated surface at d_p=1.6 mm and $N_p = 250$

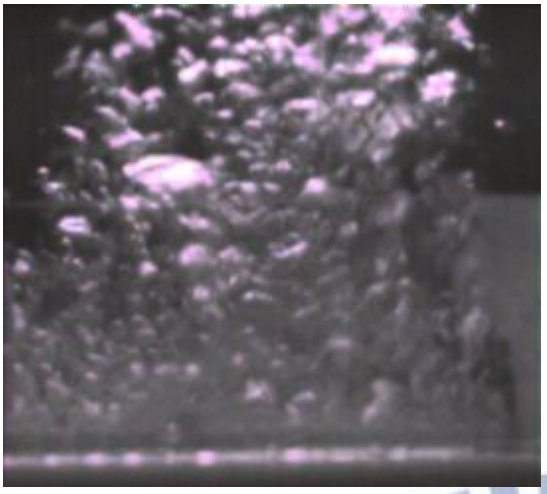

(2) t=0 s

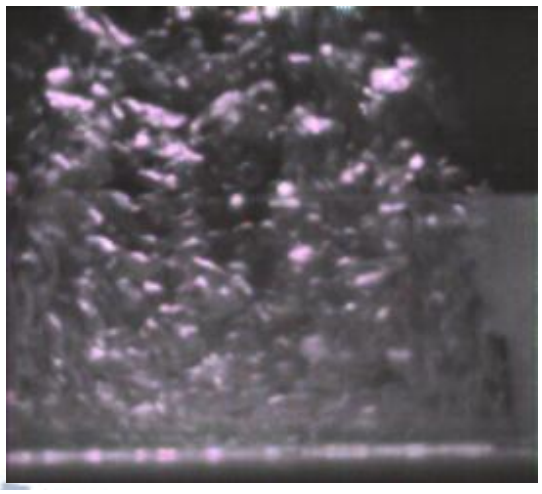

(1) t=1.2 s

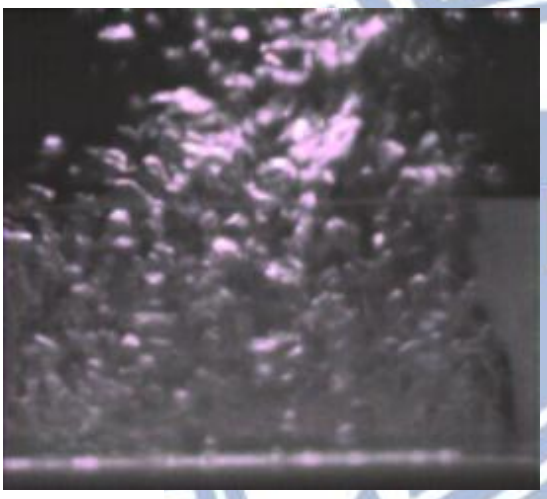

(3) t=0.4 s

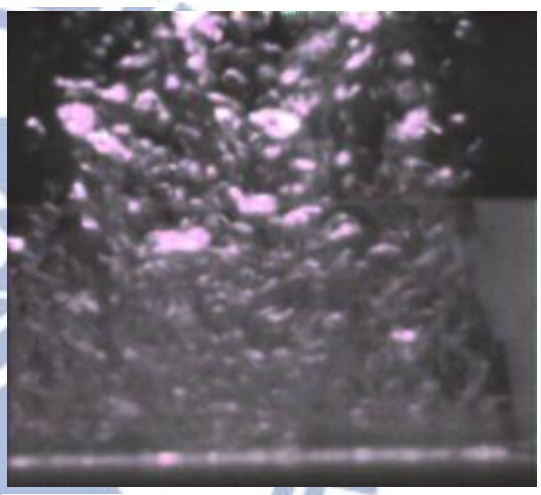

(5) t=1.6 s

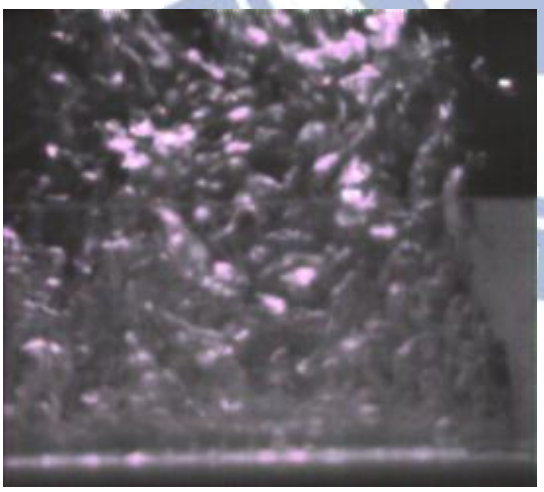

(4) t=0.8 s

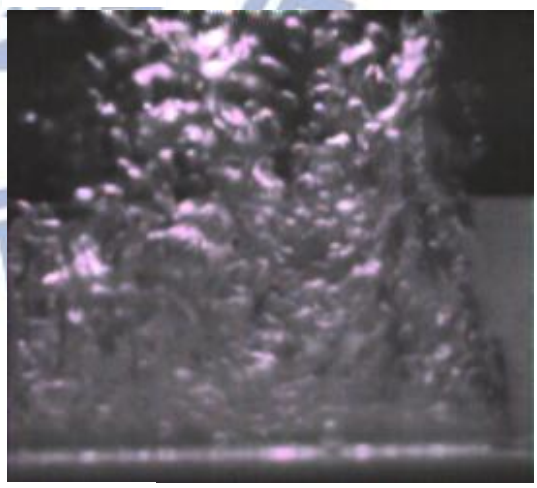

(6) t=2.0 s

Fig. 4.49 Photos taken from side view of boiling flow at selected time instants for q= 5.42 W/ m^2 with zirconia particles on heated surface at d_p=1.6 mm and $N_p = 250$

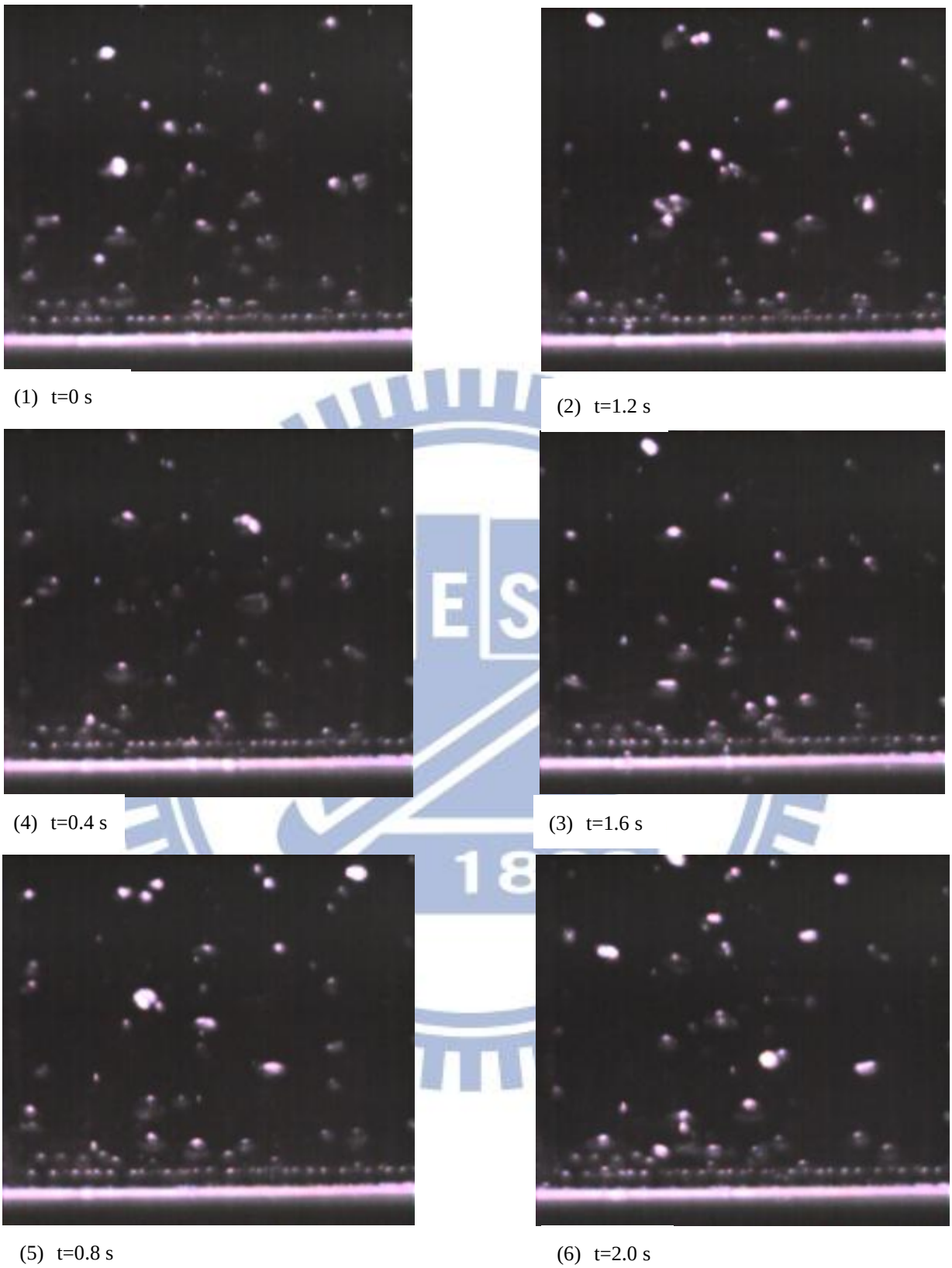

Fig. 4.50 Photos taken from side view of boiling flow at selected time instants for q= 0.22 W/ m^2 with silicon nitride particles on heated surface at d_p=1.6 mm and $N_p = 250$

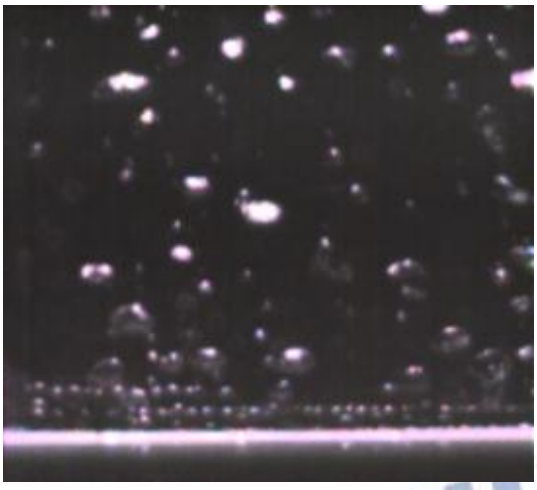

(2) t=0 s

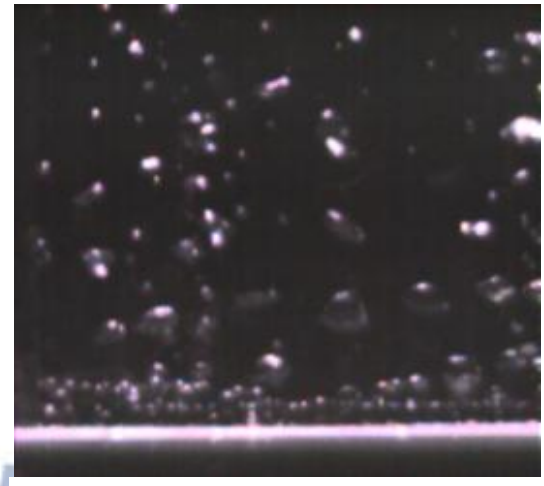

(1) t=1.2 s

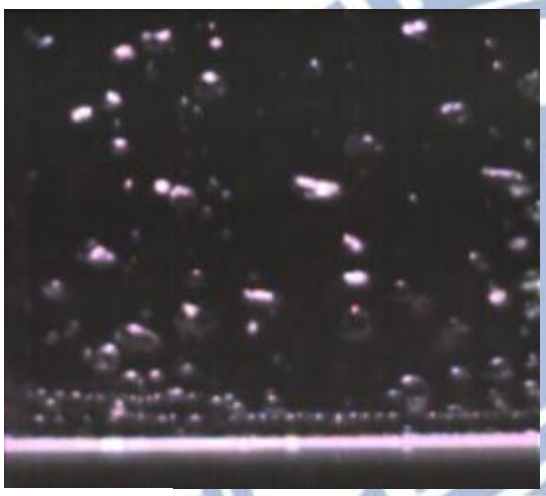

(4) t=0.4 s

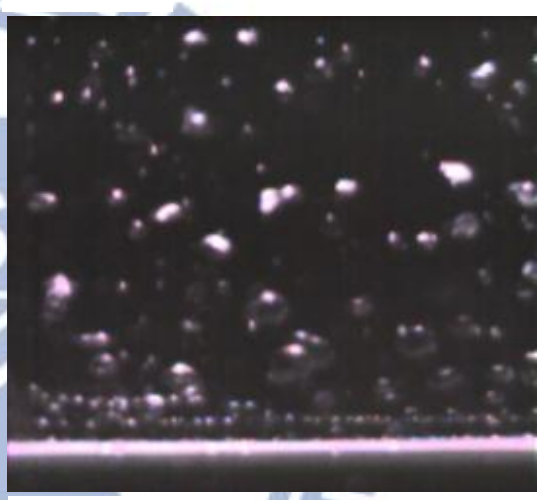

(3) t=1.6 s

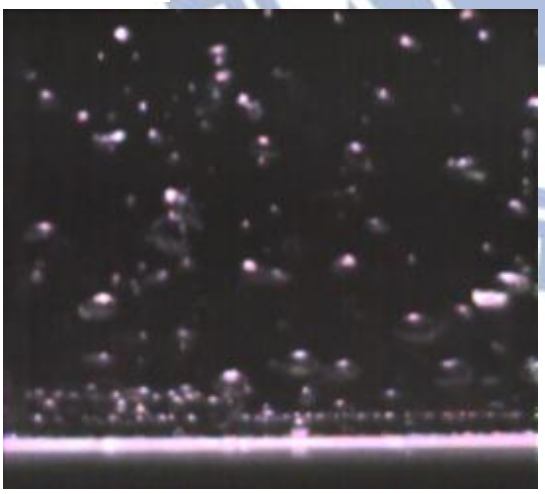

(6) t=0.8 s

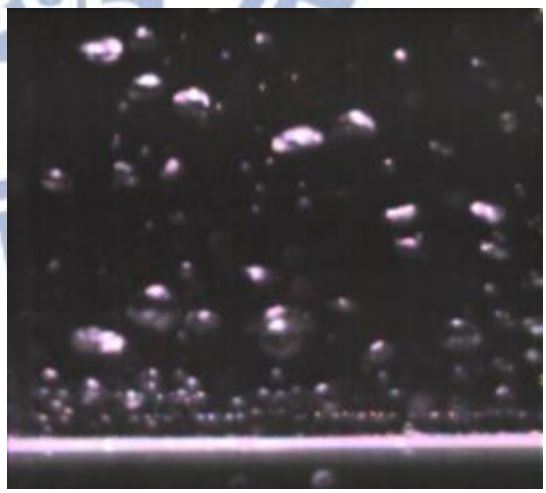

(5) t=2.0 s

Fig. 4.51 Photos taken from side view of boiling flow at selected time instants for q= 0.39 W/ m^2 with silicon nitride particles on heated surface at d_p=1.6 mm and $N_p = 250$

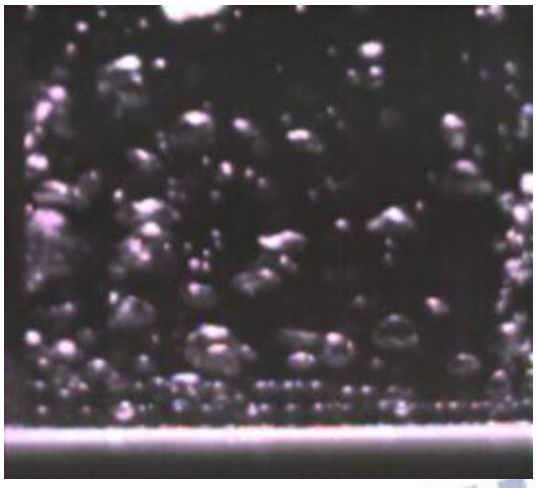

(1) t=0 s

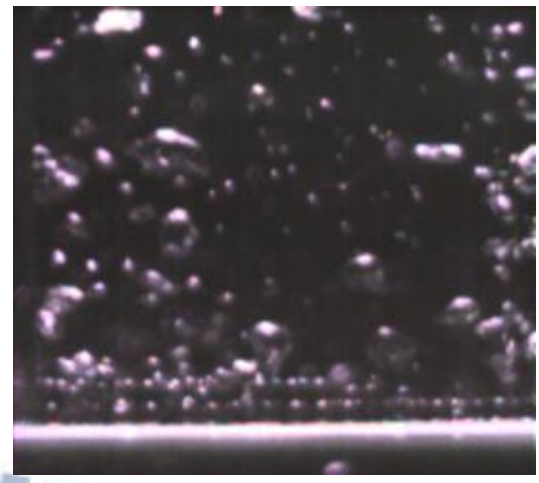

(2) t=1.2 s

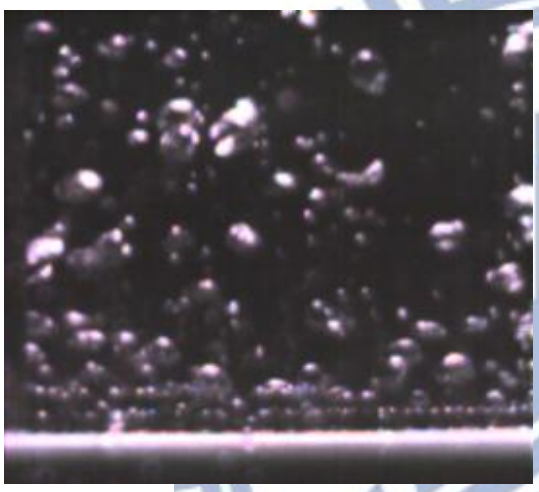

(3) t=0.4 s

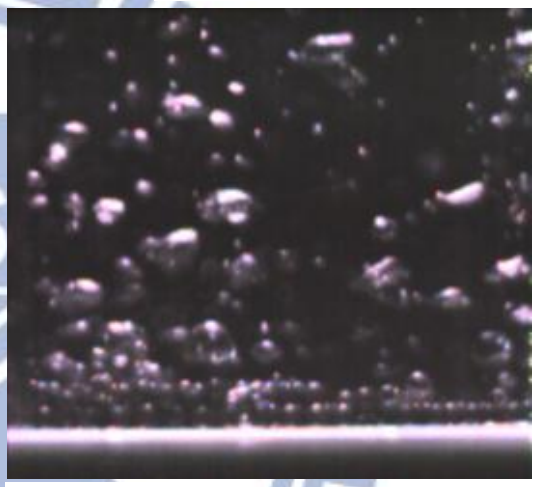

(4) t=1.6 s

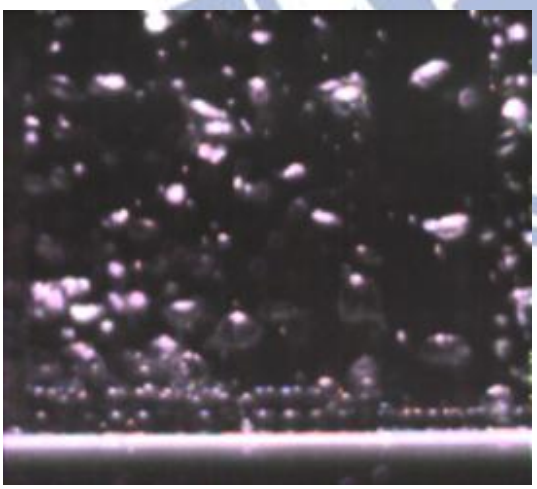

(5) t=0.8 s

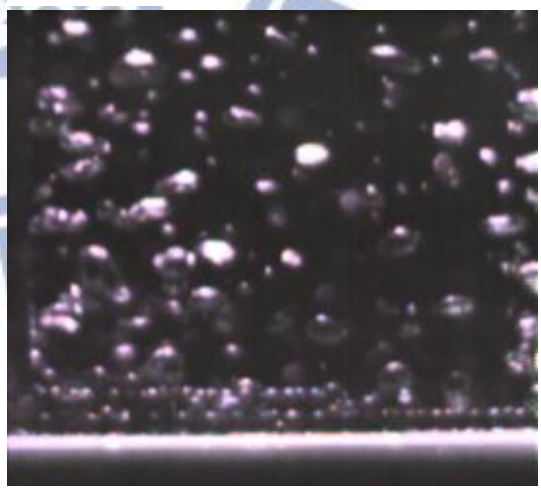

(6) t=2.0 s

Fig. 4.52 Photos taken from side view of boiling flow at selected time instants for q= 0.61 W/ m^2 with silicon nitride particles on heated surface at d_p=1.6 mm and $N_p = 250$

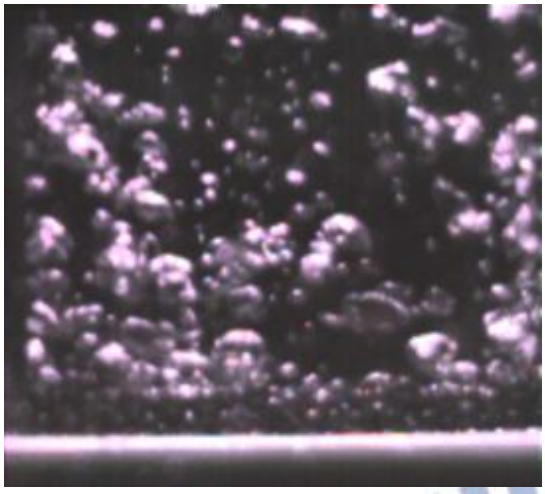

(2) t=0 s

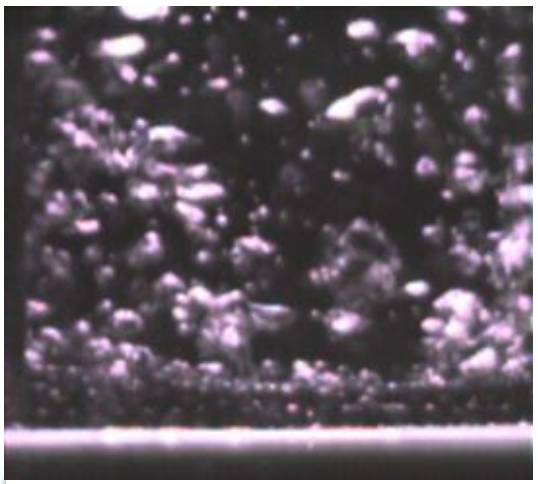

(1) t=1.2 s

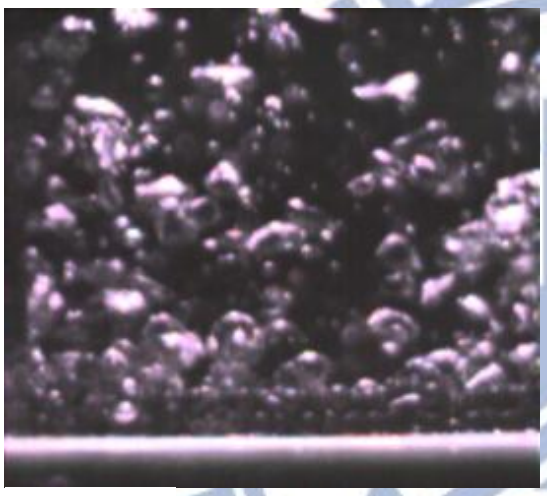

(4) t=0.4 s

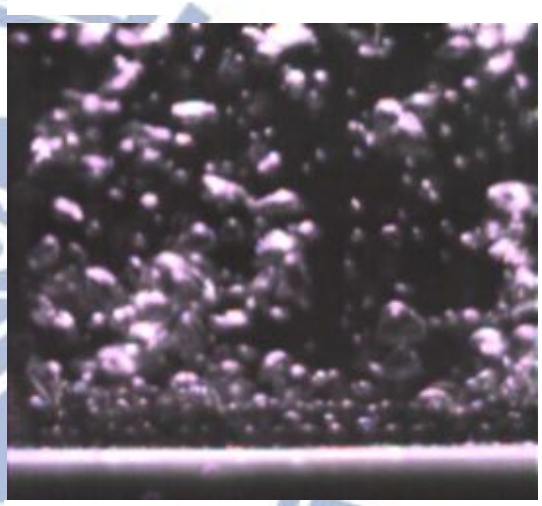

(3) t=1.6 s

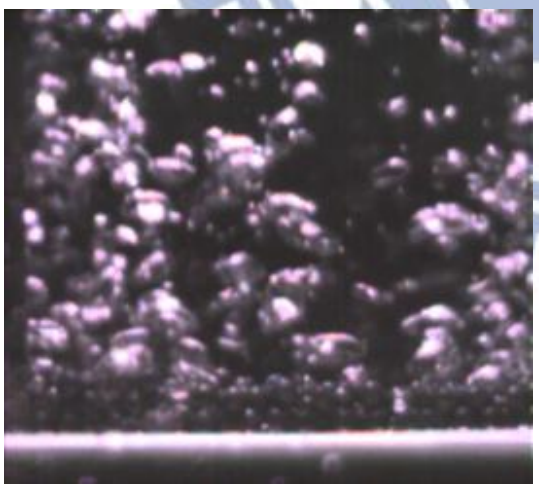

(6) t=0.8 s

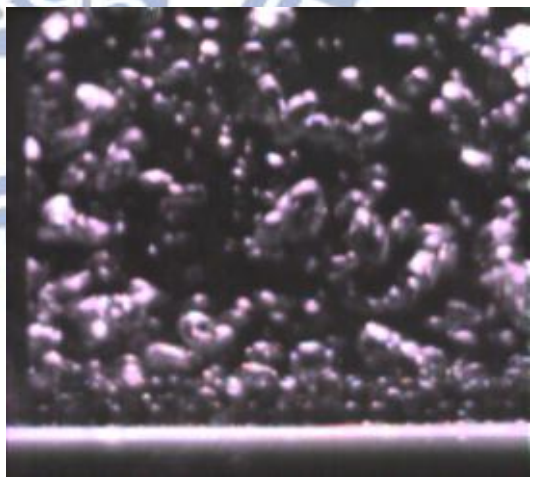

(5) t=2.0 s

Fig. 4.53 Photos taken from side view of boiling flow at selected time instants for q= 1.11 W/ m^2 with silicon nitride particles on heated surface at d_p=1.6 mm and $N_p = 250$

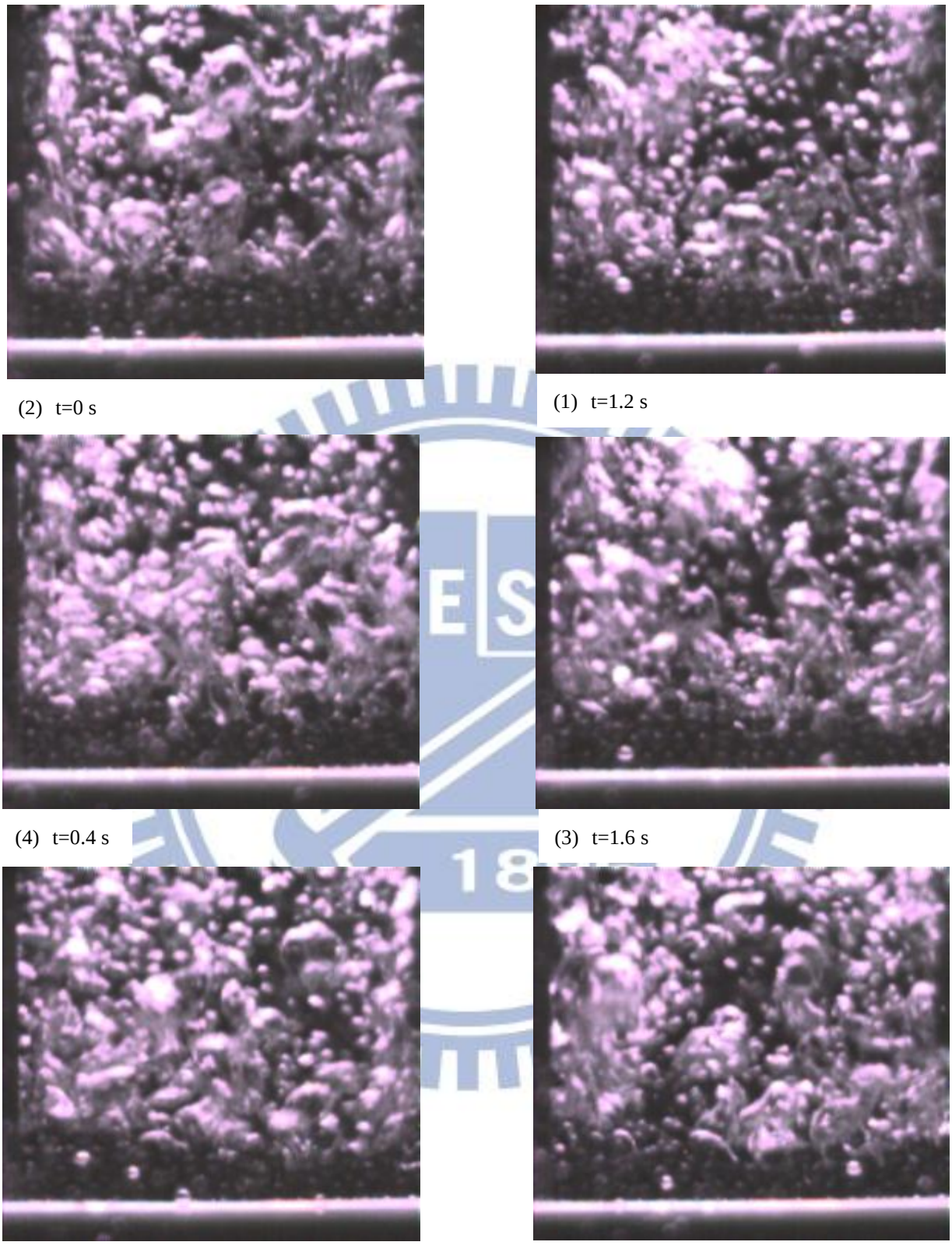

Fig. 4.54 Photos taken from side view of boiling flow at selected time instants for q= 2.67 W/ m^2 with silicon nitride particles on heated surface at d_p=1.6 mm and $N_p = 250$

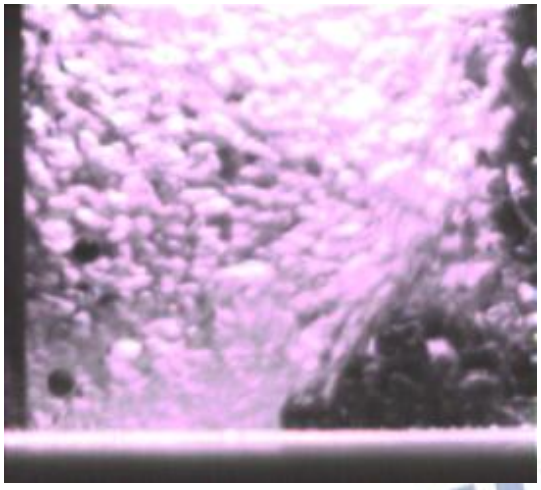

(2) t=0 s

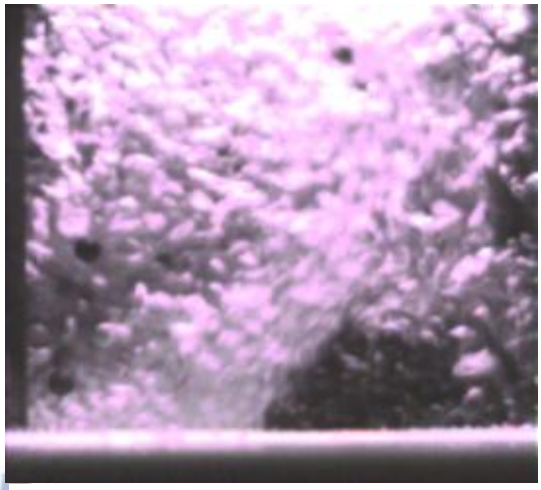

(1) t=1.2 s

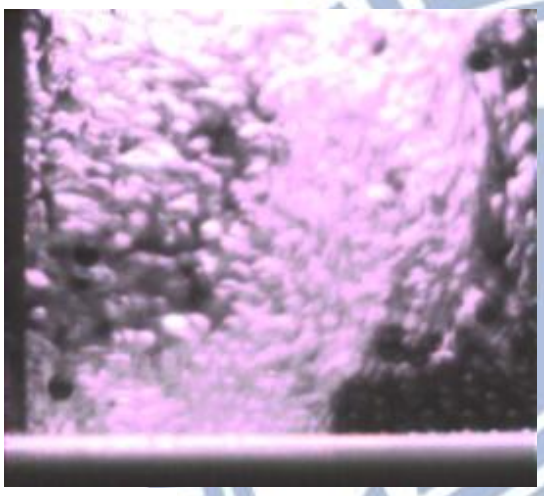

(4) t=0.4 s

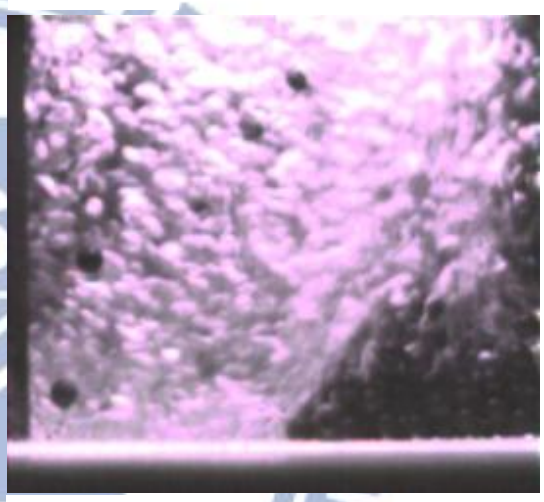

(3) t=1.6 s

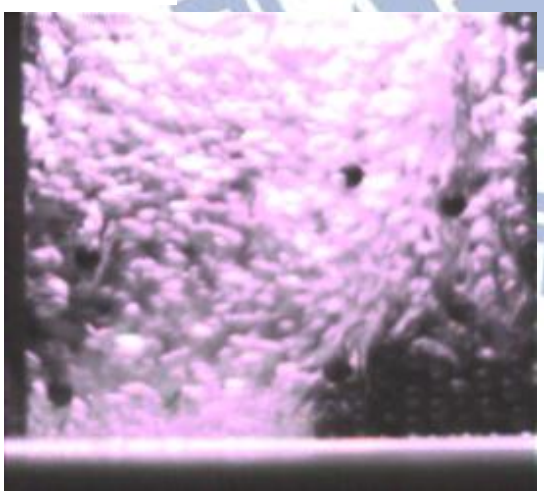

(6) t=0.8 s

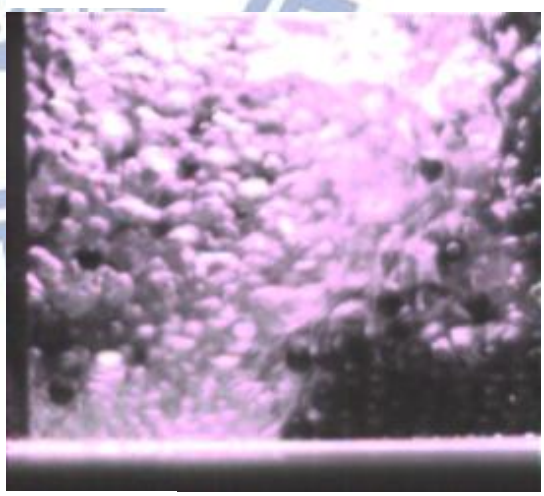

(5) t=2.0 s

Fig. 4.55 Photos taken from side view of boiling flow at selected time instants for q= 5.42 W/ m^2 with silicon nitride particles on heated surface at d_p=1.6 mm and $N_p = 250$

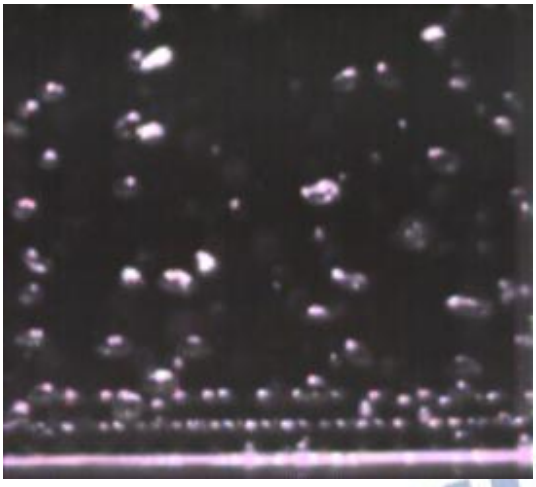

(2) t=0 s

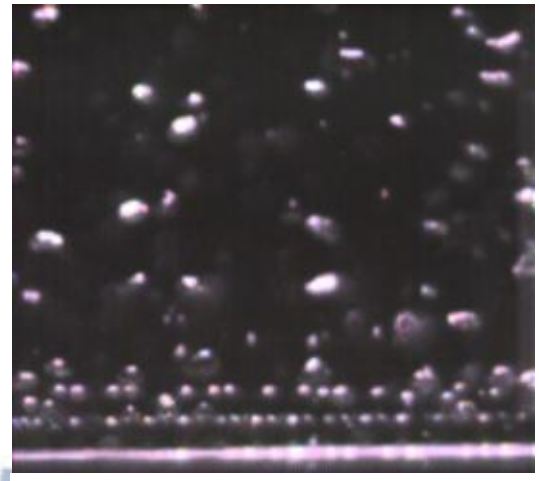

(1) t=1.2 s

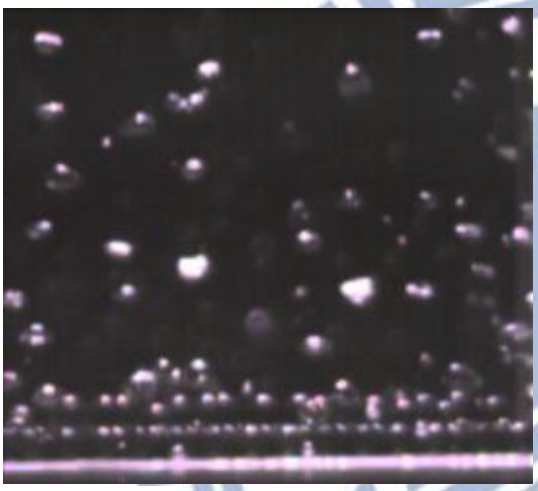

(3) t=0.4 s

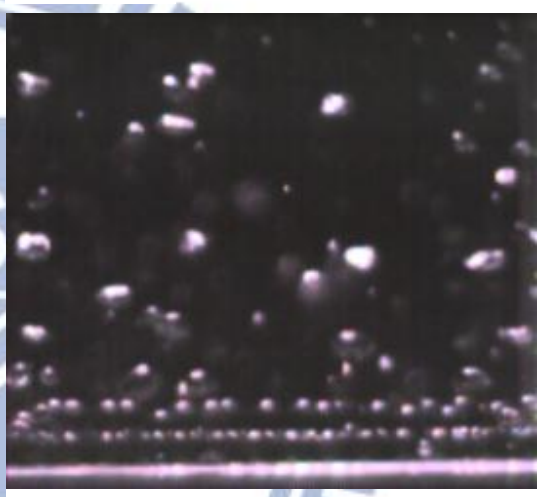

(4) t=1.6 s

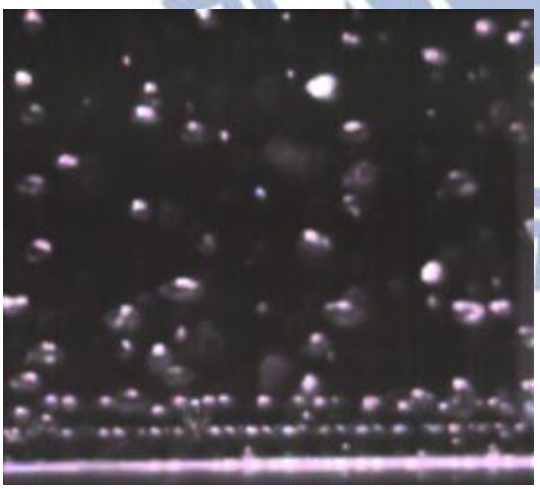

(6) t=0.8 s

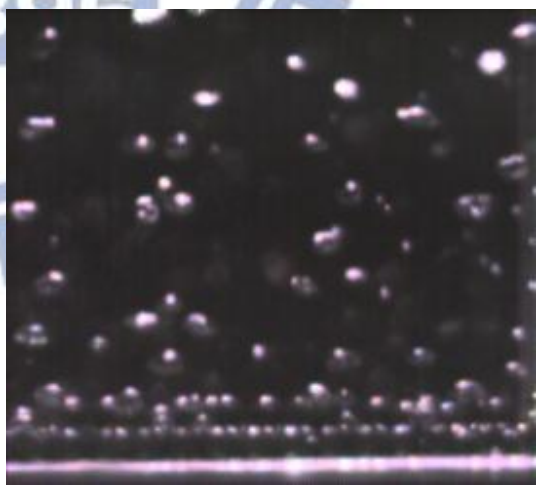

(5) t=2.0 s

Fig. 4.56 Photos taken from side view of boiling flow at selected time instants for q= 0.22 W/ m^2 with silicon nitride particles on heated surface at d_p=2.0 mm and $N_p = 150$

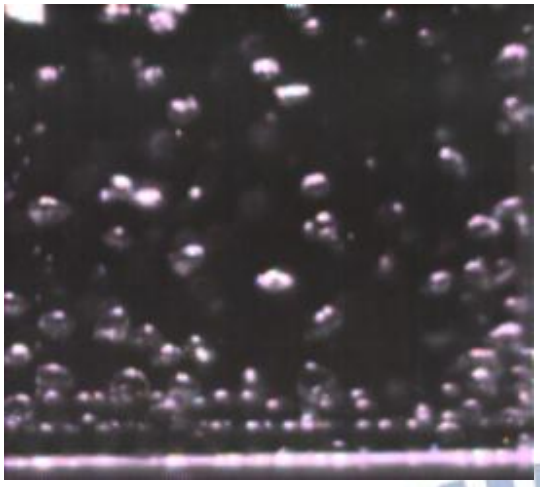

(2) t=0 s

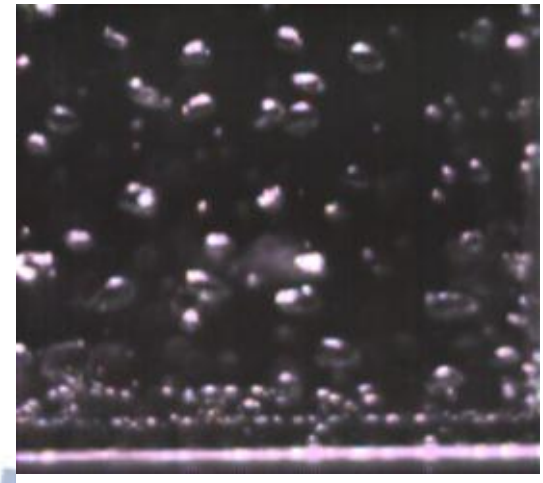

(1) t=1.2 s

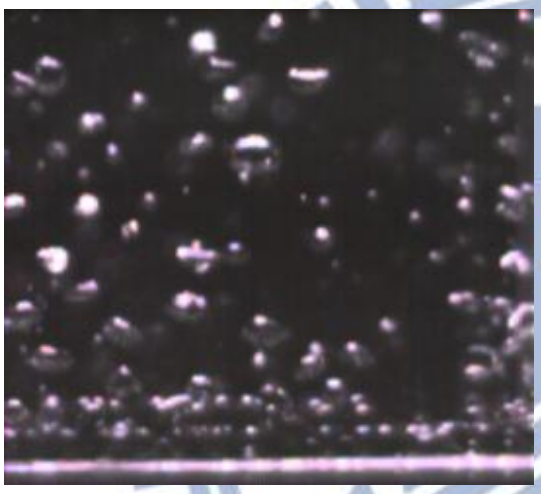

(4) t=0.4 s

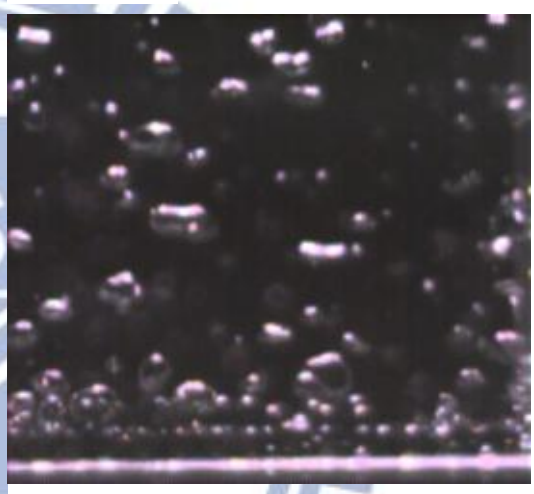

(3) t=1.6 s

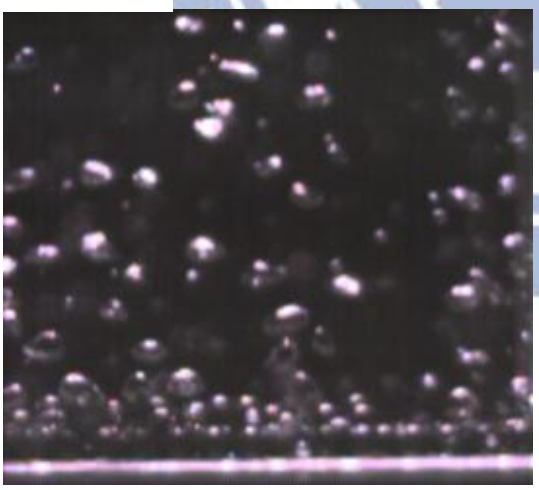

(6) t=0.8 s

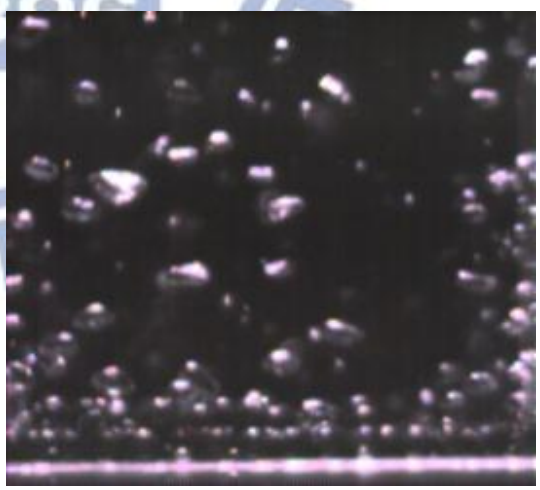

(5) t=2.0 s

Fig. 4.57 Photos taken from side view of boiling flow at selected time instants for q= 0.39 W/ m^2 with silicon nitride particles on heated surface at d_p=2.0 mm and $N_p = 150$

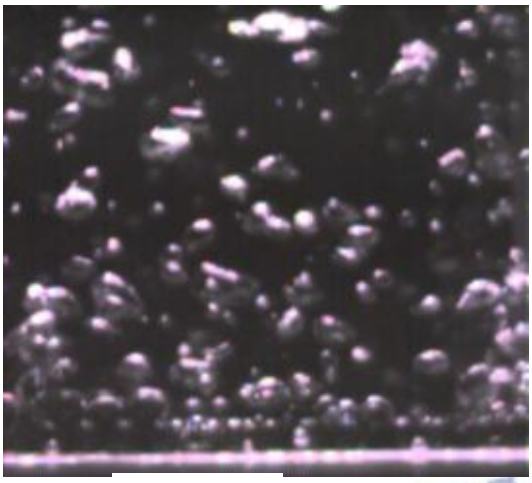

(2) t=0s

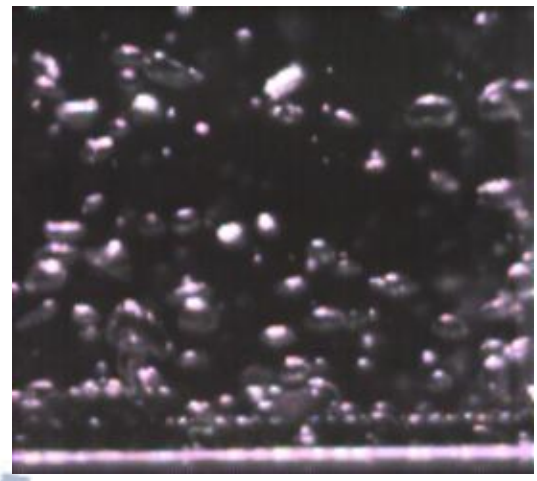

(1) t=1.2 s

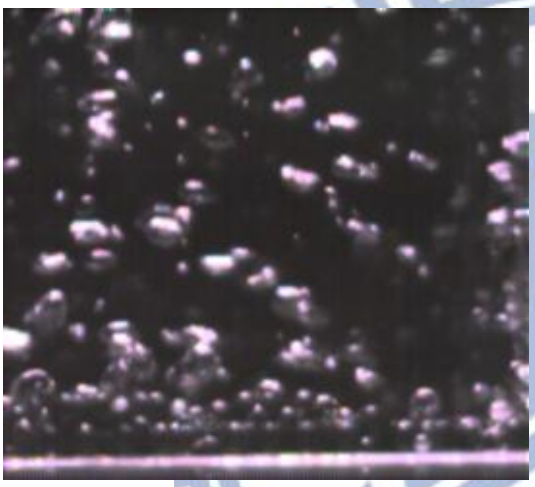

(3) t=0.4 s

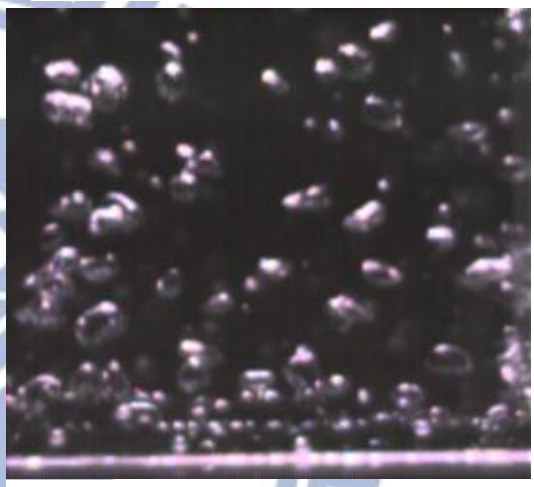

(5) t=1.6 s

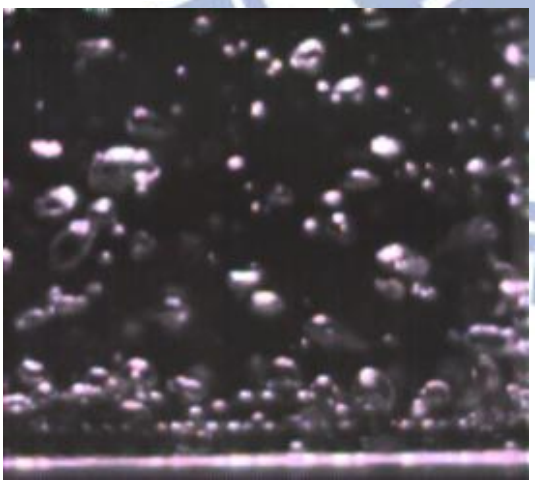

(5) t=0.8 s

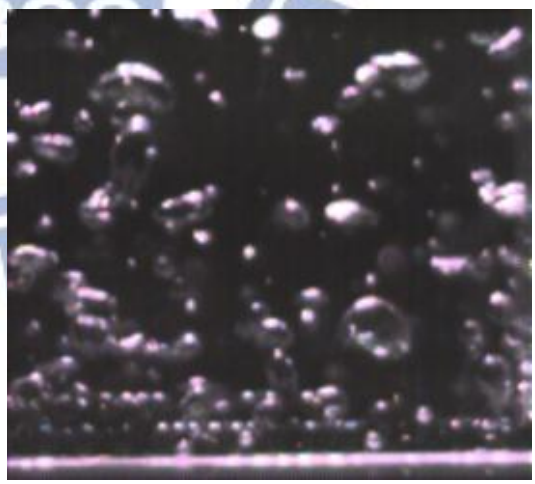

(4) t=2.0 s

Fig. 4.58 Photos taken from side view of boiling flow at selected time instants for q= 0.61 W/ m^2 with silicon nitride particles on heated surface at d_p=2.0 mm and $N_p = 150$

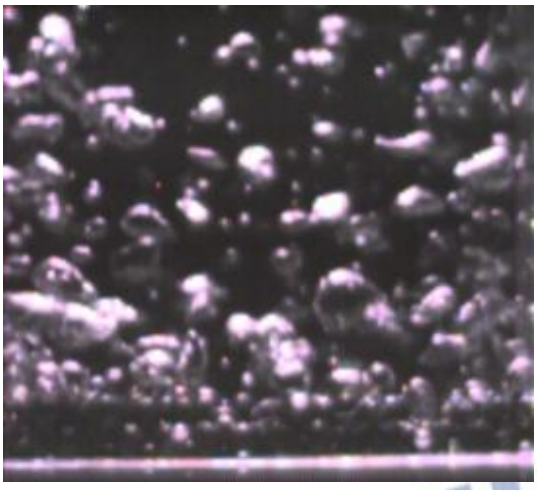

(2) t=0.4 s

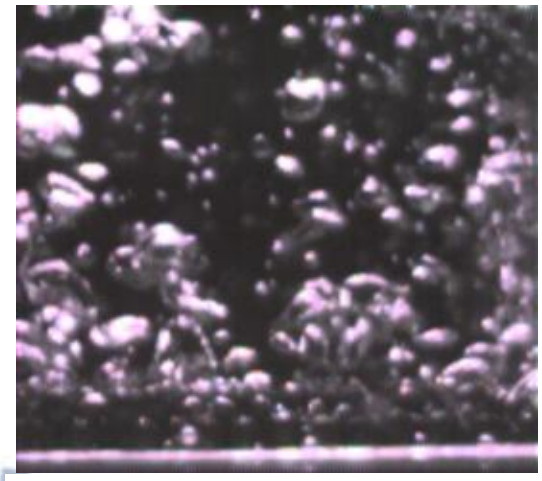

(1) t=0 s

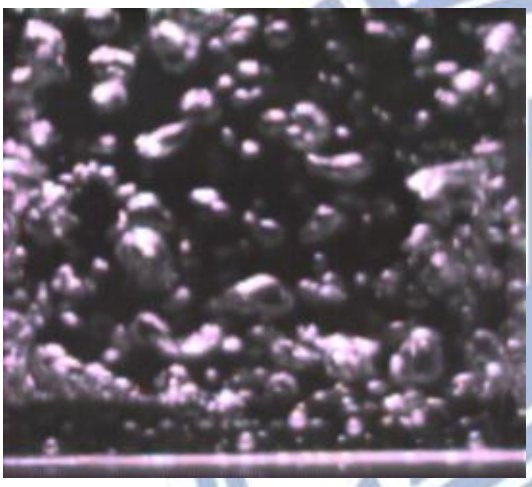

(4) t=1.2 s

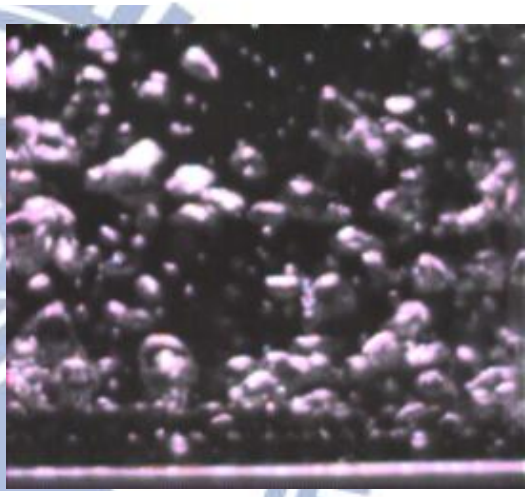

(3) t=0.8 s

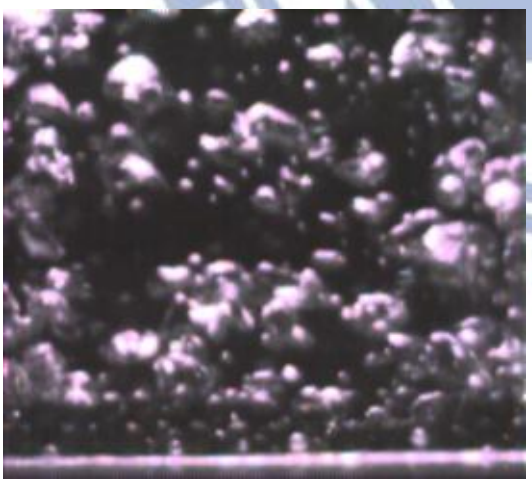

(6) t=2.0 s

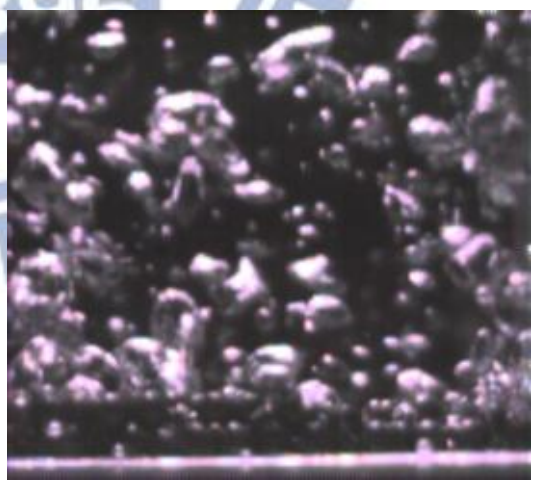

(5) t=2.0 s

Fig. 4.59 Photos taken from side view of boiling flow at selected time instants for q= 1.11 W/ m^2 with silicon nitride particles on heated surface at d_p=2.0 mm and $N_p = 150$

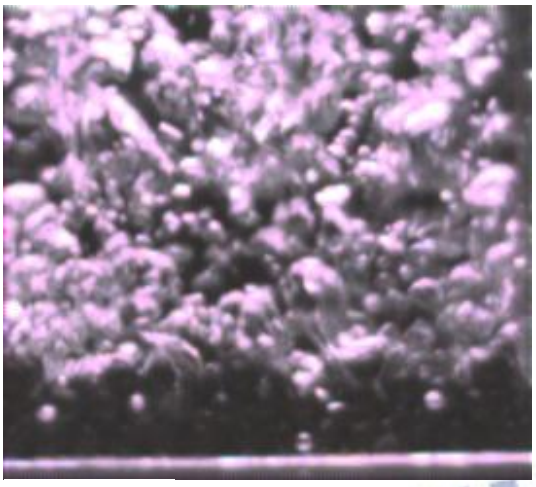

(1) t=0s

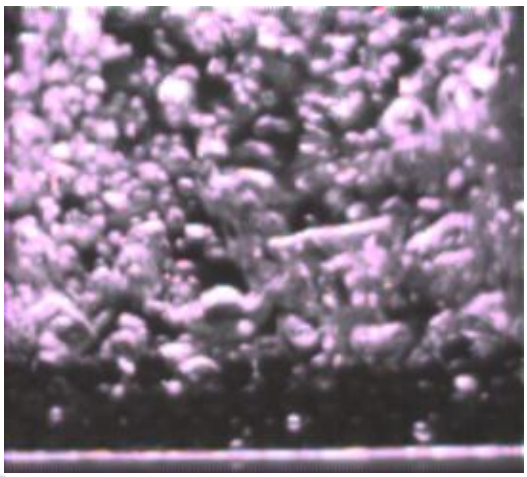

(2) t=1.2

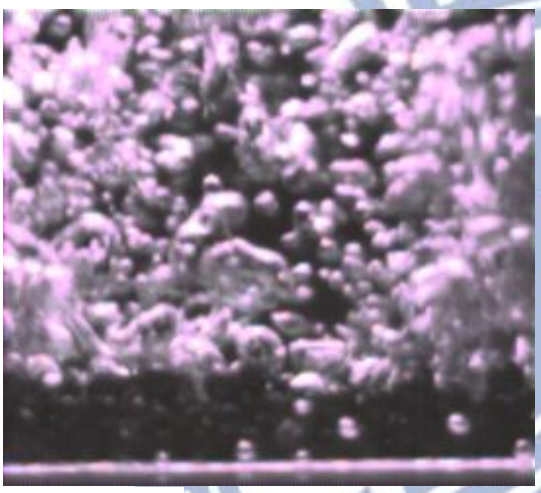

(4) t=0.4s

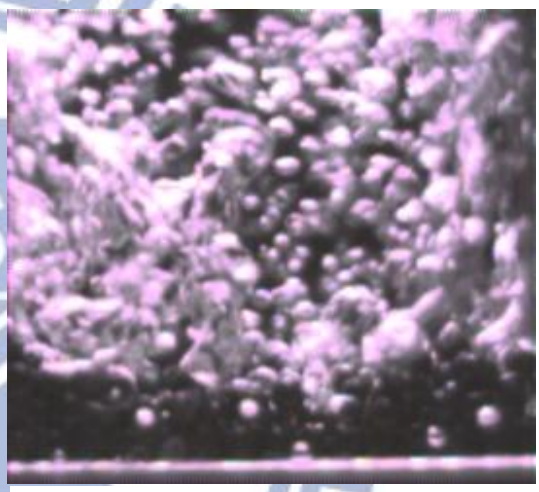

(3) t=1.6 s

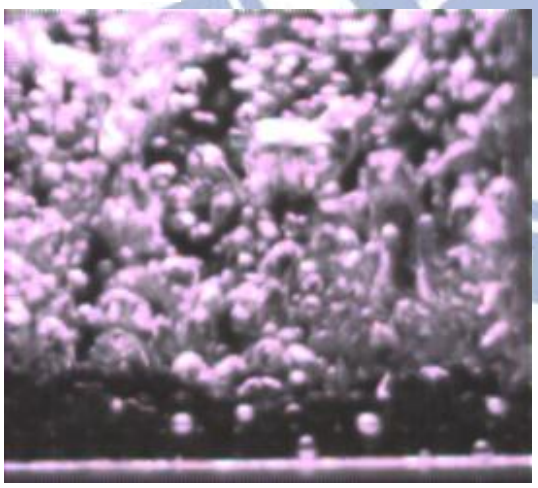

(5) t=0.8 s

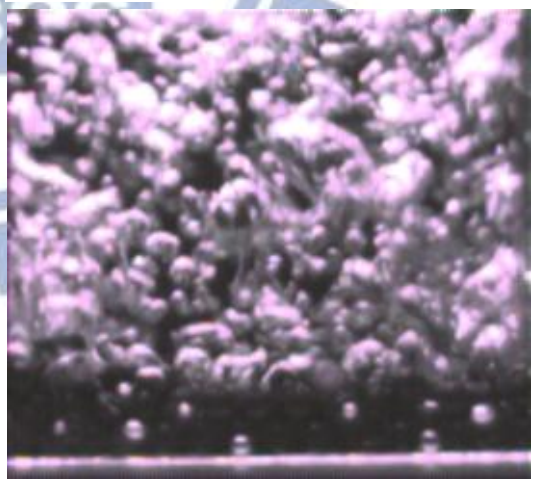

(6) t=2.0 s

Fig. 4.60 Photos taken from side view of boiling flow at selected time instants for q= 2.67 W/ m^2 with silicon nitride particles on heated surface at d_p=2.0 mm and $N_p = 150$

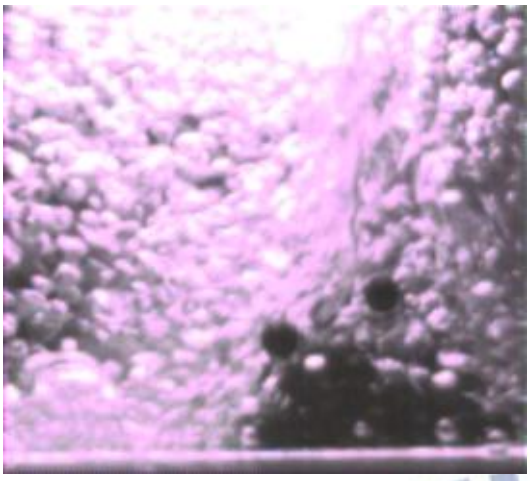

(2) t=0 s

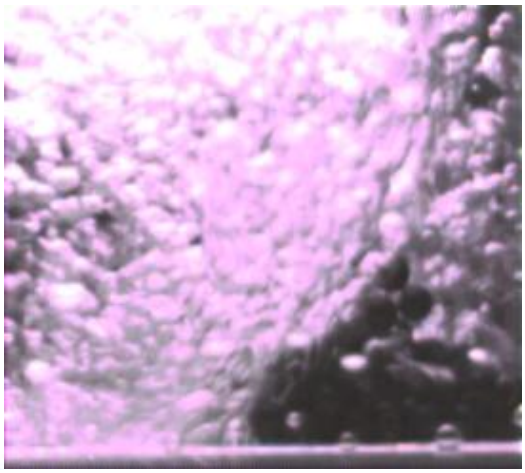

(1) t=1.2 s

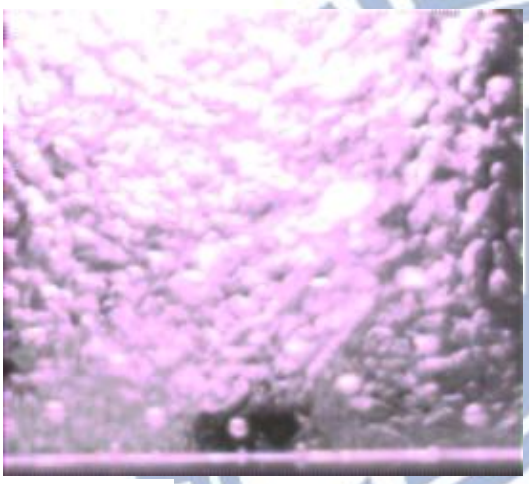

(4) t=0.4 s

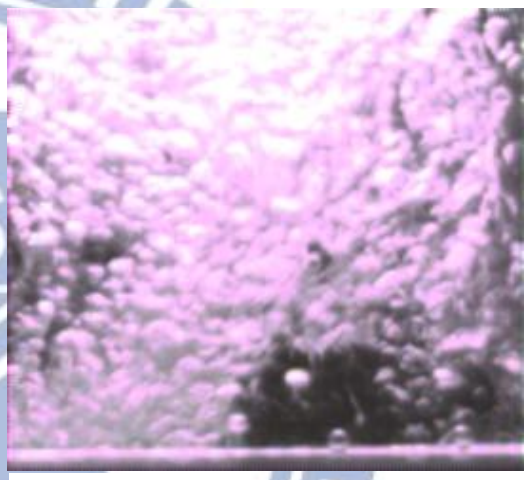

(3) t=5.42

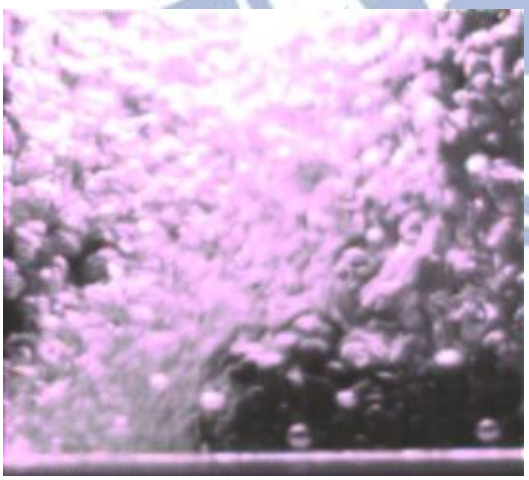

(6) t=0.8 s

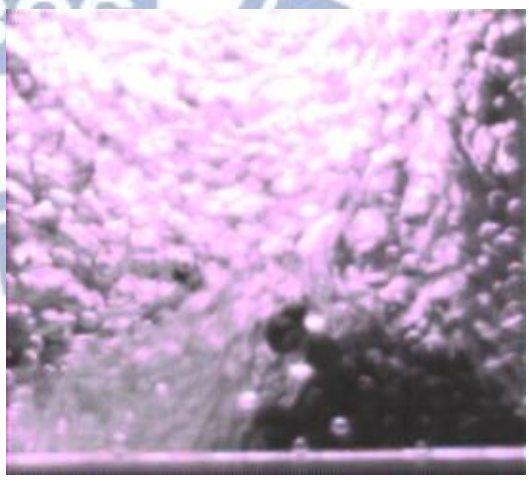

(5) t=2.0 s

Fig. 4.61 Photos taken from side view of boiling flow at selected time instants for q= 5.42 W/ m^2 with silicon nitride particles on heated surface at d_p=2.0 mm and $N_p = 150$

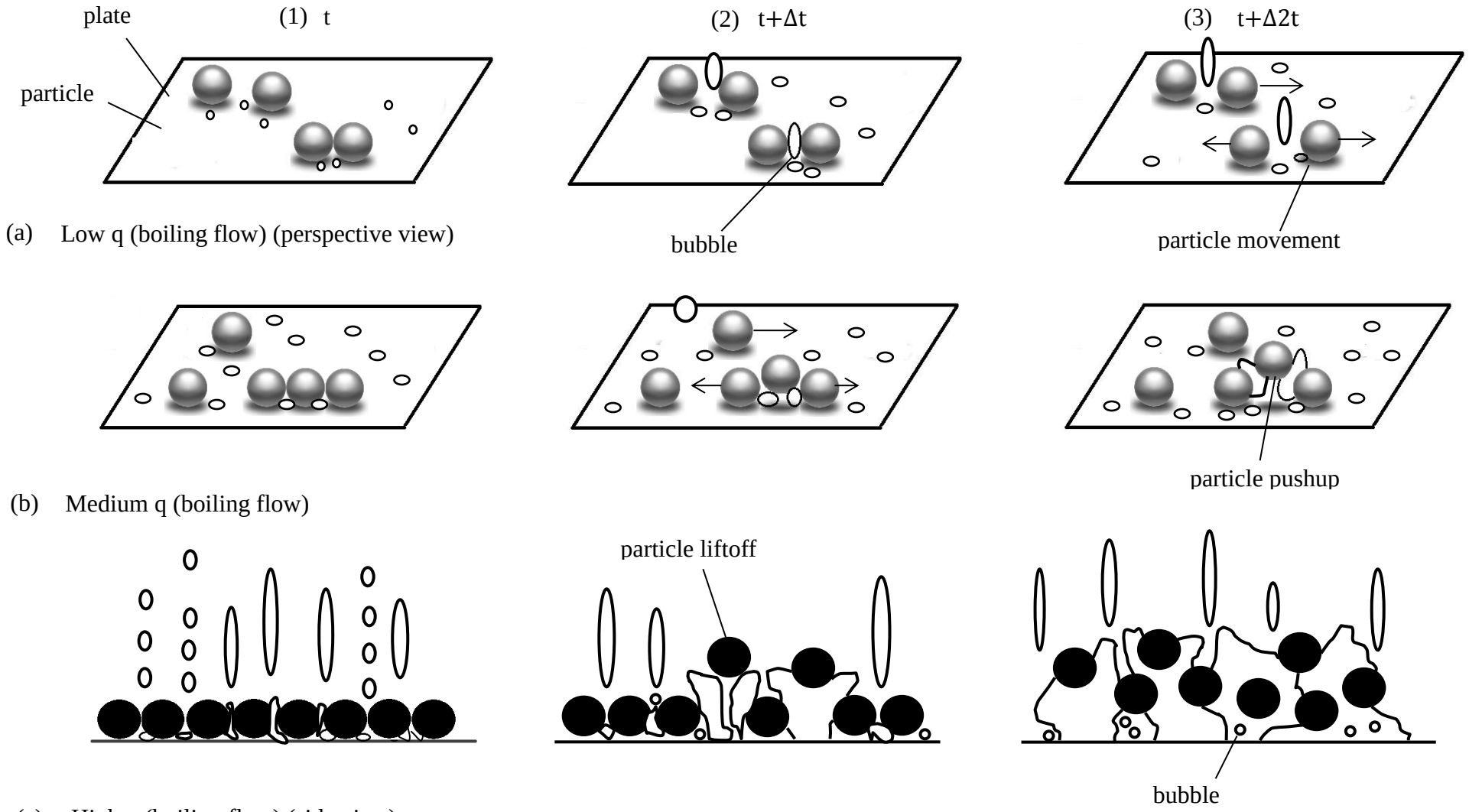

Figs. 4.62 Schematic illustration of zirconia particles-bubble interactions in boiling flow on heated surface at (a) low flux (b) medium flux (c) high flux ($\Delta t \approx 0.01$ sec.)

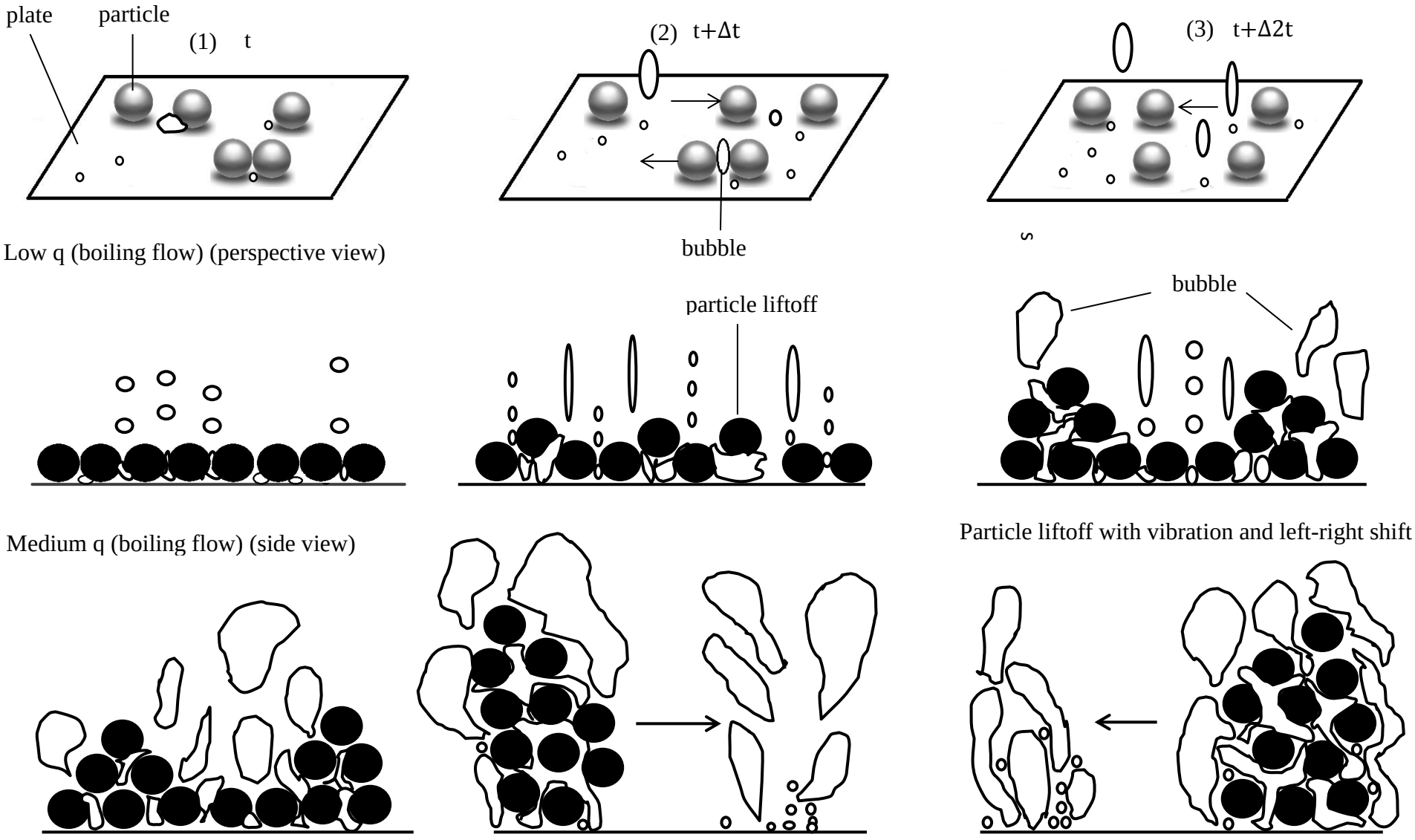

Figs. 4.63 Schematic illustration of silicon nitride particles-bubble interactions in boiling flow on heated surface at (a) low flux (b) medium flux (c) high flux ($\Delta t \approx 0.01$ sec.)

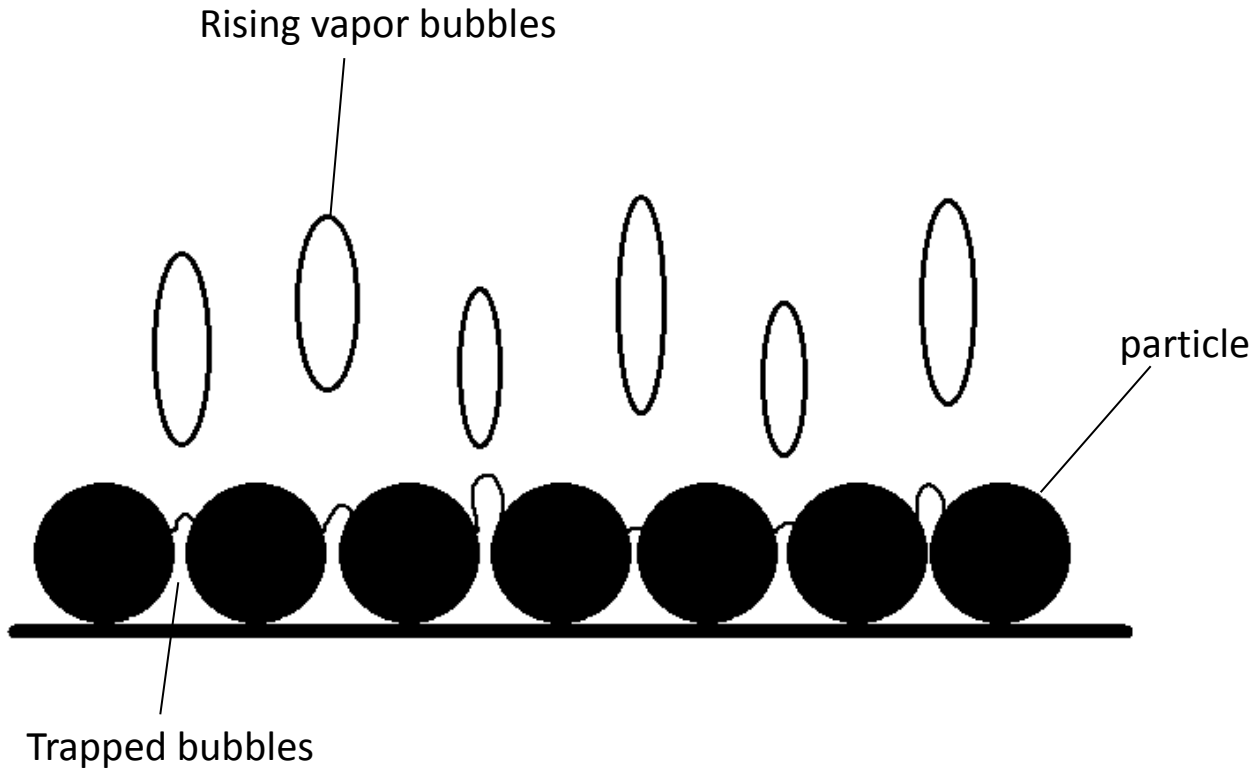

Fig. 4.64 Schematic illustration of retarding bubble growth and departure by zirconia particles at high heat flux.

(1) t (2) t+ΔT (3) t+Δ2T

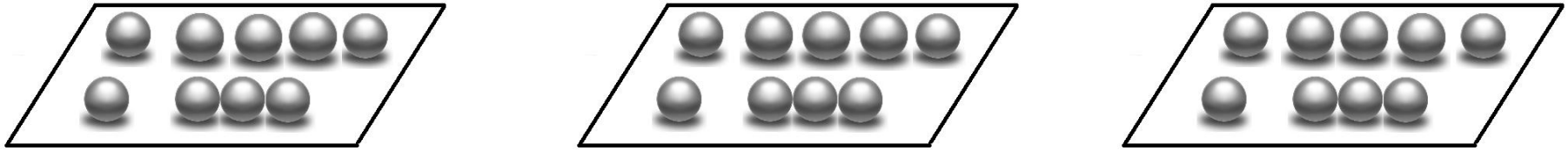

(a) (ZrO_2)

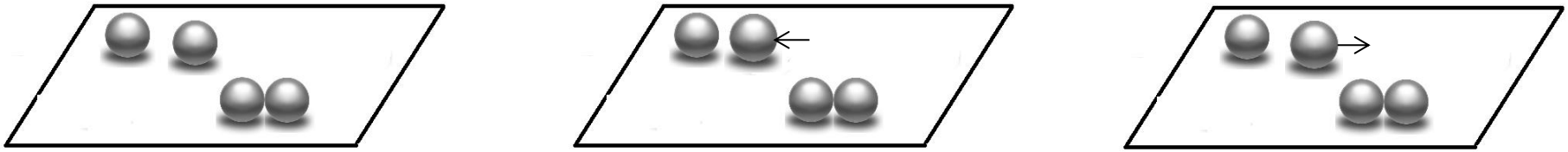

(b) (Si_3N_4)

Figs. 4.65 Schematic illustration of particles-bubble interactions in single phase on heated surface at (a) zirconia (b) silicon nitride ($\Delta t \approx 0.01$ sec.)

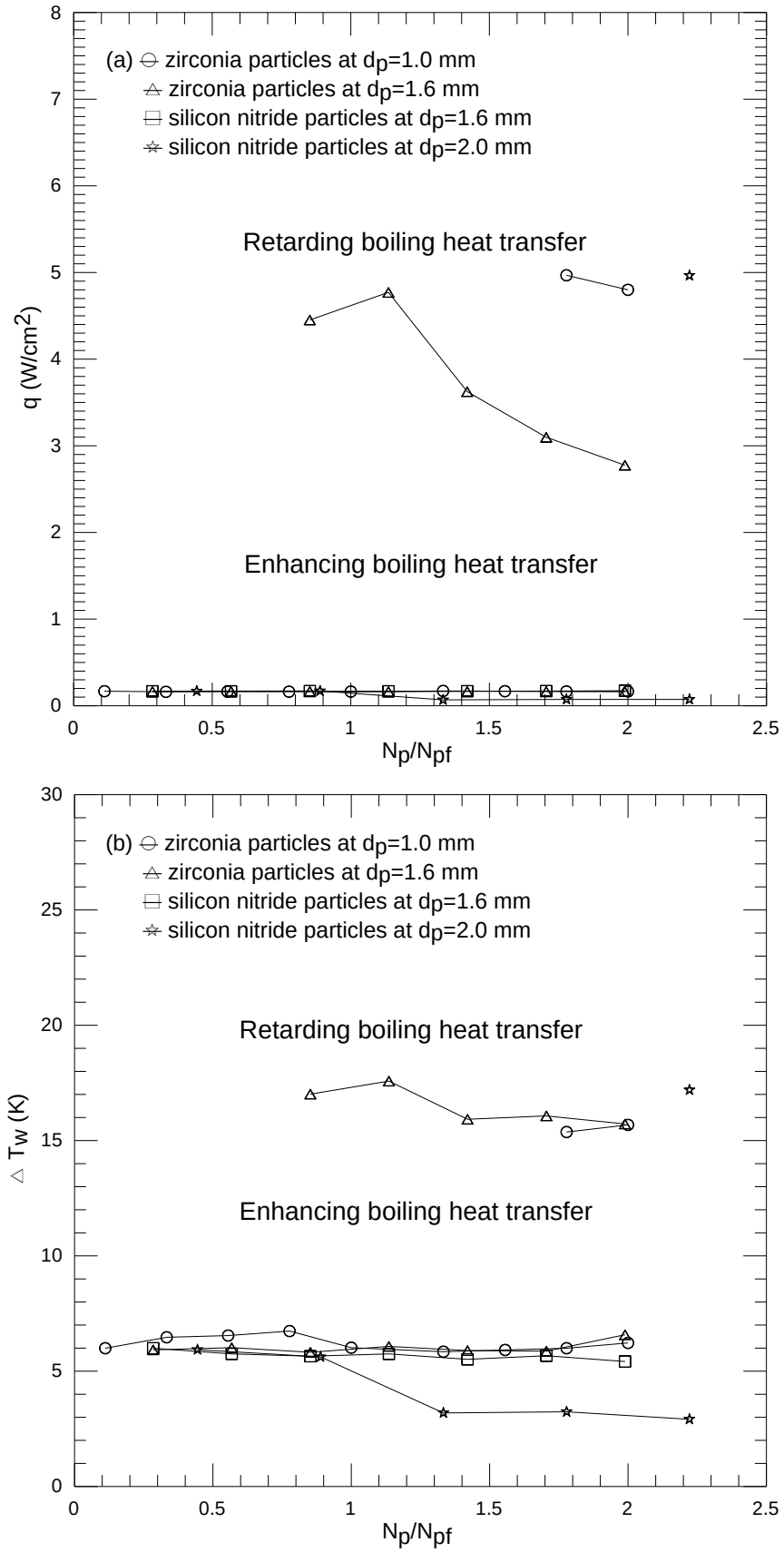

Fig. 4.66 Boundaries for boiling heat transfer augmentation and retardation for zirconia and silicon nitride particles with different d_p and N_p based on (a) q vs. N_p/N_{pf} and (b) ΔT_w vs. N_p/N_{pf}.

CHAPTER 5

CONCLUDING REMARKS

In this study we conduct an experiment to investigate the possible pool boiling heat transfer enhancement of FC-72 by placing movable ceramic particles on the boiling surface. The effects of the particle diameter, sort of particles (zirconia and silicon nitride) and particle number on the boiling heat transfer enhancement have been examined in detail. The major results obtained from this investigation can be summarized as follows.

(1) The boiling heat transfer enhancement is closely related to the particle diameter, sort of particles, particle number, and heat flux applied.

(2) The boiling and single phase heat transfer can be significantly enhanced by placing movable particles on the heated plate at low heat flux in single-phase flow and medium to high heat fluxes in boiling flow. Due to lower density of the ceramic particles, they are greatly agitated on the heated plate by the flow even at low heat flux applied. At medium to high heat flux, violent interaction between the particles and boiling flow causes substantial augmentation in boiling heat transfer. For the zirconia particles the boiling heat transfer can be enhanced up to 550% for a suitable choice of the experimental parameters. The best boiling heat transfer enhancement is slightly higher for the silicon nitride particles at 560%. Even for the particle number in the flow well exceeding N_{pf} the enhancement in the boiling heat transfer can be rather significant. Moreover, the wall superheat for the boiling incipience can be substantially reduced by the moving ceramic particles. This result is conjectured to be the consequence of that placing the particles on the heated plate has the effect of enhancing the roughness of the plate.

(3) At high heat flux (wall superheat) placing the particles in the flow can substantially retard the boiling heat transfer especially for the large particles. The boiling heat transfer retardation can be up to 40% for the large zirconia particles and 10% for the large silicon nitride particles.

(4) Interactions between the particles and bubbles are already very strong at low and medium heat fluxes for the small silicon nitride particles placed on the heated surface and hence the boiling heat transfer enhancement is already very pronounced at small particle numbers. Even at a somewhat high heat flux the retardation of the boiling heat transfer is barely seen.

(5) The pool boiling heat transfer enhancement for lighter ceramic particles is always better than heavier metallic particles at any level of heat flux applied.

References

1. G. Xu, B. Guenin, M. Vogel, “Extension of air cooling for high power processors”, Proceedings 9th Intersociety Conference on Thermal Phenomena 1 (2004) 186-193.

2. C. M. Wei, “Enhancement of FC-72 Pool Boiling Heat Transfer by Movable Particles on a Horizontal Plate” , M.S. Theses, Department of Mechanical Engineering, National Chiao Tung University, Hsinchu, Taiwan (2013)

3. S. Nukiyama, “The maximum and minimum values of the heat *Q* transmitted from metal to boiling water under atmospheric pressure”, Journal Japan Society of Mechanical Engineers 37 (1934) 367-374.
(Translated in Int. J. Heat Mass Transfer 9 (1966) 1419-1433).

4. A Bar-Cohen, “Thermal management of air-and liquid-cooled multichip modules”, IEEE Transactions on components, hybrids, and manufacturing technology 10 (2) (1987) 159-175.

5. W. J. Miller, B. Gebhart, N. T. Wright, “Effects of boiling history on a microconfigured surface in a dielectric liquid”, Int. Commun. Heat Mass Transfer 17 (4) (1990) 389-398.

6. J. Y. Chang, S. M. You, “Enhanced boiling heat transfer from micro-porous surfaces: effects of a coating composition and method”, Int. J. Heat Mass Transfer 40 (18) (1997) 4449-4460.

7. S. Vemuri, K. J. Kim, “Pool boiling of saturated FC-72 on nano-porous surface”, Int. Commun. Heat Mass Transfer 32 (2005) 27-31.

8. K. N. Rainey, S. M. You, “Pool boiling heat transfer from plain and microporous, square pin-finned surfaces in saturated FC-72”, Trans. ASME J. Heat Transfer 122 (3) (2000) 509-516.

9. K. N. Rainey, S. M. You, “Effect of pressure, subcooling, and dissolved gas on pool boiling heat transfer from microporous, square pin-finned surfaces in FC-72”, Int. J. Heat Mass Transfer 46 (1) (2003) 23-35.

10. H. Honda, H. Takamatsu, J. J. Wei, “Enhanced boiling of FC-72 on silicon chips with micro-pin-fins and submicron-scale roughness”, Trans. ASME J. Heat Transfer 124 (2) (2002) 383-390.

11. J. J. Wei, L. J. Guo, H. Honda “Experimental study of boiling phenomena and heat transfer performances of FC-72 over micro-pin-finned silicon chips”, Heat and Mass Transfer 41 (8) (2005) 744-755.

12. L. Zhang, M. Shoji “Nucleation site interaction in pool boiling on the artificial surface”, Int. J. Heat Mass Transfer 46 (2003)513-522

13. C. K. Yu. , D. C. Lu. and T. C. Cheng “Pool boiling heat transfer on artificial micro-cavity surface in dielectric fluid FC-72 ”, J. Micromech. Microeng. 16 (1989)752-759

14. Chen Li, G. P. Peterson and Y. Wang “Evaporation/Boiling in Thin Capillary Wick (I) –Wick Thickness Effects” Transaction of the ASME 128 (2006) 1312-1319

15. Chen Li, G. P. Peterson “Evaporation/Boiling in Thin Capillary Wick (II) –Effects of Volumetric Porosity and Mesh Size” Transaction of the ASME 128 (2006) 1320-1328

16. T. M. Anderson, I. Mudawar, “Microelectronic cooling by enhanced pool boiling of a dielectric fluorocarbon liquid”, Trans. ASME J. Heat Transfer 111 (3) (1989) 752-759.

17. J. P. O’Connor, S. M. You, “A painting technique to enhance pool boiling heat transfer in saturated FC-72”, Trans. ASME J. Heat Transfer 117 (2) (1995) 387-393.

18. J. P. O’Connor, S. M. You, D. C. Price, “A dielectric surface coating technique to enhance boiling heat transfer from high power microelectronics”, IEEE Transactions on components, packaging and manufacturing technology Part A 18 (3) (1995) 656-663.

19. J. Y. Chang, S. M. You, “Boiling heat transfer phenomena from micro-porous and porous surfaces in saturated FC-72”, Int. J. Heat Mass Transfer 40 (18) (1997) 4437-4447.

20. J. Y. Jung, H. Y. Kwak, “Effect of surface condition on boiling heat transfer from silicon chip with submicron-scale roughness”, Int. J. Heat Mass Transfer 49 (23-24) (2006) 4543-4551.

21. H. Honda, J. J. Wei, “Enhanced boiling heat transfer from electronic components by use of surface microstructures”, Experimental Thermal and Fluid Science 28 (2-3) (2004) 159-169.

22. K. N. Rainey, S. M. You, “Effects of heater size and orientation on pool boiling heat transfer from microporous coated surfaces”, Int. J. Heat Mass Transfer 44 (14) (2001) 2589-2599.

23. K. N. Rainey, S. M. You, S. Lee, “Effect of pressure, subcooling, and dissolved gas on pool boiling heat transfer from microporous surfaces in FC-72” Trans. ASME J. Heat Transfer 125 (1) (2003) 75-83.

24. H. M. Chou, R. F. Horng, Y. S. Liu, J. L. Wong, “The effect of grooved pattern on enhanced boiling heat transfer in a cylindrical tank base with a constant surface area”, Int. Comm. Heat Mass Transfer 29 (7) (2002) 951-960.

25. S. Hasegawa, R. Echigo, S. Irie, “Boiling characteristics and burnout phenomena on heating surface covered with woven screens”, Journal of Nuclear Science and Technology 12 (11) (1975) 722-724.

26. J. Y. Tsay, Y. Y. Yan, T. F. Lin, “Enhancement of pool boiling heat transfer in a horizontal water layer through surface roughness and screen coverage”, Heat and Mass Transfer 32 (1-2) (1996) 17-26.

27. J. W. Liu, D. J. Lee, A. Su, “Boiling of methanol and HFE-7100 on heated surface covered with a layer of mesh”, Int. J. Heat Mass Transfer 44 (1) (2001) 241-246.

28. A. Franco, E. M. Latrofa, V. V. Yagov, “Heat transfer enhancement in pool boiling of a refrigerant fluid with wire nets structures”, Experimental Thermal and Fluid Science 30 (3) (2006) 263-275.

29. H. M. Kurihara, J. E. Myers, “The effects of superheat and surface roughness on boiling coefficients”, A.I.Ch.E. Journal 6 (1) (1960) 83-91.

30. M. Shi, Y. Zhao, Z. Liu, “Study on boiling heat transfer in liquid saturated particle bed and fluidized bed”, International Journal of Heat and Mass Transfer 46(2003) 4695-4702.

31. M. MATIJEVIC, M. DJURIC, Z. ZAVARGO, M. NOVAKOVIC, “Improving Heat Transfer with Pool Boiling by Covering of Heating Surface with Metallic Spheres”, HEAT TRANSFER ENGINEERING 13(3)(1992) 49-57.

32. D. Wen, Y. Ding, “Experimental investigation into the pool boiling heat transfer of aqueous based γ -alumina nanofluids”, J. Nanoparticle Res.7 (2) (2005) 265-274.

33. I. C. Bang, S. H. Chang, “boiling heat transfer performance and phenomena of Al2O3-water nano-fluids from a plain surface in a pool”, Int. J. Heat Mass Transfer 48 (12) (2005) 2420-2428.

34. J. H. Jeong, Y. C. Kwon, “Effects of ultrasonic vibration on subcooled pool boiling critical heat flux”, Heat Mass Transfer (2006) 42 : 1155-1161.

35. M. Cipriani, P. Di Marco, W. Grassi, “Effect of an externally applied electric field on pool film boiling of FC-72”, HEAT TRANSFER ENGINEERING 26 (2010) : 3-13.

36. Y. V. Navruzov, P. V. Mamontov, A. V. Stoychev, “Subcooled liquid Pool Boiling Heat Transfer on a Vibration Heating Surface”, Heat Transfer Research 24 (6) (1992) 771-776.

37. S. J. Kline, F. A. McClintock, “Describing uncertainties in single sample experiments”, Mechanical Engineering 75 (1953) 3-8.

38. R. J. Moffat, “Contributions to the theory of single-sample uncertainty analysis”, Journal of Fluids Engineering 104 (2) (1982) 250-260.

39. E. Radziemska, W. M. Lewandowski, “The effect of plate size on the natural convective heat transfer intensity of horizontal surfaces”, Heat Transfer Engineering 26 (2) (2005) 50-53.